การสืบหาพารามิเตอร์ในการสปัตเตอร์สำหรับการเตรียมซิงค์ออกไซด์ที่โดปด้วยธาตุหมู่ห้าอันนำไปสู่ฟิล์มบางออกไซด์นำไฟฟ้าโปร่งใสชนิดพี

นายเกรียงไกร วันทอง

วิทยานิพนธ์นี้เป็นส่วนหนึ่งของการศึกษาตามหลักสูตรปริญญาวิทยาศาสตรดุษฎีบัณฑิต
สาขาวิชาฟิสิกส์ ภาควิชาฟิสิกส์
คณะวิทยาศาสตร์ จุฬาลงกรณ์มหาวิทยาลัย
ปีการศึกษา 2552

INVESTIGATION OF SPUTTERING PARAMETERS IN PREPARATION OF GROUP-V DOPED ZnO LEADING TO P-TYPE TRANSPARENT CONDUCTING OXIDE THIN FILMS

Mr. Kriangkrai Wantong

A Dissertation Submitted in Partial Fulfillment of the Requirements
for the Degree of Doctor of Science Program in Physics
Department of Physics
Faculty of Science
Chulalongkorn University
Academic year 2009

Thesis Title	Investigation of Sputtering Parameters in Preparation of Group-V Doped ZnO Leading to p-type Transparent Conducting Oxide Thin Films
By	Mr. Kriangkrai Wantong
Field of Study	Physics
Thesis Advisor	Chanwit Chityuttakan, Ph.D.
Thesis Co-Advisor	Assistant Professor Sojiphong Chatraphorn, Ph.D.

Accepted by the Faculty of Science, Chulalongkorn University in Partial Fulfillment of the Requirements for the Doctoral Degree

S. Hannongbua

……………………………………… Dean of the Faculty of Science
(Professor Suphot Hannongbua, Dr.rer.net.)

THESIS COMMITTEE

Wichit Sritrakool

……………………………………… Chairman
(Associate Professor Wichit Sritrakool, Ph.D.)

Chanwit Chityuttakan

……………………………………… Thesis Advisor
(Chanwit Chityuttakan, Ph.D.)

……………………………………… Thesis Co-Advisor
(Assistant Professor Sojiphong Chatraphorn, Ph.D.)

……………………………………… Examiner
(Assistant Professor Thiti Bovornratanaraks, Ph.D.)

……………………………………… Examiner
(Assistant Professor Sakuntam Sanorpim, Ph.D.)

Supab Choopun

……………………………………… External Examiner
(Assistant Professor Supab Choopun, Ph.D.)

เกรียงไกร วันทอง : การสืบหาพารามิเตอร์ในการสปัตเตอร์สำหรับการเตรียมซิงค์ออกไซด์ที่โดปด้วยธาตุหมู่ห้าอันนำไปสู่ฟิล์มบางออกไซด์นำไฟฟ้าโปร่งใสชนิดพี. (INVESTIGATION OF SPUTTERING PARAMETERS IN PREPARATION OF GROUP-V DOPED ZnO LEADING TO P-TYPE TRANSPARENT CONDUCTING OXIDE THIN FILMS) อ.ที่ปรึกษาวิทยานิพนธ์หลัก : ดร. ชาญวิทย์ จิตยุทธการ, อ. ที่ปรึกษาร่วม : ผศ. ดร.โศจิพงศ์ ฉัตราภรณ์, 105 หน้า.

ฟิล์มบาง ZnO ที่โดปด้วยธาตุหมู่ V ถูกค้นคว้าเพื่อหาเงื่อนไขของการสปัตเตอร์ที่ให้สมบัติการนำไฟฟ้าชนิดพี ฟิล์มบาง ZnO ที่ได้จากการสปัตเตอร์เป้าที่โดปด้วยฟอสฟอรัสแสดงสมบัติการนำไฟฟ้าชนิดเอ็นโดยเป็นผลหลักที่เกิดจากการแทนที่ของฟอสฟอรัสเข้าสู่ตำแหน่งของ Zn ฟิล์มบาง ZnO โดยส่วนใหญ่ที่โดปด้วยไนโตรเจนที่ได้จากการสปัตเตอร์เป้า ZnO บริสุทธิ์ภายใต้แก๊สผสมระหว่าง N_2 กับ Ar และจากการสปัตเตอร์เป้า Zn บริสุทธิ์ภายใต้แก๊สผสมระหว่าง N_2O กับ Ar มีสภาพต้านทานที่สูงมากระดับ 10^5 $\Omega\cdot$cm และไม่ได้แสดงสมบัติการนำไฟฟ้าชนิดพี โดยสิ่งที่เกิดขึ้นนี้สัมพันธ์กับการที่ส่วนใหญ่ของอะตอมของไนโตรเจนไม่สามารถเข้าสู่ตำแหน่งของออกซิเจนได้และอาจจะปรากฏเป็นอินเตอร์สติเทียลภายในฟิล์ม มีเพียงปริมาณเล็กน้อยของไนโตรเจนที่แทนที่ตำแหน่งของออกซิเจนและแสดงตัวเป็นแอกเซปเตอร์ ไม่สามารถชดเชยโดเนอร์เพื่อที่จะแสดงสมบัติการนำไฟฟ้าชนิดพีได้ ท้ายที่สุดแล้ว การเตรียม ZnO บริสุทธิ์โดยแทรกชั้นบางๆ ของ Zn:N ตรงกลางโดยการสปัตเตอร์และมีการอบภายหลังที่เหมาะสมจะนำไปสู่ฟิล์ม ZnO ชนิดพี โครงสร้างผลึกของฟิล์มถูกกระจายเข้าสู่สภาวะกึ่งเสถียรโดยแสดงสมบัติการนำไฟฟ้าชนิดพีโดยการอบภายใต้สุญญากาศในช่วงเวลาสั้นๆ และจะถูกกระจายอีกครั้งไปสู่สถานะที่เสถียรโดยมีแสดงสมบัติการนำไฟฟ้าชนิดเอ็นโดยการอบภายใต้สุญญากาศในช่วงเวลาที่ยาว อุณหภูมิและเวลาในกระบวนการอบภายหลังจากจุดสิ้นสุดของกระบวนการสปัตเตอร์เป็นพารามิเตอร์ที่สำคัญที่นำไปสู่สภาพการนำไฟฟ้าชนิดพี กระบวนการอบนี้นำไปสู่การเปลี่ยนเฟสของ Zn_3N_2 และการแพร่ของอะตอมของไนโตรเจนและออกซิเจน

ภาควิชา ฟิสิกส์ ลายมือชื่อนิสิต เกรียงไกร วันทอง
สาขาวิชา ฟิสิกส์ ลายมือชื่อ อ.ที่ปรึกษาวิทยานิพนธ์หลัก
ปีการศึกษา 2552 ลายมือชื่อ อ.ที่ปรึกษาวิทยานิพนธ์ร่วม S. Chatraph

4873808723 : MAJOR PHYSICS

KEYWORDS : ZINC OXIDE / P-TYPE / NITROGEN / SPUTTERING / ZINC NITRIDE

KRIANGKRAI WANTONG : INVESTIGATION OF SPUTTERING PARAMETERS IN PREPARATION OF GROUP-V DOPED ZnO LEADING TO P-TYPE TRANSPARENT CONDUCTING OXIDE THIN FILMS. THESIS ADVISOR : CHANWIT CHITYUTTAKAN, Ph.D., THESIS CO-ADVISOR : SOJIPHONG CHATRAPHORN, Ph.D., 105 pp.

Group-V doped ZnO thin films were investigated for the sputtering parameters of p-type conductivity. Phosphorus-doped ZnO thin films obtaining from sputtering of phosphorus-doped ZnO target exhibit n-type conductivity which is a main result of substitution of phosphorus into the zinc site. Most of nitrogen-doped ZnO thin films obtaining from sputtering of pure ZnO target under a mixture of N_2 and Ar gases and from sputtering of pure Zn target under a mixture of N_2O and Ar exhibit very high resistivity in the order of 10^5 Ω·cm and do not exhibit p-type conductivity. This relates to that most of nitrogen atoms cannot occupy oxygen sites and may appear as interstitial in the films. Small amount of nitrogen occupying oxygen sites and acting as acceptors cannot compensate the donors to exhibit p-type conductivity. Finally, preparation of intrinsic ZnO with the insertion of the ultra-thin Zn:N middle layer by sputtering with suitable post annealing leads to p-type ZnO films . The film crystalline structure was distributed to quasi-stable states with p-type conductivity by short-time vacuum annealing and then redistributed to stable states with n-type conductivity by long-time vacuum annealing. The temperature and time of annealing process after the end of sputtering process are the main parameters leading to p-type conductivity. This leads to the phase formation of Zn_3N_2 and the diffusion of nitrogen and oxygen atoms.

Department : Physics
Field of Study : Physics
Academic Year : 2009

Student's Signature Kriangkrai Wantong
Advisor's Signature Chanwit Chityuttakan
Co-Advisor's Signature S.

Acknowledgements

I would like to express my sincere gratitude and appreciation to my thesis advisors, Dr. Chanwit Chityuttakan and Assistant Professor Dr. Sojiphong Chatraphorn for their supervision, kindness suggestion and advice throughout the course of this dissertation. I am also grateful to Associate Professor Dr. Wichit Sritrakool, Assistant Professor Dr. Thiti Bovornratanaraks, Assistant Professor Dr. Sakuntam Sanorpim and Assistant Professor Dr. Supab Choopun for serving as the committee. All of whom have made valuable comments and have been helpful in the production of this dissertation.

I would like to thank Mr. Bancha Athibenjakul and Mr. Rachsak Sakdanuphab, Ph. D. students, who worked hard together and contributed courteous assistance during the work.

I would like to acknowledge the financial supports from the 90th Anniversary of Chulalongkorn University Fund (Ratchadaphisek-somphot Endowment Fund) and from Thailand Center of Excellent in Physics (ThEP Center).

I would like to acknowledge the Department of Geology, Faculty of Science, Chulalongkorn University for the access to the XRD facility, the Material Science Research Institute, Chulalongkorn University, for the access to the high temperature XRD facility, and the Gem and Jewelry Institute of Thailand for the access the Raman spectroscopy facility.

I would like to thank to my friends and colleagues including many Master students considered as younger brothers and younger sisters, whose names are not mentioned here, who helped and encouraged me in various ways.

Finally, a deep affectionate gratitude is acknowledged to my mother, father, and sisters for encouragement throughout the entire study.

Contents

List of Tables

List of Figures

CHAPTER I

INTRODUCTION

Zinc oxide (ZnO) is widely used in many applications, such as piezoelectric transducers, varistors, phosphors, and transparent conducting films [1]. N-type transparent conducting oxide (TCO) film is used in various photo-electronic devices such as window layers of solar cells [2] and flat panel displays [3]. In addition, p-type TCO is required for fabrications of complicated devices using together with n-type TCO. Due to n-type properties of ZnO by nature [4] because its native defects such as oxygen vacancies (V_O) and zinc interstitials (Zn_i) act as donor states, it is easy to fabricate excellent n-type semiconductors by doping with group-III elements such as Al, Ga, etc., and achieve high carrier concentration to the order of 10^{21} cm^{-3}, and resistivity in the order of 10^{-4} $\Omega\cdot cm$ [5]. On the other hand, it is difficult to make stable p-type ZnO with high carrier concentration because of the oxygen vacancies, zinc interstitials, and size mismatch between the dopants and oxygen sites. Oxygen vacancies and zinc interstitials contribute n-type carriers. Size mismatch leads to the low crystalline quality. Recently, many research groups competed for p-type ZnO fabrication with better electrical properties and stability. In principle, p-type ZnO may be doped using group-V elements such as N, P, As and Sb to occupy the oxygen sites. These group-V doped ZnO thin films can be fabricated by several techniques such as metal-organic vapor deposition (MOCVD) [6], molecular beam epitaxy (MBE) [7, 8], pulsed laser deposition (PLD) [9 - 12], spray pyrolysis [13], and sputtering [14 - 21]. Among these growth techniques, sputtering is a suitable technique which could be applied to larger area deposition.

Future p-type ZnO material should be used in many applications such as an ultraviolet electroluminescence device [22] and a tandem solar cell. The tandem cell is suggested in order to improve solar cell efficiency. It consists of two or more units of stacking solar cells. In order to connect electrical circuit of the upper unit to the lower unit while keeping high optical transmittance, it requires p-type TCO thin films. Generally, heavily doped n-type ZnO thin film is used as a window layer of the cell.

Thus, if heavily doped p-type ZnO could be created, the tunneling junction would be made. The lattice would be matched because both layers are made of the same kind of material i.e. ZnO. The junction would act as a tunneling diode that leaves the carrier to move in one direction. In addition, the n-type and p-type ZnO junction from n and p TCO's could be fabricated in the same system such as the sputtering. Thus, the production time and number of fabrication tools could be decreased.

In this work, a sputtering technique is proposed to fabricate group-V doped ZnO thin films on soda-lime glass substrates which are commonly used in many industries. Objective of this work is to fabricate ZnO thin film with group-V dopants using the sputtering technique and investigate key parameters in the process leading to p-type TCO thin films. In order to achieve p-type ZnO films, many conditions or parameters such as types of elements, temperature and time of thermal treatment, and composition of reactive gas were investigated. To avoid lattice mismatch, group-V elements with small atomic radii such as nitrogen (period 1) and phosphorous (period 2) should be considered. Firstly, phosphorus-doped ZnO (ZnO:P) was investigated for p-type ZnO because phosphorus oxide (P_2O_5) which is in a solid form can be easily doped directly into ZnO target. Secondly, nitrogen which is the smallest element of group-V and commonly appears as nitrogen (N_2) gas was used in the research. Nitrogen-doped ZnO (ZnO:N) was investigated by sputtering with pure ZnO target under the mixture of N_2 and Ar gases. Thirdly, in order to help nitrogen atom to occupy oxygen site easier, pure metallic Zn target was used instead of ZnO target in sputtering process under N_2 gas. Various thermal treatments with oxygen filling were investigated. Then, apart from N_2 gas, nitrous oxide (N_2O) gas was used as sputtering gas. Chemical bond of N_2O should be broken by dissociation collision under sputtering process easier than that of N_2. Thus, the mixture of N_2O and Ar gases were investigated. Finally, many failures of previous research procedures originated from the high electronegativity of oxygen leading to the difficulty of nitrogen in occupying oxygen site. To force nitrogen into the oxygen site, encapsulation of zinc-nitrogen (Zn:N) layer between two ZnO layers with suitable thermal treatment for phase formation and diffusion was investigated to achieve p-type ZnO:N.

The as-deposited films and thermal treatment films can be verified to have p-type conductivity by Hall effect measurement. Nitrogen related defect complexes

(NRDC) that incorporated in the nitrogen doped ZnO (ZnO:N) films could be verified by Raman spectroscopy [23].

This dissertation consists of six chapters. In the following chapters, Chapter II, the literature reviews are given. Chapter III describes the theoretical background of sputtering and characterization. The experimental procedures are given in Chapter IV. Next, Chapter V describes the experimental results and the discussion. Finally, Chapter VI is the conclusions of the dissertation.

CHAPTER II

LITERATURE REVIEWS

The chapter begins with literature reviews discussing about zinc oxide, phosphorus-doped ZnO, arsenic-doped ZnO, antimony-doped ZnO, and nitrogen-doped ZnO.

2.1 Zinc oxide

Zinc oxide (ZnO) or zincite is II-VI compound semiconductor with wide and direct band gap of about 3.3 eV. Its crystal structure commonly appears in a form of hexagonal wurtzite (space group $P6_3mc$ with oxygen and zinc at site *2b*) as shown in Fig. 2.1. Its values of a and c are 3.24982 Å and 5.20661 Å [24], respectively. Its density is 5.675 g/cm^3 [24]. The energy band structure of bulk ZnO [25] is depicted in Fig. 2.2.

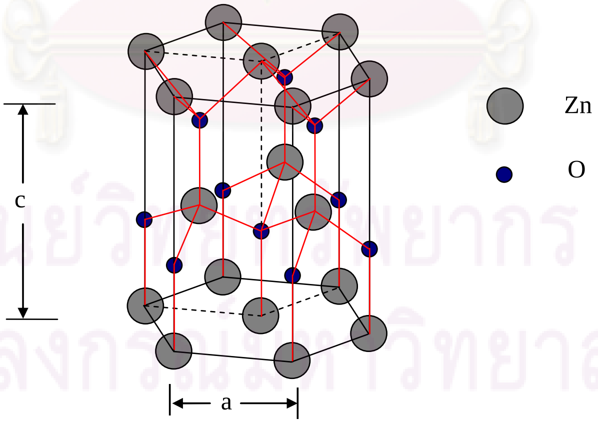

Figure 2.1: Wurtzite structure of ZnO.

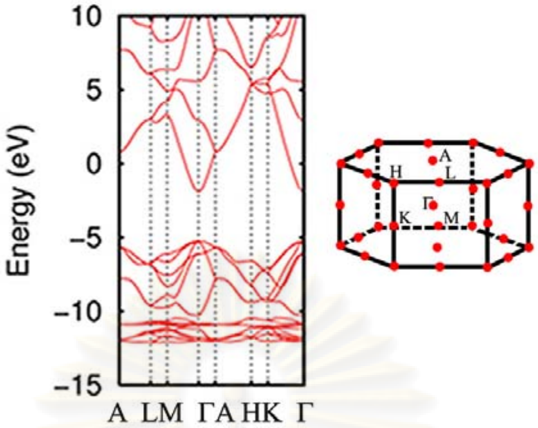

Figure 2.2: Calculated band structure of bulk ZnO using hybrid density function [25].

Refractive index (n) of ZnO can be calculated from the formula [26]:

$$n^2 = C_1 + \frac{C_2\lambda^2}{\lambda^2 - C_3^{\ 2}} - C_4\lambda^2 \ , \tag{2.1}$$

where C_1 = 2.81418, C_2 = 0.87968, C_3 = 0.3042 μm, C_4 = 0.00711 μm^{-2}, and λ is the photon wavelength (μm) in visible region. The refractive index in the visible region (0.4 – 0.7 μm) of ZnO is depicted in Fig. 2.3. The medium value of refractive index is 2.02 at the wavelength of 0.55 μm.

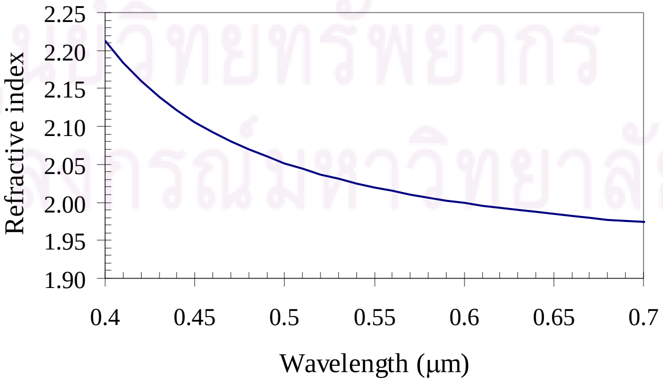

Figure 2.3: Refractive index of ZnO in the visible region.

Typical ZnO exhibits n-type conductivity by nature because of it native defects such as oxygen vacancy (V_O) and zinc interstitial (Zn_i). Both defects act as shallow donors. Hall mobility and carrier concentration of bulk ZnO are shown in Figs. 2.4 and 2.5, respectively.

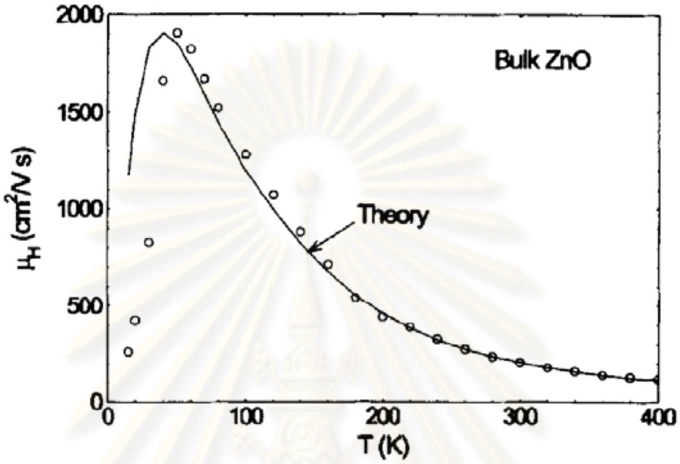

Figure 2.4: Experimental (circle) and theoretical (solid line) Hall mobility as a function of temperature in bulk ZnO [4].

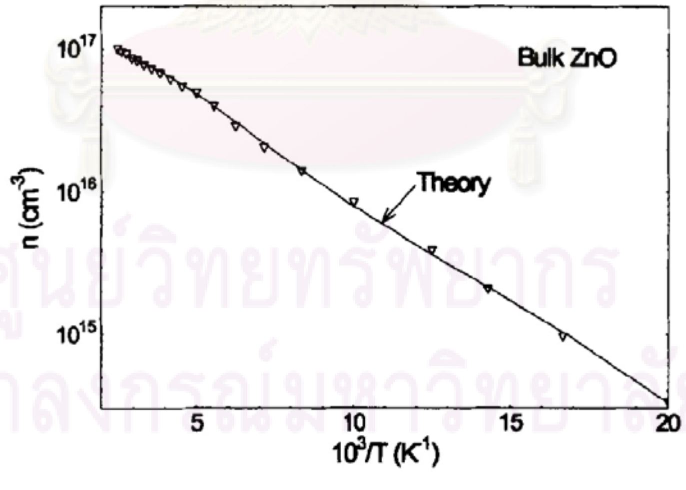

Figure 2.5: Experimental carrier concentration (triangles) and theoretical fit (solid line) as a function of inverse temperature in bulk ZnO [4].

Hall mobility of ZnO relies on scattering mechanisms including (1) optical-mode lattice vibrations, polar potential; (2) acoustic-mode, deformation potential; (3) acoustic-mode, piezoelectric potential; and (4) coulomb scattering from ionized impurities or defects. In addition, these scattering mechanisms depend on (1) relative low-frequency dielectric constant $\varepsilon_0 = 8.12$, relative-high frequency dielectric constant $\varepsilon_\infty = 3.72$ and polar-optical (Debye) temperature, $T_{po} = 837$ K; (2) acoustic-mode deformation potential $E_1 = 15$ eV [4]; (3) piezoelectric coupling $P_\perp = 0.21$ (current is perpendicular to the *c*-axis); and acceptor concentration, $N_A = 2.0 \times 10^{15}$ cm^{-3} [4]. Look *et al.* [4] reported that the ratio of accepter concentration to donor concentration N_A/N_D or compensation ratio of bulk ZnO equals to 0.02.

ZnO is easy to be doped by group-III elements such as Al, Ga, and In into its Zn site and obtain n-type ZnO. In contrast, doping group-V elements into its O site for p-type conductivity is difficult. In addition, the problem also includes non-repeatability, instability, low crystallinity and low transmission of the p-type ZnO films. Thus, p-type ZnO fabrication is very interesting and challenging work done by many research groups and is reviewed in the next sections. The promising candidates group-V elements to achieve p-type ZnO are N, P, and As.

2.2 Phosphorus-doped ZnO films

Heo *et al.* [9] prepared phosphorus doped ZnO film on sapphire substrates by pulsed laser deposition (PLD) technique at 400°C in oxygen pressure of 20 mTorr. Solid phosphorus doped ZnO targets are fabricated using ZnO powder with P_2O_5 doping level of 0 – 5%. Figure 2.6 shows the degradation in ZnO crystallinity with the increment of phosphorus content.

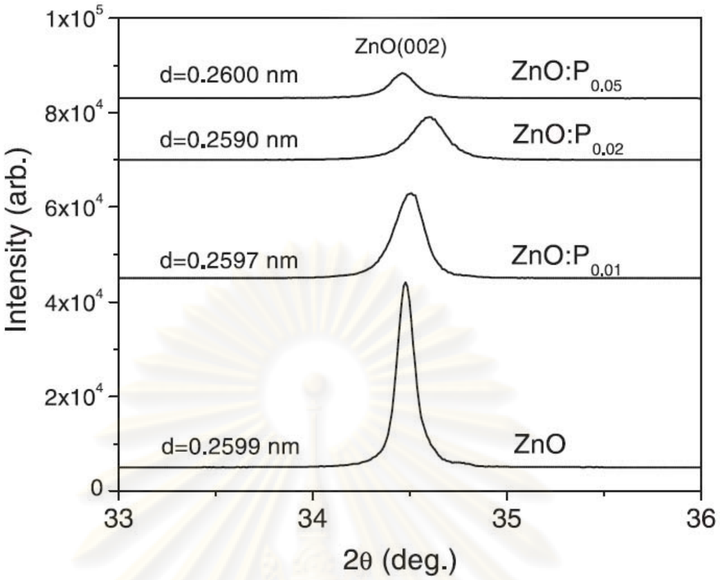

Figure 2.6: X-ray diffraction patterns of the ZnO:P films with various phosphorus contents, indicating a shift of lattice spacing with increasing phosphorus content [9].

The films do not exhibited p-type conductivity. But the films show n-type conductivity with hall mobility of 18 – 20 cm^2/V·s. From Fig. 2.7, the carrier concentration increases with the increment of phosphorus content. The result indicated that donor state could be introduced by substitution of P on the Zn site. P^{+5} and P^{-3} oxidation states were identified by the splitting of binding energy of P 2s peak using x-ray photoelectron spectroscopy (XPS) as shown in Fig. 2.8. This refers to possible substitution of P on the O site, but not enough to compete against P substitution on Zn site.

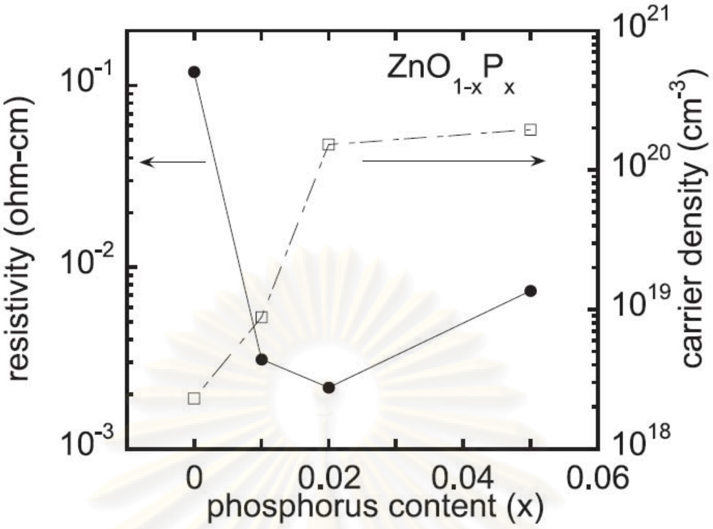

Figure 2.7: Resistivity and carrier concentration for as-grown ZnO:P films with various phosphorus content [9].

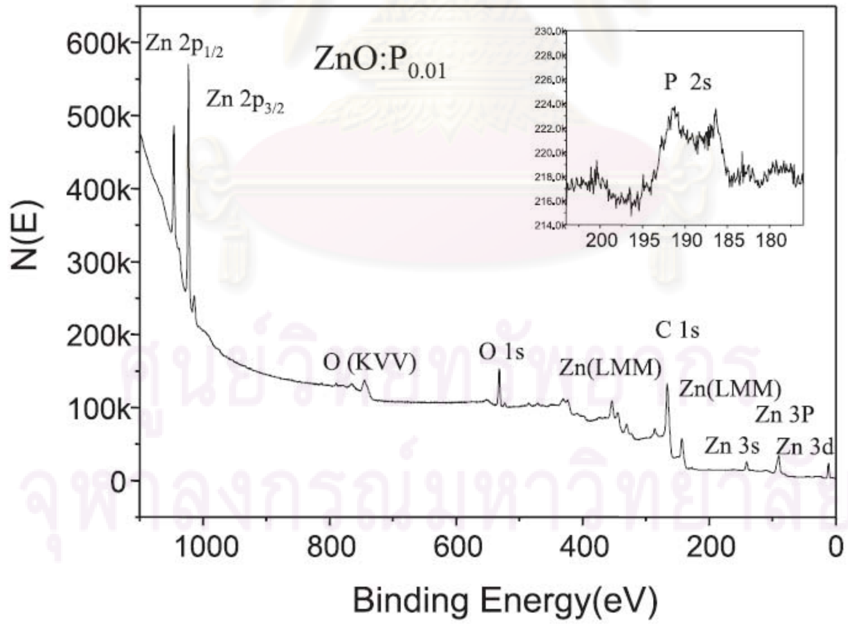

Figure 2.8: X-ray photoelectron spectrum for as-grown ZnO:P$_{0.01}$ film [9].

Xiu *et al.* [7, 8] prepared phosphorus-doped ZnO films on sapphire substrates by molecular beam epitaxy (MBE) using Zn and GaP effusion cells with the oxygen flow rate of 6 SCCM (SCCM denotes cubic centimeter per minute at STP). After the growth, the as-grown films were annealed under vacuum at 800°C for 20 minutes to activate phosphorus dopants. Growth conditions and electrical properties at room temperature (RT) of the films are summarized in Table 2.1:

Table 2.1: Growth conditions and RT electrical properties of phosphorus-doped ZnO films [8].

Sample	Zn cell temperature (°C)	GaP cell temperature (°C)	Thickness (μm)	Conduction type	Carrier concentration (cm^{-3})	Mobility (cm^2/V s)
a	320	710	0.29	*n*	2.0×10^{19}	31.3
b	340	710	0.53	Ambiguous	N/A	N/A
c	350	710	0.40	*p*	1.2×10^{18}	4.2
d	360	710	0.55	Ambiguous	N/A	N/A
e	370	710	0.62	*n*	2.3×10^{18}	45.2
f	350	680	0.40	*n*	7.8×10^{17}	2.4
g	350	750	0.74	*p*	6.0×10^{18}	1.5

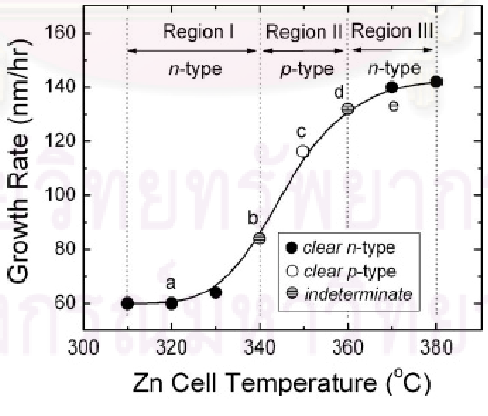

Figure 2.9: Phosphorus-doped ZnO growth rate as a function of Zn cell temperature. Three regions were identified: Region I, oxygen-extremely-rich region (n-type); region II, oxygen-rich region (p-type); and region III, stoichiometric and Zn rich region (n-type) [8].

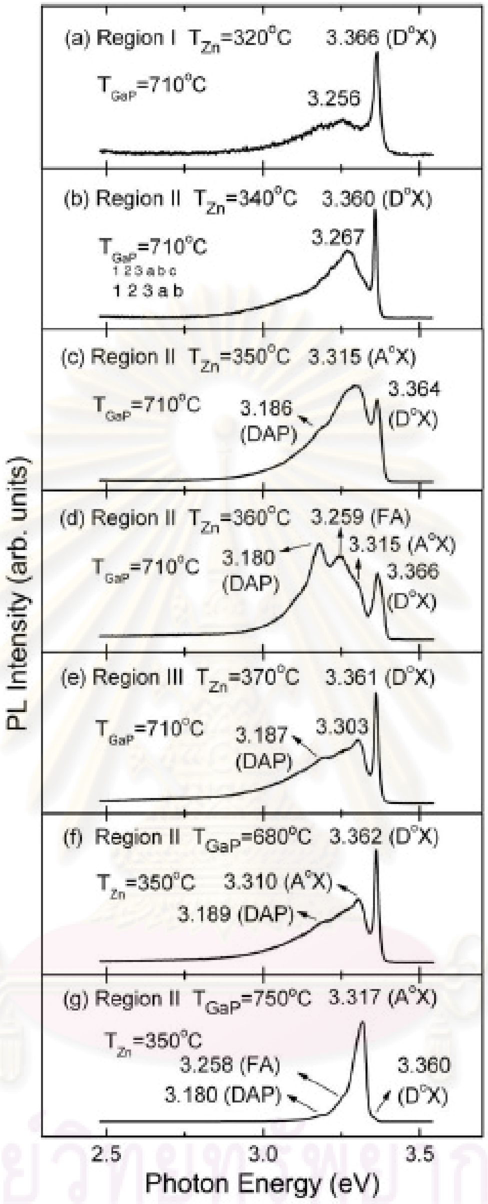

Figure 2.10: PL spectra at 8.5 K of phosphorus-doped ZnO films [8].

The ideas to control p-type conductivity are the temperatures of Zn effusion cell and GaP effusion cell. Figure 2.9 shows a narrow window to obtain p-type ZnO:P at Zn cell temperature of 350^{o}C. Low temperature (8.5 K) photoluminescence was used to identify states in band gaps of the films. Donor-bound excitons (D^0X), acceptor-bound excitons (A^0X), free electron to acceptor (FA), and donor-acceptor pair (DAP) transition are identified. From Fig. 2.10, dominant A^0X peak was observed for sample g with high p-type conductivity. The PL spectra show the existence of competitions between D^0X and A^0X for the ZnO:P flms.

Lim *et al.* [10] prepared phosphorus-doped ZnO multi-layer thin film as shown in Fig. 2.11 on sapphire substrates by pulse laser deposition (PLD). The phosphorus doped ZnO (ZnO:P) layer was encapsulated by ZnO top layer. In order to activate carriers, the as-grown films were annealed under 400^{o}C for 40 minutes. All of the films prepared at various oxygen partial pressures exhibited n-type conductivity. There electrical properties are illustrated as Fig. 2.12. Due to a large number of oxygen vacancies, the films exhibited n-type conductivity. The resistivity increases with the increment of oxygen partial pressure corresponding to the decrement of oxygen vacancies.

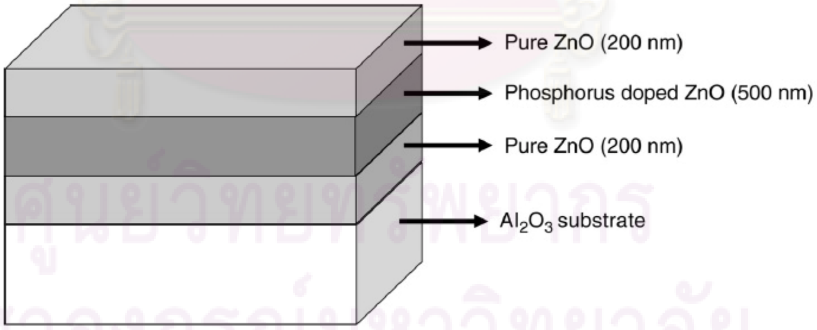

Figure 2.11: A schematic of ZnO/ZnO:P/ZnO thin films [10].

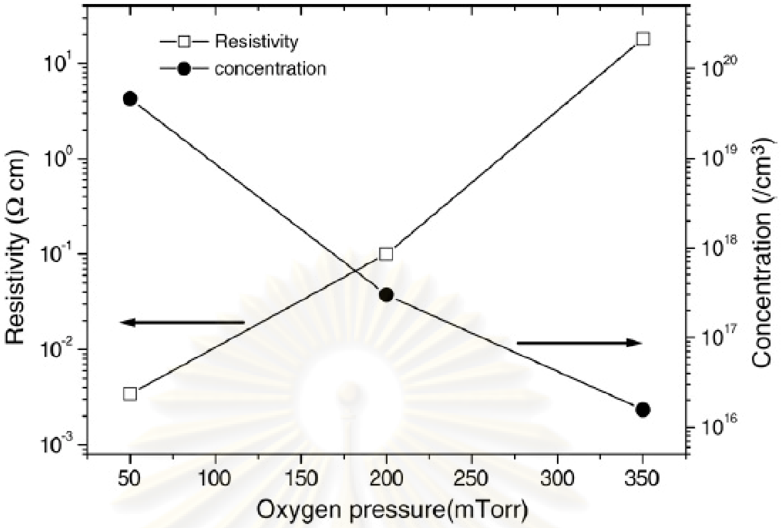

Figure 2.12: A plot of electron concentration and resistivity versus oxygen pressure as a result of Hall measurement of ZnO/ZnO:P/ZnO multi-layer thin films [10].

2.3 Arsenic-doped ZnO films

Ryu *et al.* [12] prepared arsenic-doped ZnO (ZnO:As) films on (001) GaAs substrates by pulse laser deposition (PLD). GaAs substrates were selected as a p-type dopant source because As atoms could diffuse from the substrate into the ZnO film. ZnO:As films grown with substrate temperatures of 400^{o}C and 450^{o}C exhibited p-type conductivity with hole concentrations of 10^{18} – 10^{21} cm^{-3}, mobilities of 0.1 – 50 cm^{2}/V·s, and resisitivity of 10 – 10^{-5} Ω·cm. In contrast, ZnO:As films grown with substrate temperature of 300^{o}C and 350^{o}C exhibited n-type conductivity with electron concentrations of 10^{15} – 10^{16} cm^{-3}, mobilities of 1 – 50 cm^{2}/V·s, and resistivities of 10 – 10^{3} Ω·cm. Large uncertainties of these values may be a result of the contributions from the interference layers between the ZnO film and GaAs substrate which are still unclear.

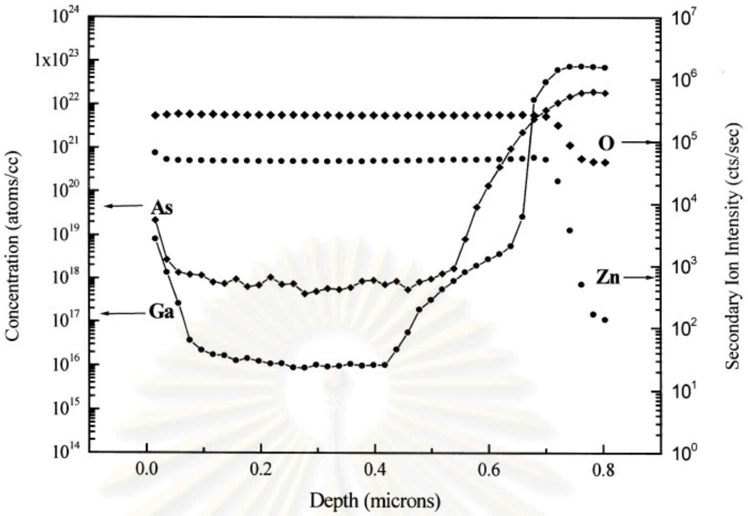

Figure 2.13: Dynamic SIMS results for a p-type ZnO film doped with As, Zn, and O intensities, in secondary ion intensity, are plotted for reference [12].

The diffusion of As atoms for the ZnO:As film prepared at 400°C was examined by secondary ion mass spectroscopy (SIMS) as shown in Fig. 2.13. The depth profile of each element was measured from surface of the film and the As atom concentration was in the order of 10^{17} to 10^{18} cm^{-3}.

2.4 Antimony-doped ZnO films

Wang *et al.* [18] prepared Sb-doped ZnO (ZnO:Sb) on (100) Si substrate by radio frequency (RF) magnetron sputtering technique. The as-grown films exhibited n-type conductivity with resistivities of 1 – 10 Ω·cm. The as-grown films were annealed at various temperatures in nitrogen pressure for one hour. After annealing at 400°C, the ZnO:Sb film exhibited higher resistance. Furthermore, the film annealed at 800°C became semi-insulating with a resistivity of 10^4 Ω·cm as shown in Fig. 2.14.

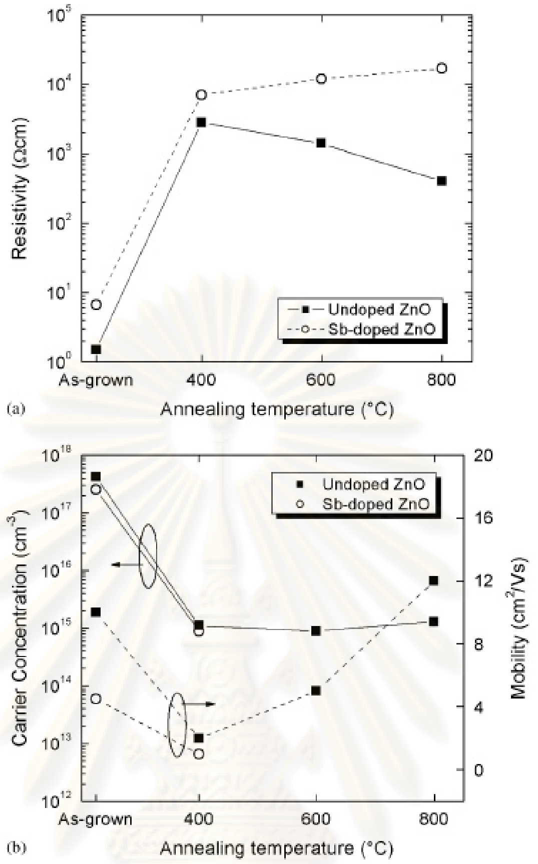

Figure 2.14: Annealing temperature dependence of (a) resistivity and (b) carrier concentration and mobility of Sb-doped and undoped ZnO thin films [18].

2.5 Nitrogen-doped ZnO films

Li *et al.* [6] prepared nitrogen-doped ZnO (ZnO:N) thin films on Corning 1737 glass by low-pressure metal-organic chemical vapor deposition (MOCVD) technique using diethylzinc (DEZ) and nitric oxide (NO) precursors. The optical transmittances of undoped ZnO and ZnO:N films are illustrated as Fig. 2.15. The ZnO:N film exhibits yellow shading corresponding to the lower transmittance in the region of 400 – 600 nm because of the increased absorption near the band edge. Nitrogen concentration as high as 2.60 × 10^{21} cm^{-3} were achieved. The p-type conductivity was achieved in the growth temperature of about 400°C. The electrical properties are shown in Table 2.2.

The best carrier concentration was 8.36×10^{17} cm^{-3} with mobility of 4.55 $cm^2/V \cdot s$. Carbon and hydrogen impurities from MOCVD process lead to several defect complexes such as CH_x, NH_x, and NC_x which incorporate into the ZnO crystalline and passivate nitrogen acceptor.

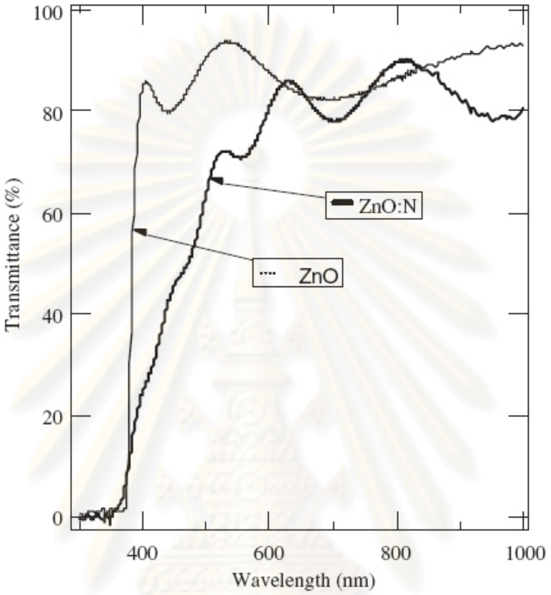

Figure 2.15: Optical transmittances of ZnO and ZnO:N films. Both films were deposited on glass substrate at 400^{o}C [6].

Table 2.2: Electrical properties of ZnO films deposited on glass substrate at deposition temperature of 400^{o}C [6].

Doping condition	Sample ID	CC (cm^{-3})	μ ($cm^2/V\,s$)	ρ (Ωcm)	Conductivity type
Undoped	L3353.2	-8.42×10^{18}	3.2	0.235	n
	L4084.1	-8.38×10^{16}	6.3	11.8	n
N-doped	L3357.2	2.90×10^{14}	579	37.2	p
	L4098.2[a]	8.36×10^{17}	4.55	1.64	p

(For Hall measurement, the error bars are very small for carrier concentrations higher than 10^{15} cm^{-3} and mobilities greater than 1 $cm^2/V\,s$. In this table, the sample L3367.2 has a large error bar. Carrier concentration data was measured in the region between 2.9×10^{14} and 4.8×10^{14} cm^{-3}.

[a] Sapphire substrate.

Kerr *et al.* [23] used Raman spectroscopy to analyze p-type ZnO:N films prepared at 400^{o}C by MOCVD technique. Raman features are summarized in Table 2.3. The formation of nitrogen related defect complex due to N incorporation in the ZnO film is detected from the Raman peak broadening at 570 cm^{-1} including the addition peaks at 280, 510 and 642 cm^{-1} as shown in Fig. 2.16.

Table 2.3: Summary of Raman features [23].

Sample I.D.	F_{NO} (sccm)	T_g (°C)	Film thickness (µm)	Raman features (ZnO) (cm^{-1})	Raman features (Nitroge-related) (cm^{-1})	Raman features (Carbon-related) (cm^{-1})	Raman features (unindentified) (cm^{-1})
Pure ZnO powder				335, 390, 433, 535, 589, 669, 995	None	1134	
Undoped ZnO (with varied T_g)	∅	**300**	0.21		None	None	
	∅	**400**	0.28		None	None	
	∅	**500**	0.34		None	None	
	∅	**550**	1.21	433	None	1134	
Nitrogen doped ZnO (with varied NO gas flow)	**40**	400	0.54		280, 510, 570, 642	1500 broad	773
	36	400	0.45		280, 510, 570, 642	1500 broad	773 (weak)
	30	400	0.44		280, 510, 570, 642	1500 broad	773 (weak)
Nitrogen doped ZnO (with varied T_g)	20	**400**	0.40		280, 510, 570, 642	1500 broad	773 (weak)
	36	**500**	0.39			1361 and 1564	
	36	**300**	0.10		570	None	

Data in bold highlights the changing parameters.

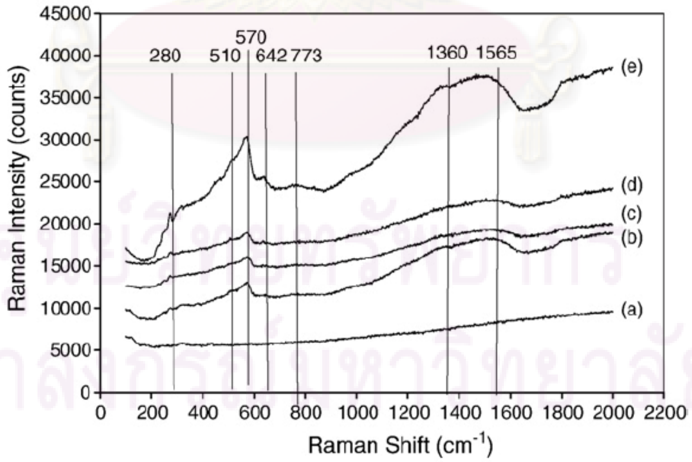

Figure 2.16: The effect of NO gas flow rate on the Raman spectra of ZnO:N films fabricated at 400^{o}C with (a) F_{NO} = 0 sccm, (b) F_{NO} = 20 sccm, (c) F_{NO} = 30 sccm, (d) F_{NO} = 36 sccm, and (e) F_{NO} = 40 sccm [23].

Tu *et al.* [14] prepared ZnO:N films on Corning glass by RF magnetron sputtering under the mixture of Ar and N_2 gases at room temperature. The target was made of pure ZnO (99.99%) and the sputtering power was 200 W. Flow rate of Ar was kept constant at 20 SCCM and the flow rate of N_2 was varied from 6 to 15 sccm. The electrical properties are shown in Table 2.4. The best p-type carrier concentration was 2.11×10^{19} cm^{-3} with low mobility of 0.092 $cm^2/V{\cdot}cm$. The Raman feature peaks appeared at 275, 436, 508, 581, 640, and 854 cm^{-1} as shown in Fig. 2.17. Zinc nitride (Zn_3N_2) phase also be observed in the XRD spectra as shown in Fig. 2.18 of their ZnO:N films.

Table 2.4: Hall measurement of ZnO:N films prepared by RF magnetron sputtering with various ratios of N_2/Ar sputtering gas [14].

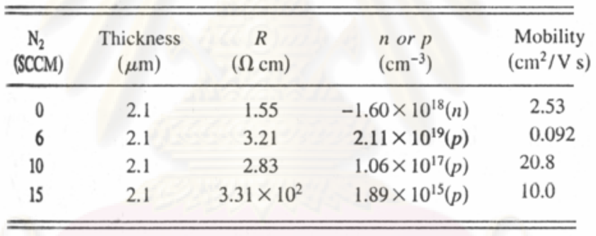

N_2 (SCCM)	Thickness (μm)	R (Ω cm)	n or p (cm^{-3})	Mobility ($cm^2/V\,s$)
0	2.1	1.55	$-1.60\times10^{18}(n)$	2.53
6	2.1	3.21	$2.11\times10^{19}(p)$	0.092
10	2.1	2.83	$1.06\times10^{17}(p)$	20.8
15	2.1	3.31×10^{2}	$1.89\times10^{15}(p)$	10.0

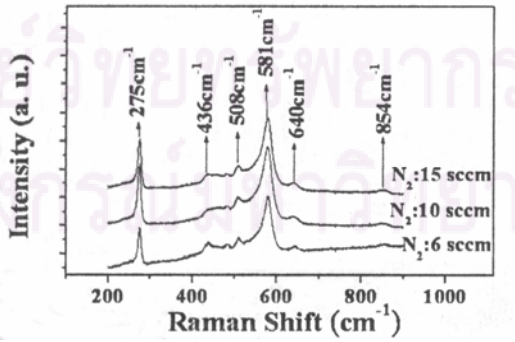

Figure 2.17: The micro Raman spectrum of ZnO:N films produced by RF magnetron sputtering system with various N_2 flow rates of sputtering gas [14].

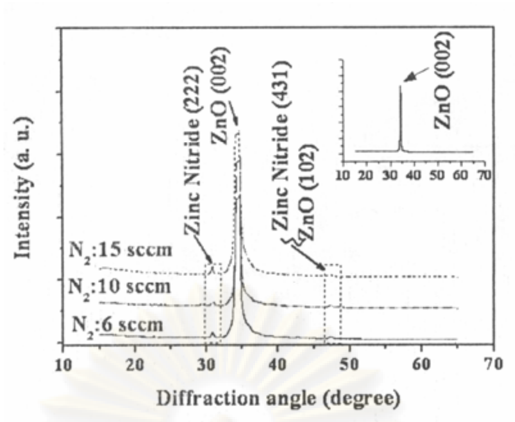

Figure 2.18: X-ray diffraction (XRD) pattern of ZnO:N films. The inset is an XRD pattern of undoped ZnO film [14].

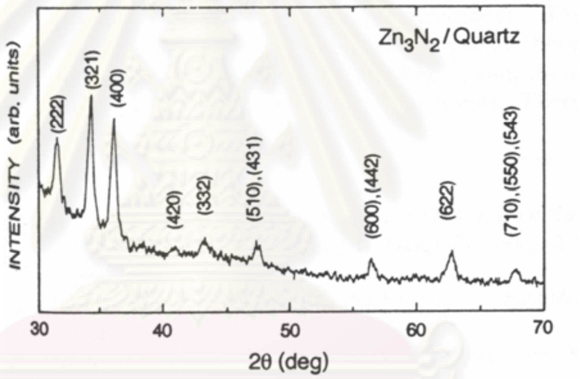

Figure 2.19: Typical x-ray diffraction pattern of the Zn_3N_2 film [28].

Table 2.5: Summary of electrical properties of samples annealed at different temperature in oxygen ambient [31].

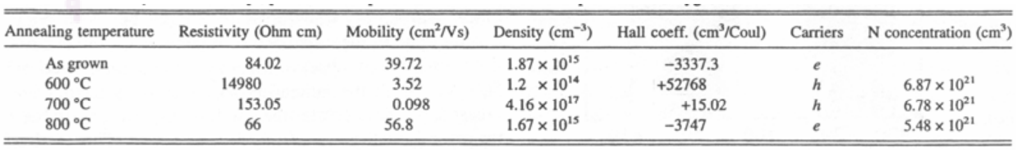

Annealing temperature	Resistivity (Ohm cm)	Mobility (cm^2/Vs)	Density (cm^{-3})	Hall coeff. (cm^3/Coul)	Carriers	N concentration (cm^3)
As grown	84.02	39.72	1.87×10^{15}	−3337.3	*e*	
600 °C	14980	3.52	1.2×10^{14}	+52768	*h*	6.87×10^{21}
700 °C	153.05	0.098	4.16×10^{17}	+15.02	*h*	6.78×10^{21}
800 °C	66	56.8	1.67×10^{15}	−3747	*e*	5.48×10^{21}

Zinc nitride (Zn_3N_2) is black or grey in color and has the anti-scandium oxide structure (Sc_2O_3) structure. This structure is also called anti-bixbyite structure (cubic) with the lattice parameter *a* of 9.77687 Å [27]. Polycrystalline zinc nitride film is an n-type semiconductor. Its band gap is quite varied such as direct band gap of 3.2 eV [28] and indirect band gap of 2.11 eV [29]. The space group of anti-bixbyite structure is *Ia3*. The atoms which occupy sites in anti-bixbyite structure [30] are nitrogen (anion) at sites *8d* and *24d* and zinc (cation) at site *48e*. From the work of Kuriyama *et al.* [29], the Zn_3N_2 films were prepared by direct reaction between NH_3 and zinc (99.999% pure). Zinc film on a quartz substrate was obtained from evaporation and Zn_3N_2 film was obtained by annealing the Zn film in NH_3 flow for 4 hours. Typical x-ray diffraction pattern of Zn_3N_2 film is shown as Fig. 2.19.

Li *et al.* [31] prepared p-type ZnO thin films by thermal oxidization of Zn_3N_2 thin films. The Zn_3N_2 films were grown on fused silica substrates by using plasma-enhanced chemical vapor deposition from a mixture of $Zn(C_2H_5)_2$ and NH_3 gases. The film was annealed at 500^oC or higher temperature in O_2 atmosphere for one hour, the Zn_3N_2 transform to be ZnO. The electrical properties of the films are summarized in Table 2.5. The best p-type carrier concentration of 4.16×10^{17} cm^{-3} with mobility of 0.098 cm^2/V·s was obtained at annealing temperature of 700^oC. Due to thermal energy, oxygen atoms can diffuse into the film and N atoms are replaced by O atoms. As a result, the crystal structure of Zn_3N_2 changed to be ZnO structure leading to the ZnO:N films.

Yao *et al.* [15] prepared ZnO:N film on quartz at 237^oC by RF magnetron sputtering of a ZnO target under N_2 gas. The as-grown ZnO:N exhibited very high resistivity. After anneal at 587^oC for one hour under 10^{-4} Pa, the resistivity was 456 Ω·cm, mobility was 0.01 cm^2/V·s. Their p-type ZnO:N films are not stable in the dark and transform into n-type gradually. Furthermore, they can be reverted to meta-stable p-type by irradiation of sunlight for a few minutes.

Among group-V elements, the two smallest elements are N and P which have possibility in occupying O site of ZnO. For phosphorus doping, the p-type ZnO with p-type carrier concentration in the order of 10^{18} cm^{-3} achieved from MBE technique with annealing up to 800^{o}C [7, 8]. But, disadvantage of MBE system is the limit of substrate size that is not suitable for large area application. Occupying of P into Zn site of ZnO leads to the failure of fabrication of p-type ZnO:P [9]. P-type nitrogen doped ZnO can be obtained from MOCVD process [23] that can be applied to large scale fabrication. But the disadvantage of the process is the carbon and hydrogen impurities leading to the passivation of nitrogen acceptor or low p-type carrier concentration in the order of 10^{17} cm^{-3}. Sputtering which can be applied to large area is also interested. Sputtering with ZnO ceramic target under the mixture of N_2 and Ar gases provided the maximum p-type carrier concentration of 10^{19} cm^{-3} with low mobility of 0.092 cm^{2}/V·s [14].

CHAPTER III

THEORETICAL BACKGROUND OF SPUTTERING AND CHARACTERIZATION

The chapter begins with a brief description of sputtering and analysis techniques for physical properties of the films.

3.1 Sputtering

Sputtering is an ejection process of target atoms caused by a series of collisions between atoms of the target. An ionized atom of plasma impacts the target surface and implants into the target material leading to the series of collisions. Sputtering which is well known in many material industries or research laboratories is one of plasma processes.

3.1.1 Basics of plasma

In a simple picture, plasma is defined as an ionized gas with equal numbers of positive and negative charges. It consists of charged particles (electrons and positive ions) and neutral atoms or molecules of gas. The concentrations of negative and positive charges are the same, $n_e = n_i$. The ratio of electron concentration to the total concentration is defined as the ionized rate [32].

$$\text{Ionized rate} = \frac{n_e}{n_e + n_n}, \tag{3.1}$$

where, n_e = electron concentration, n_i = ion concentration, and n_n = neutral concentration. Ionization rate which relied on inelastic collision depends on electron energy and type of gas used in the system. The three most important mechanisms in plasma are the inelastic collisions between electron and neutral atom such as ionized collision (which generates and maintains plasma), excitation-relaxation, and dissociation collision. The collision which impacting electron transfers enough energy to the orbital electron of the neutral atom to be free from its confinement is called ionization collision (as shown in Fig. 3.1):

$$e^- + A \rightarrow A^+ + 2e^- \tag{3.2}$$

If the orbital electron receives not enough energy, it is excited to the higher energy level. This leads to the excitation process (as shown in Fig. 3.2):

$$e^- + A \rightarrow A^* + e^- \tag{3.3}$$

Due to the instability of the high level, the orbital electron will return to the original state with the emission of electromagnetic wave with a frequency related to a type of gas. This is call relaxation process (as shown in Fig. 3.3):

$$A^* \rightarrow A + h\nu \tag{3.4}$$

Sometime, the chemical bonds of a molecule can be broken by high energy. This process is called dissociation (as shown in Fig. 3.4):

$$e^- + CD \rightarrow C + D + e^- , \tag{3.5}$$

where, e^- is electron, A is neutral atom, A^+ is positive ion, A^* is excited state of A, $h\nu$ is the energy of a photon, h is Plank's constant, and ν is the frequency of the electromagnetic wave, CD is a molecule, and C and D are free radicals.

The mean free path (MFP) or λ is defined as the average distance for a particle that can travel before it collides with another particle. It can be expressed as [32]:

$$\lambda = \frac{1}{\sqrt{2}n\sigma} , \tag{3.6}$$

where n is the particle density, and σ is the collision cross section.

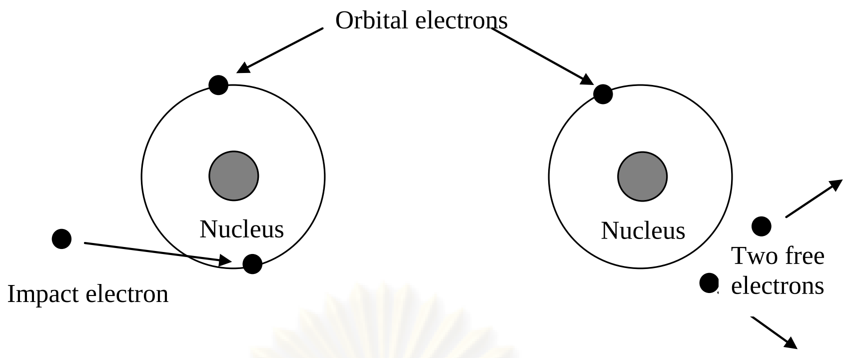

(a) (b)

Figure 3.1: Ionization collisions (a) before and (b) after electron impact [32].

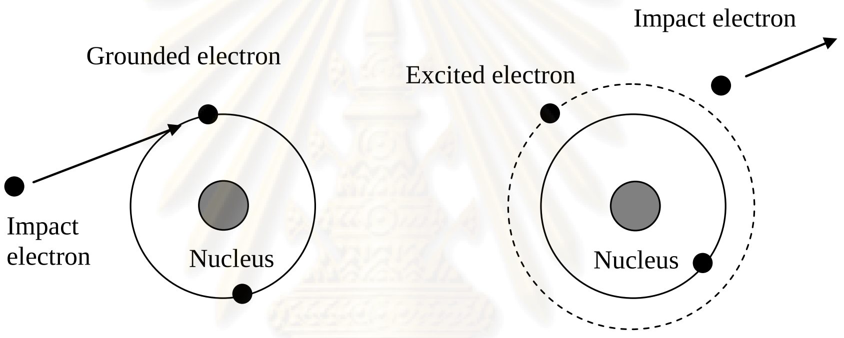

(a) (b)

Figure 3.2: (a) Before and (b) after excitation collision [32].

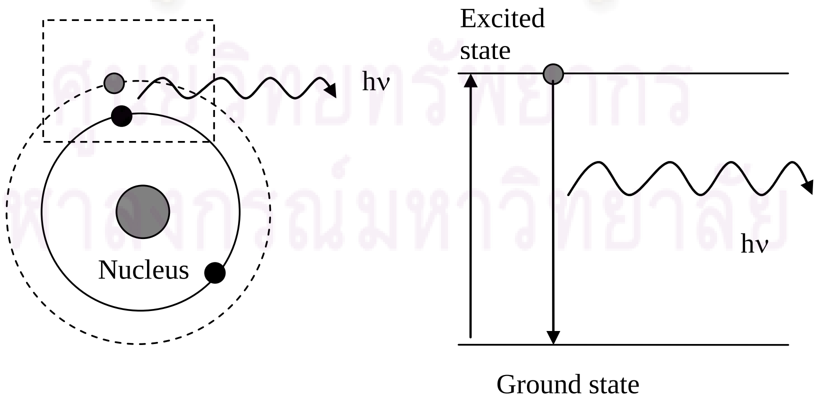

Figure 3.3: Relaxation process [32].

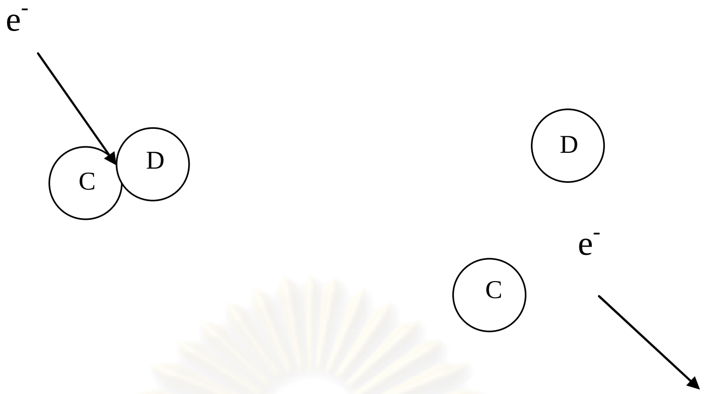

Figure 3.4: Dissociation process [32].

Higher particle density (or higher pressure as shown in Fig. 3.5(a)) corresponds to high collision or short MFP. In contrast, lower particle density (or lower pressure as shown in Fig. 3.5(b)) corresponds to low collision or long MFP. MFP depends on pressure and a kind of gas (different cross section). The spiral motions of electrons obtained from the applied magnetic field as shown in Fig. 3.6 also increase the probability of collisions. From Boltzmann distribution as shown in Fig. 3.7, most of electron has energy about 2 - 3 eV, but a small fraction of electron has enough energy of about 15 eV for ionization.

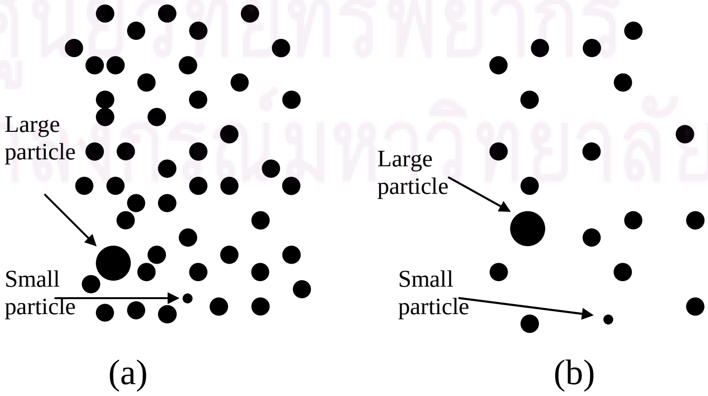

Figure 3.5: (a) High pressure short MFP and (b) low pressure long MFP [32].

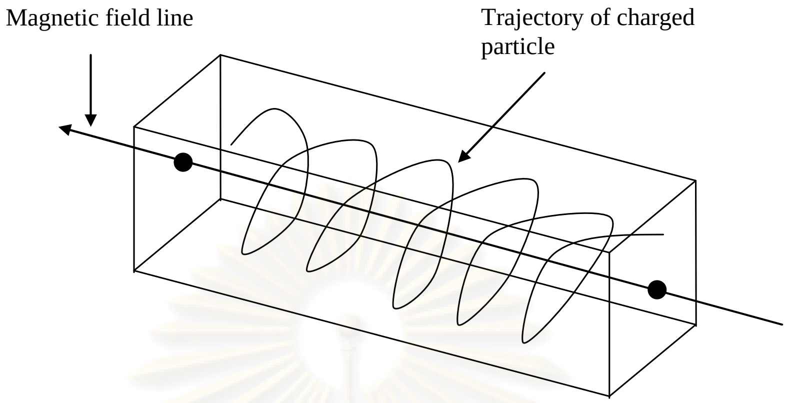

Figure 3.6: Gyro-motion of a charged particle in a magnetic field [32].

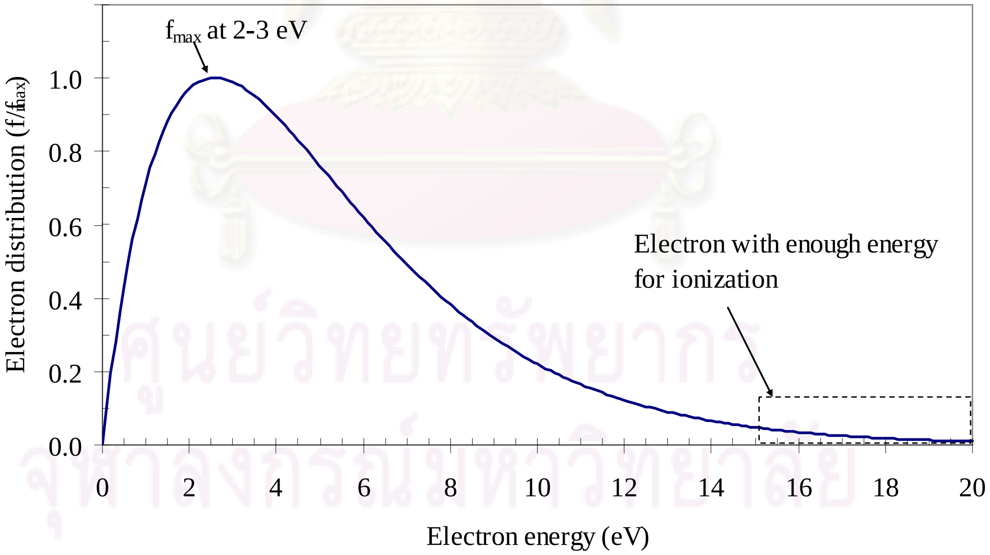

Figure 3.7: Electron energy distribution.

3.1.2 Sputtering process

Figure 3.8 illustrates the simple diagram of direct current (DC) sputtering system. The system consists of a vacuum chamber, a vacuum pump, and electrodes with a target on the negative side. The sputtering gas such as Ar and N_2 is injected into the chamber at suitable pressure i.e. 10^{-3} – 10^{-2} mbar. When the voltage is applied between the electrodes, the positive ions are obtained from ionization collision between the accelerated electrons and the sputtering gas. After that, the positive ions are accelerated by electric field and impact or collide to the target surface at the negative side. The incident ions implant into the target and transfer momentum to the target atoms leading to a series of collisions between atoms of the target and leading to the knock-out of sputtering atoms from the target surface. Finally, the film is deposited on a substrate commonly placing in the opposite position of the target. In addition, radio frequency (RF) sputtering can also be employed to deposit dielectric thin film by sputter the non-conducting target. In order to increase sputtering rate, the magnetic filed is also applied to the sputtering system.

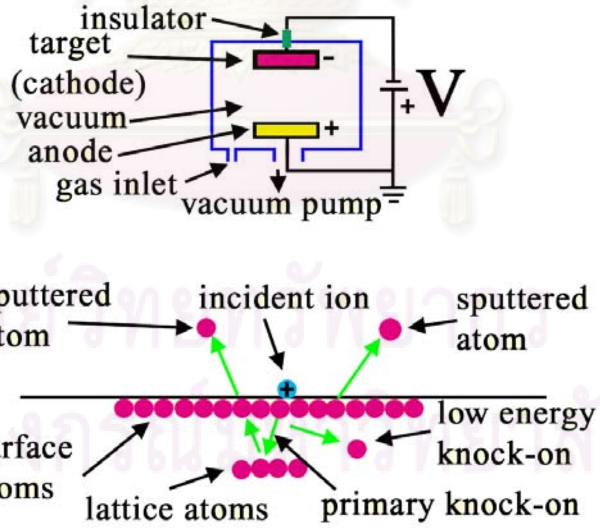

Figure 3.8: Simple diagram of DC sputtering system.

3.2 Electrical Property

Electrical property of a semiconductor is considered as a carrier transport property. The current density $\vec{J}$ passing through a specimen of conductor is defined as

$$\vec{J} = nq\vec{v} = nq\mu\vec{E}\,, \tag{3.7}$$

where, n is the carrier concentration, q is the charge of carrier and $\vec{v}$ is the drift velocity of the carrier, μ is the mobility of the carrier and $\vec{E}$ is the electric field.

From Ohm's law, the current density is directly proportional to the electric field ($\vec{J} = \frac{1}{\rho}\vec{E}$). Then, the resistivity ρ can be written as

$$\rho = \frac{1}{\sigma} = \frac{1}{nq\mu} \tag{3.8}$$

3.2.1 The linear four-point probe

Due to its convenience, the linear four-point probe is widely used in semiconductor industries for measuring resistivity of materials [33]. Consider Fig. 3.9, the probes are placed in line with current I passing through the outer two probes. The potential V developed across the inner two probes is measured. For probes placing on a semi-infinite specimen, the resistivity ρ is [33]:

$$\rho = \frac{2\pi(V/I)}{[1/S_1 + 1/S_3 - 1/(S_1+S_2) - 1/(S_2+S_3)]}\,, \tag{3.9}$$

where S_1, S_2, and S_3 are the probe spacing. If the probe spacings are all equals, then Eq. 3.9 reduces to [33]:

$$\rho = 2\pi S\frac{V}{I} \tag{3.10}$$

In the case of a sample cannot be considered as infinite, the corrections summarized in Table 3.1 are required.

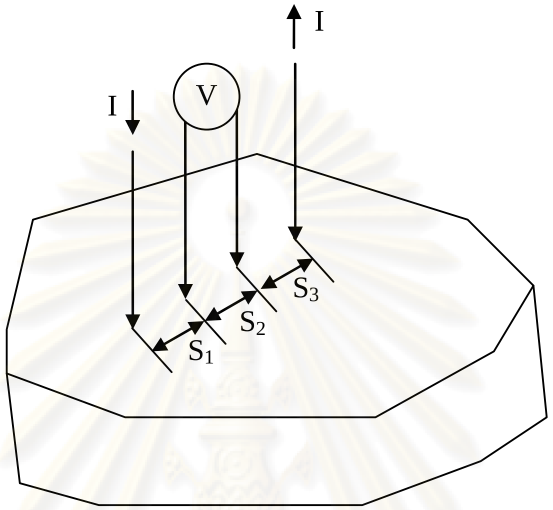

Figure 3.9: Linear four-point probe.

Table 3.1: Linear four-point probe corrections [33].

Configuration	Corrections
Thick sample, boundaries > $10S$ from probe	No correction required, $\rho = 2\pi S(V/I)$
Thick sample, near edge	For non-conducting boundaries the meter read as much as 100% high
Thin sample, with thickness $d < 0.1S$, and boundaries > $20S$ from probes	$\rho = 4.53d(V/I)$, $R_s = 4.53(V/I)$

3.2.2 The van de Pauw method

Van de Pauw method is also four-point probe measurement. The contacting points are placed on the periphery of the sample as shown in Fig. 3.10. Its resistivity is calculated from [33]:

$$\rho = \frac{\pi d}{2\ln 2}(R_{AB,CD} + R_{BC,DA})\, f\left(\frac{R_{AB,CD}}{R_{BC,DA}}\right), \tag{3.11}$$

where $f\left(\frac{R_{AB,CD}}{R_{BC,DA}}\right)$ is correction factor as shown in Fig. 3.11, and d is the thickness of the sample. $R_{AB,CD}$ is the potential difference between the contacts C and D per unit current through the contacts A and B, and $R_{BC,DA}$ is the potential difference between the contacts D and A per unit current through the contacts B and C. This method requires contacts on the periphery with very small contacts. A sample must be uniform with no isolated holes in the interior of the sample.

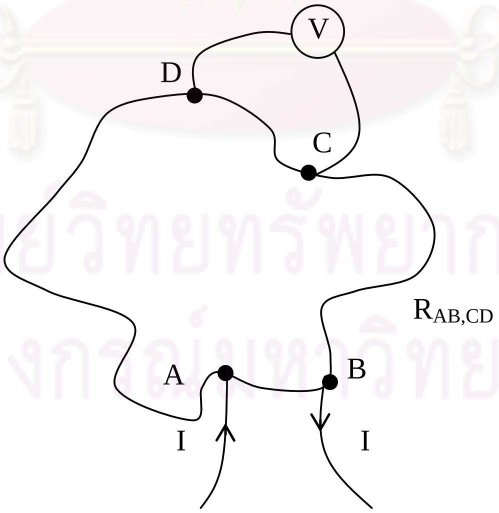

Figure 3.10: A sample of arbitrary shape used with the van der Pauw method.

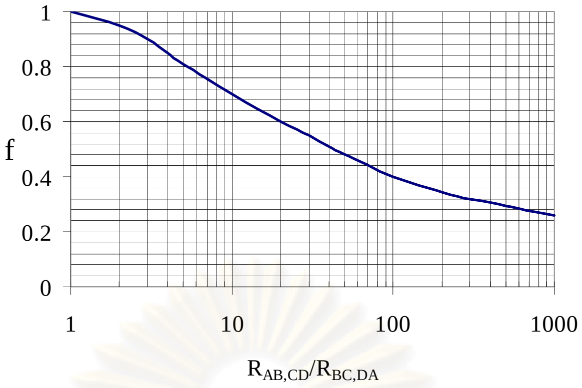

Figure 3.11: Correction factor as a function of $\frac{R_{AB,CD}}{R_{BC,DA}}$.

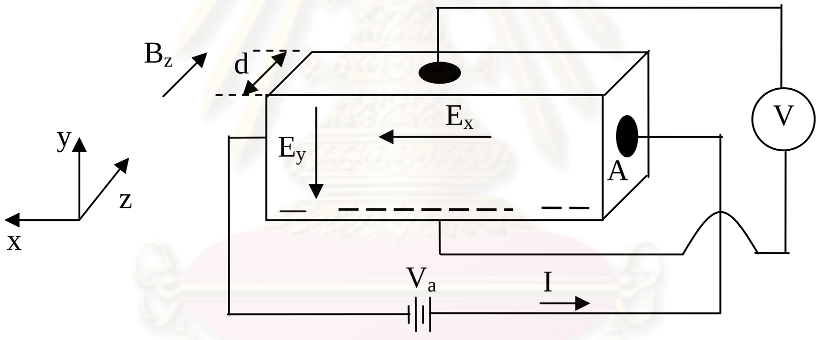

Figure 3.12: Configuration for Hall effect measurement on a rectangular-shaped n-type sample.

3.2.3 The Hall effect

Consider an experimental configuration for a rectangular shaped sample shown in Fig. 3.12. The magnetic force $\vec{F}$ acting on a carrier with charge q is defined by

$$\vec{F} = q\vec{v} \times \vec{B}\,, \tag{3.12}$$

where $\vec{v}$ is the velocity of the carriers and $\vec{B}$ is the applied magnetic field. Carriers (or electrons) are accumulated on the lower side of the sample. The magnetic force in the y-direction driving a carrier is

$$F_y = qv_x B_z = q\mu_n E_x B_z \, , \tag{3.13}$$

where μ_n is the mobility of the electron. The electric field E_y in the *y*-direction is created by the effect of accumulated electrons. The Hall field E_H is defined as:

$$E_y = E_H = \frac{V_H}{d} \, , \tag{3.14}$$

where d is the film thickness and V_H is the Hall voltage which is measured at equilibrium such that the force resulting from the Hall field cancels the effect of the magnetic force.

$$qE_y = q\mu_n E_x B_z \tag{3.15}$$

Then, the mobility can be calculated from the measured Hall field,

$$\mu_n = \frac{E_y}{E_x B_z} \tag{3.16}$$

In experiments, external controlled parameters are J_x and B_z. The Hall coefficient R_H is defined as

$$R_H = \frac{E_y}{J_x B_z} = \frac{1}{nq} \tag{3.17}$$

When a sample which is in arbitrary shape as discussed in van der Pauw measurement are placed under a magnetic field, mobility measurement can be obtained by feeding a current from the contact A to C. The voltage is measured across the contact B and D. The voltage is usually measured both with forward magnetic field ($+\vec{B}$) and reverse magnetic field ($-\vec{B}$). Van der Pauw shows that the Hall coefficient is given by [34]

$$R_H = \frac{d}{2B} \Delta R_{AC,BD}, \tag{3.18}$$

where $\Delta R_{AC,BD}$ specifies the change in resistance with the forward and reverse magnetic fields. Therefore, the Hall mobility can be calculated from

$$\mu = \frac{R_H}{\rho} = \frac{d}{2B\rho} \Delta R_{AC,BD}. \tag{3.19}$$

Then, carrier concentration can be calculated from Eq. 3.8.

3.3 Optical Properties

3.3.1 Interference and film thickness calculation

When light transmits through a film as shown in Fig. 3.13, the path difference of two beams is the cause of interference pattern which relates to refractive index and the film thickness [35]. The film thickness can be calculated from the interference fringes of the optical transmission as shown in Fig. 3.14 of the thin film. The interference fringes correspond to the condition:

$$2nd = m\lambda, \tag{3.20}$$

where $m = 0,1,2,...$ for constructive interferences and $m = \frac{1}{2}, \frac{3}{2},...$ for destructive interferences. Consider two maxima ($T_{\max}$) or two minima ($T_{\min}$) of the transmission patterns according to wavelengths λ_1 and λ_2, the number of oscillations (M) between the two extrema is

$$M = m_1 - m_2. \tag{3.21}$$

where m_1 and m_2 are the numbers of maxima or minima.

Or

$$M = 2nd\left|\frac{1}{\lambda_1} - \frac{1}{\lambda_2}\right| = \frac{2nd}{\lambda_1\lambda_2}\left|\lambda_2 - \lambda_1\right|. \tag{3.22}$$

Therefore, the film thickness (d) can be calculated from

$$d = \frac{M\lambda_1\lambda_2}{2n\left|\lambda_2 - \lambda_1\right|} \tag{3.23}$$

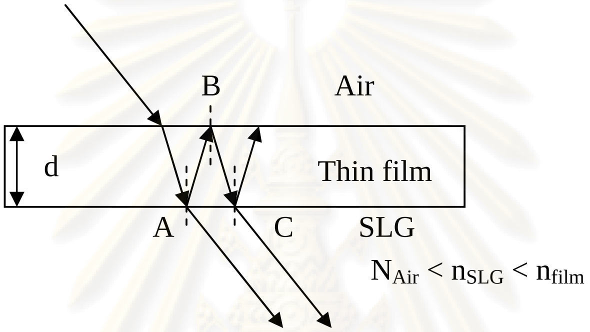

Figure 3.13: Interference in light beam transmitted from a thin film is due to a combination of beam 1 and beam 2.

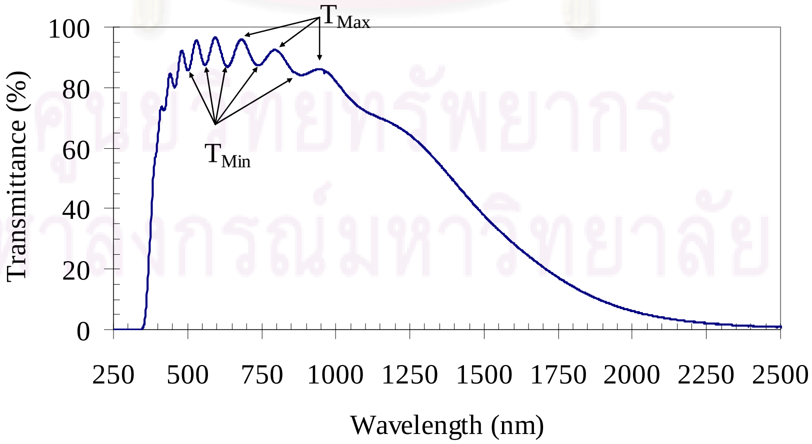

Figure 3.14: Optical transmittant spectrum of the ZnO thin film as a function of wavelength and the result shows the oscillations due to interference in thin film.

3.3.2 Optical absorption properties

When light travels in the media (or films), its intensity will decrease as:

$$I = I_0 e^{-\alpha x} \tag{3.24}$$

where I_0 is the initial intensity of light, x is the distance from surface, and α is the absorption coefficient. In addition, absorption coefficient is related to the imaginary part κ of the refractive index:

$$\alpha = \frac{4\pi\kappa}{\lambda}, \tag{3.25}$$

where λ is the wavelength of light. Absorption property relates to the dynamic behaviors of the electrons and ions in media under the influence of electromagnetic radiation. The electron absorbs energy of radiation equal to or higher than band gap of semiconductors for inter-band (band-to-band) transition from the maximum point of valence band to the minimum point of conduction band. So, the absorption edge is defined by the minimum energy of radiation for inter-band transition of the electrons. The inter-band transition can be divided into the following:

allowed direct transition [36]

$$\alpha = \frac{A}{h\nu}(h\nu - E_g)^{\frac{1}{2}}, \tag{3.26}$$

forbidden direct transition [36]

$$\alpha = \frac{B}{h\nu}(h\nu - E_g)^{\frac{3}{2}}, \tag{3.27}$$

and, indirect transition [36]

$$\alpha = \frac{C}{h\nu}(h\nu - E_g)^{2}, \tag{3.28}$$

where A, B, C are constants, $h\nu$ is the photon energy and E_g is the energy gap of the semiconductor.

Consider normal incidence, as shown in Fig. 3.15, the absorption coefficient can be calculated directly from the transmission of the films. The transmission (T) and the reflection (R) can be expressed in terms of the intensity of incident wave I_0, intensity of transmitted wave I_t and intensity of reflected wave I_r as the following [36];

$$T = \frac{I_t}{I_0} = \frac{(1-R)^2 e^{-\alpha d}}{1+R^2 e^{-2\alpha d}} \tag{3.29}$$

$$R = \frac{I_r}{I_0} = \frac{(n-1)^2 + k^2}{(n+1)^2 + k^2} \tag{3.30}$$

If the film has a large thickness (d), then $R^2 e^{-2\alpha d} << 1$ and Eq. 3.29 reduces to

$$T = (1-R)^2 e^{-\alpha d} . \tag{3.31}$$

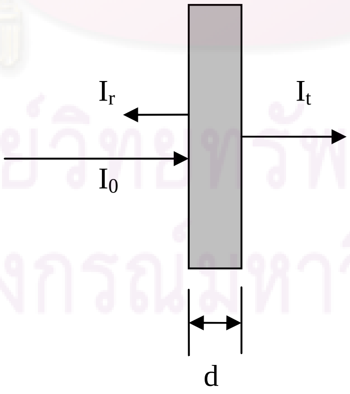

Figure 3.15: Transmission and reflection of the film.

Generally, the change of photon energy of incident wave affects the reflection (R) slightly. Then, the term $(1-R)^2$ can be approximated to a constant. Then, the optical absorption coefficient is

$$\alpha = \frac{1}{d}\ln\left(\frac{I_0}{I_t}\right) + C \,, \qquad (3.32)$$

where C is a constant. Since the reflection is approximated by a constant, the absorption coefficient is higher than the real value. In experiments, the background absorption coefficient (α_0) caused by the imperfection of thin film is subtracted for the correct absorption coefficient determination.

3.4 Structural Properties by X-ray diffraction (XRD)

The crystal structure of any material can be identified from its x-ray diffraction (XRD) pattern. X-ray is an electromagnetic wave that has high transmission through the medium because of its short wavelength of 0.5 Å to 3 Å which is shorter than the inter-planar spacing (d) in crystal. A sample in a form of powder or in a form of polycrystalline film can be seen that it is composed of the arranged parallel planes of atoms. Then, the incident beams of X-ray are reflected from these planes in crystal, with each plane reflecting only a small fraction of the radiation. The angle of incidence is equal to the angle of reflection. The diffracted beams are found when the reflections from parallel planes interfere constructively and destructively, as shown in Fig. 3.16. The path difference for X-ray diffracted from adjacent planes is $2d\sin\theta$, where θ called Bragg angle is measured from the plane. Constructive interference of the radiation occurs when the path difference is an integer number n of wavelengths (λ) of X-ray, corresponding to Bragg's law [37]

$$2d\sin\theta = n\lambda \qquad (3.33)$$

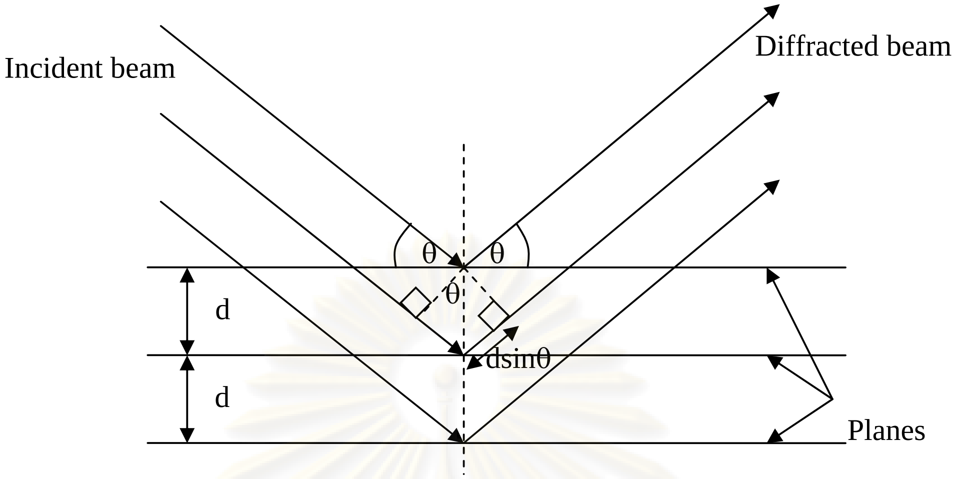

Figure 3.16: Diffraction of X-ray from parallel planes in the crystal followed by Bragg's law.

The interference pattern can be observed by measuring intensities of diffracted X-ray at varied diffraction angles (2θ), which are the angles between reflected beams and incident beams. For the same element or material, the XRD pattern looks like the same. The inter-planar spacing of (*hkl*) plane or d_{hkl} can be defined by Miller indicies: *h,k,l*. For Zn and ZnO of which crystal structure is wurzite or hexagonal can be expressed as [37]

$$\frac{1}{d_{hkl}^2}=\frac{4}{3}\left(\frac{h^2+hk+k^2}{a^2}\right)+\frac{l^2}{c^2} \qquad (3.34)$$

For Zn_3N_2 of which crystal structure is cubic can be expresses as [37]

$$\frac{1}{d_{hkl}^2}=\frac{h^2+k^2+l^2}{a^2} \qquad (3.35)$$

3.5 Raman effect

Raman effect is a phenomena which a photon is scattered inelastically by a crystal, with creation or annihilation of a phonon with frequency Ω [38]:

$$\omega = \omega' \pm \Omega\,; \qquad \vec{k} = \vec{k}' \pm \vec{K}\,, \tag{3.36}$$

where ω, $\vec{k}$ refer to the incident photon; ω', $\vec{k}'$ refer to the scattered photon; and Ω, $\vec{K}$ refer to phonon created or destroyed in the scattering event. Photons at frequency $\omega+\Omega$, which is called anti-Stoke line and $\omega-\Omega$ which is called Stoke line, can be emitted, corresponding to the absorption or emission of a phonon of frequency Ω. A simple diagram of Raman scattering is depicted as in Fig. 3.19. In the thermal equilibrium at temperature *T*, the intensity ratio of the two lines is

$$\frac{I(\omega+\Omega)}{I(\omega-\Omega)} = e^{\frac{-\hbar\Omega}{k_B T}}\,. \tag{3.37}$$

The intensity of Stoke line is higher than that of anti-Stoke line.

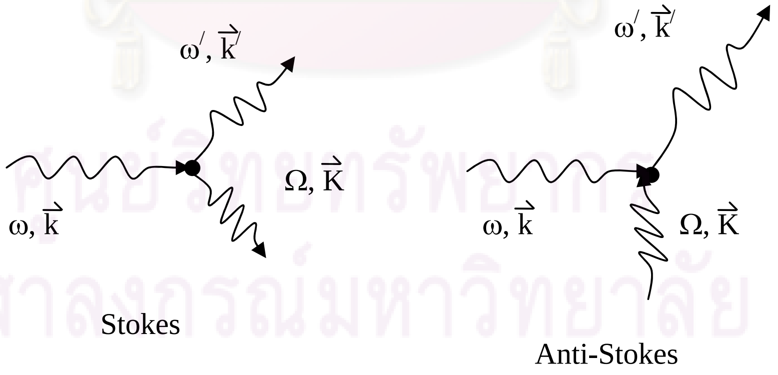

Figure 3.17: Raman scattering of a photon with emission or absorption of a phonon [38].

CHAPTER IV

EXPERIMENTAL PROCEDURES

This chapter describes the experimental procedures including fabrication of ZnO ceramic targets, ZnO thin film fabrication, characterizations.

4.1 Fabrication of ZnO Target

Ceramic ZnO target can be fabricated from raw material, i.e. 99.99% ZnO powder including the required dopants such as Al_2O_3 and P_2O_5. Then follow these procedures:

1. The compositions of raw materials of a target are calculated for the diameter of 50 mm and the thickness of 6 mm., and then calcined at 500^{o}C for 5 hours in a furnace shown in Fig 4.1 with a temperature profile shown in Fig. 4.2.

2. The compositions are mixed together and grinded using a ball milling in a plastic container to obtain smaller grain as shown in Fig 4.3. Moisten the mixture with de-ionized water, and stir in a container. Then put the mixture in the mold (diameter = 50 mm).

3. Press and heat the target in the mold with the pressure up to 4,000 psi as shown in Fig 4.4, and the temperature up to 150^{o}C using the profile illustrated in Fig 4.5. The total time of the target pressing is seven hours. After that, remove the target from the iron mold. Figure 4.6 is an example of the target just removed from the mold.

4. Sinter the target at 1,200^{o}C for one hour under atmospheric pressure as illustrate in Fig. 4.7 and used the profile depicted in Fig. 4.8. The total sintering time is 12 hours. Then, remove the target from the furnace, and measure the dimension of the target. Polish the surface of the ZnO target for the desired thickness of 6.0 mm. Then, install the ZnO target in the sputtering system as shown in Fig. 4.9.

Figure 4.1: Preparation of raw materials for fabrication of ZnO target.

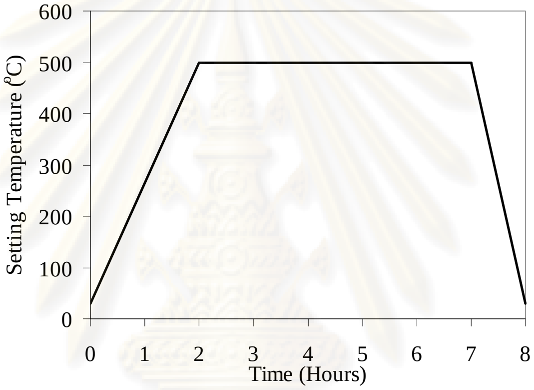

Figure 4.2: Profile of calcination of ZnO powder.

Figure 4.3: Ball milling of the raw material in a plastic container.

Figure 4.4: Pressing a target by hydrolic press with warming.

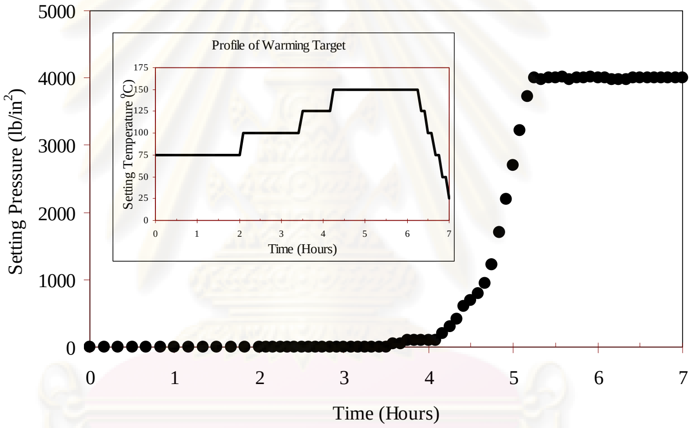

Figure 4.5: Profile of target pressing.

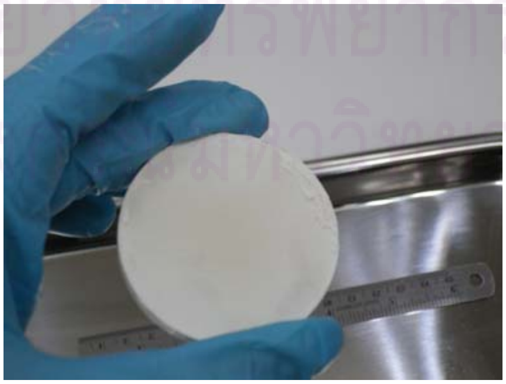

Figure 4.6: A ZnO ceramic target just removed from the mold.

Figure 4.7: Sintering a target in a furnace.

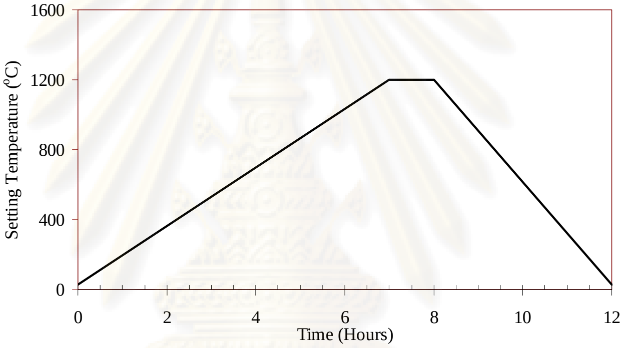

Figure 4.8: Profile of target sintering.

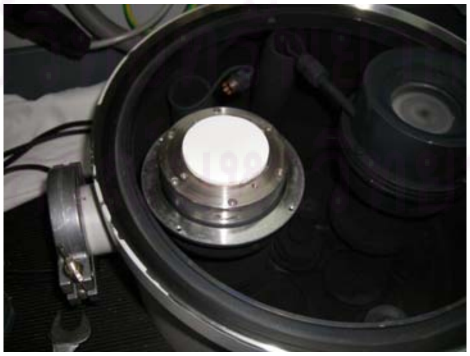

Figure 4.9: Installation of ZnO target in sputtering system.

4.2 ZnO thin film fabrications

The films in this work were deposited on 4.85 × 5.85 cm^2 soda-lime glass (SLG) substrates by RF/DC magnetron sputtering. To avoid any contaminations on the surface of SLG substrates, the substrates were cleaned as the following procedure. Firstly, the soda-lime glass substrates were washed with soft sponge and detergent. Secondly, they were cleaned with the mixture of detergent and de-ionized water in an ultrasonic bath at 60^oC for one hour. Thirdly, they were cleaned in de-ionized water in the ultrasonic bath at 60^oC for one hour again and then dried with nitrogen compressed air. Finally, they were kept in a humidity-controlled cabinet.

The typical starting material for fabrication of ZnO thin films is the ZnO ceramic target which is easy to be doped during its fabrication process such as phosphorus. In addition, any gas dopant can be used as the mixture of working gas during sputtering process such as N_2, N_2O, and O_2. The targets which were made and used in this research are summarized in Table 4.1. Since nitrogen may not compete against oxygen to occupy oxygen site in ZnO, alternative idea that one should change the starting material to be a pure metallic Zn (99.99%) target as shown in Fig. 4.10 and use N_2, N_2O, O_2, or the mixture of them with Ar as the working gas. The probability of nitrogen to occupy the oxygen size should be increased. The diagram of the sputtering used in this research is shown as Fig. 4.11.

Table 4.1 Summary of fabricated ZnO targets.

Target Code	Compositions
LHK02	2.5% Al_2O_3 + 97.5% ZnO
LHK06	2.5% P_2O_5 + 97.5% ZnO
LHK07	99.99% ZnO
LHK09	99.99% ZnO

Figure 4.10: Pure metallic Zn target.

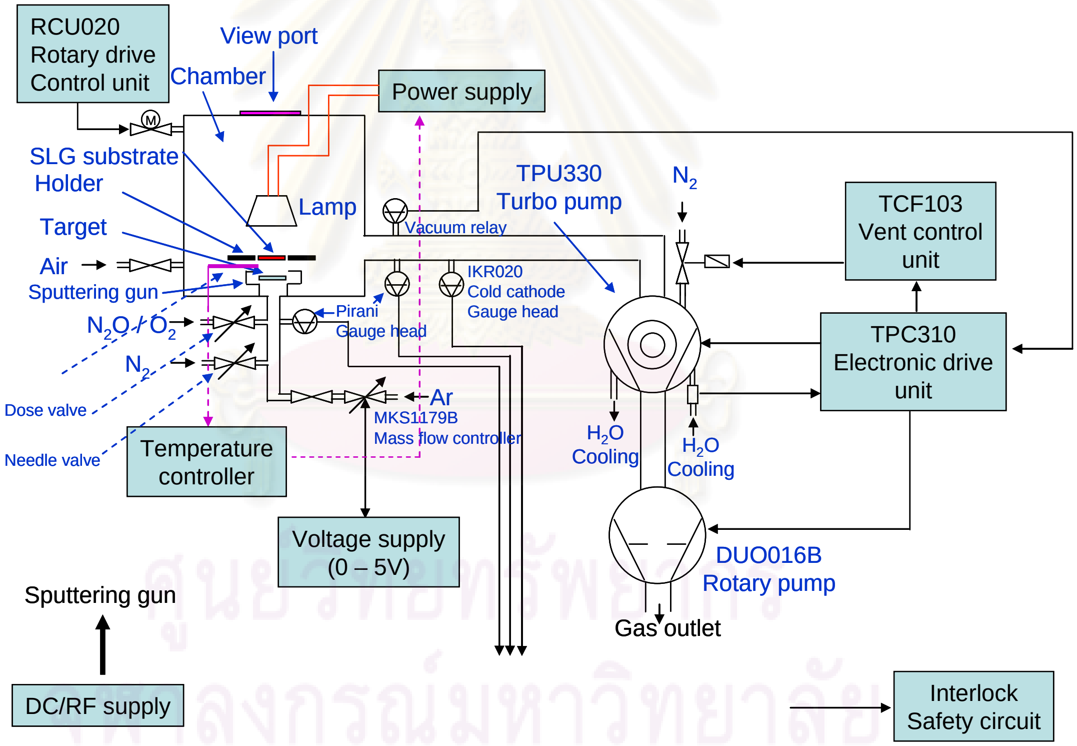

Figure 4.11: Diagram of sputtering system.

4.3 Characterizations

Characterization of the films consists of optical transmittance, x-ray diffraction (XRD), linear four-point probe, Hall effects, atomic force microscopy (AFM), and Raman spectroscopy.

4.3.1 Optical transmittance

As discussed in section 3.3, the optical transmittance is employed to investigate optical band gaps and thicknesses of the films. UV/VIS/NIR spectrometer (PerkinElmer Lambda900) is an instrument for measuring optical transmission, optical absorption and optical reflection between the wavelength of 200 nm and 2600 nm.

Optical transmittance is shown as Fig. 3.14 and the thickness can be calculated from Eq. 3.23. For a ZnO thin film which has direct band gap according to Eq. 3.26, a graph $\left((\alpha-\alpha_o)h\nu\right)^2$ versus $h\nu$ or photon energy was plotted as shown in Fig. 4.12.

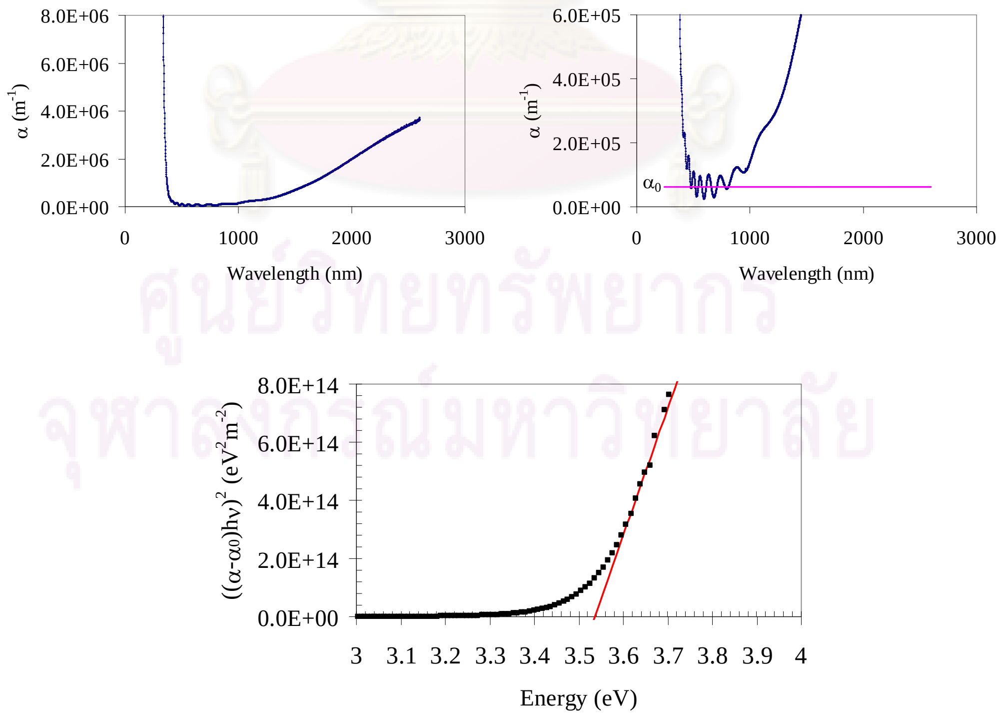

Figure 4.12: Graphical method to find optical band gap of a thin film.

The α_0 is an absorption background due to an environment. In order to find an absorption coefficient, Eq. 3.32 can be written as:

$$\alpha = \frac{1}{d}\ln(\frac{1}{T}), \qquad (3.1)$$

where d is the film thickness and $T = \frac{I_t}{I_0}$. Then a linear region in the graph is selected and plotted as a straight line. The required optical gap is the intercept on energy axis.

4.3.2 X-ray diffraction (XRD)

As a brief discussion in section 3.4, x-ray diffraction spectrometer is an effective tool to identify the crystal structure of the film. An example of XRD spectrum of a ZnO film scanning from 2θ of 15^o to 80^o with XRD wavelength of 1.5405 Å ($K_{\alpha 1}$) is shown in Fig. 4.13.

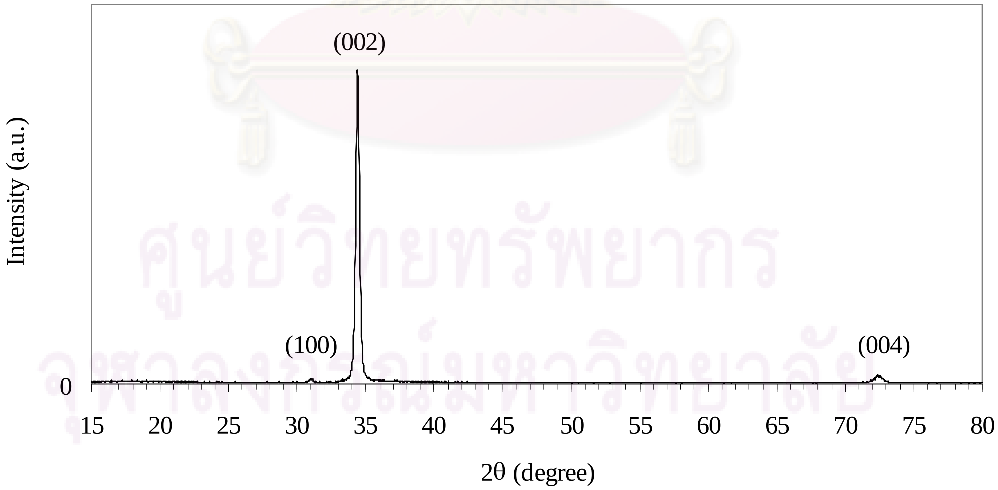

Figure 4.13: An XRD spectrum of a ZnO thin film.

The XRD spectra should be compared to the powder diffraction file of Joint Committee on Powder Diffraction Standards (JCPDS file). The standard ZnO is the card no. 36-1451. From Fig. 4.12, the positions of the peaks were compared and identified for the crystal planes such as (100), (002), and (004). The positions of the peaks can be fitted yielding important parameters such as peak center (position), full width at half maximum (FWHM). Inter-planar spacing can be calculated form Eq. 3.33. Then the lattice parameters (a and c) can be calculated from Eq. 3.34 (hexagonal structure of ZnO and Zn) or Eq. 3.35 (cubic structure of Zn_3N_2). Next, the average grain size t can be calculated from the Scherrer's formula:

$$t = \frac{0.9\lambda}{B\cos\theta}, \tag{4.2}$$

where λ is the wavelength of measured x-ray (1.5405 Å), B is the full width at half maximum, and θ is the half diffraction angle of crystal orientation peak.

In order to observe the change of crystal structure of the film under high temperature, high temperature configuration of XRD as shown in Fig. 4.14 is required. It consists of a platinum heater on which a sample is placed within the measuring chamber with the vacuum pressure of 10^{-5} mbar.

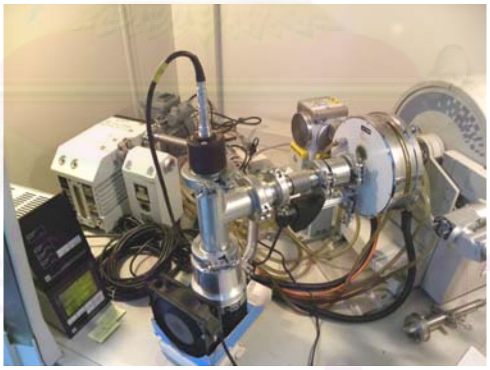

Figure 4.14: X-ray diffraction spectrometer with high temperature configuration, Phillips X'Pert, at Metallurgy and Material Science Research Institute, Chulalongkorn University.

The temperature of the platinum heater is monitored by a thermocouple (type-S). In addition, precise surface temperature of the sample surface could be monitored by a pyrometer.

4.3.3 Hot probe measurement

A hot probe is a qualitative technique to identify type of carrier (n-type or p-type) in a semiconductor. The setup consists of a heat reservoir such as a soldering gun and a micro-voltmeter with two probes in contact to the sample surface. The distance between the two probes is about 1 cm. One probe is made to be hotter than another. Consider Fig. 4.15, high temperature probe contacted the sample surface would drive carriers in the sample away from the probe making the probe being negative comparing to another. In a case of n-type semiconductors, electrons are driven away. Holes are also driven away by thermal energy in a case of p-type semiconductors.

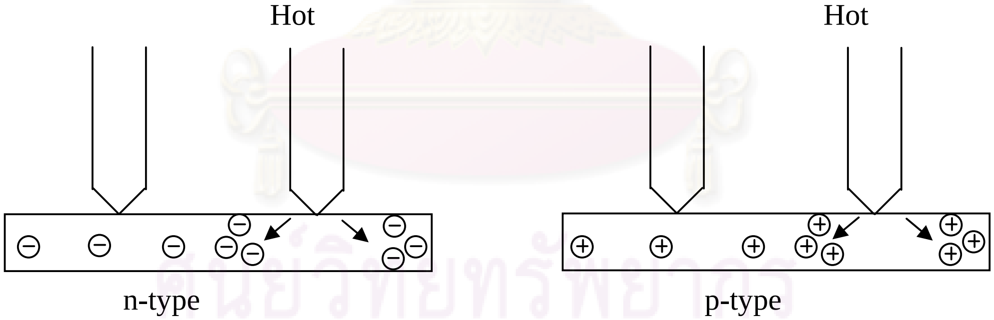

Figure 4.15: Illustration of carriers driven by hot probe.

4.3.4 The linear four-point probe

From section 3.2.1, the linear four point probe is a non-destructive method to find resistance or resistivity of a sample. The ends of the four probes are in contact with the center of a sample (or film) shown in Fig. 3.9. A current source (Keithley 237) supplies the current passing to the outer pair probes. A high impedance electrometer (Keithley 617) is used to measure the voltage developed between the inner pair probes. For a uniform flat sample as thin film, the resistivity could be calculated from:

$$\rho = 4.53\frac{V}{I}w, \tag{4.3}$$

where, ρ is resistivity, V is voltage between the inner-pair probes, I is current applied between the outer probes, and w is the film thickness, and 4.53 is the correction factor of the thin sample. To avoid errors, the probes must be far from the edge of sample at least 20S, where S is probe spacing.

4.3.5 Hall effect measurement

In order to find the carrier concentration of a sample, the Hall effect measurement setup is required. Figure 4.16 is a film sample with the size of 8 x 8 mm^2 in van de Pauw configuration is attached on a holder.

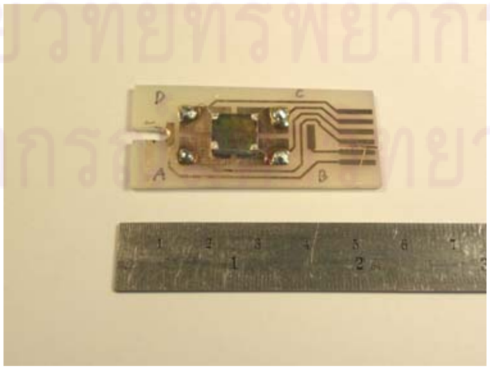

Figure 4.16: Sample with a size of 8 × 8 mm^2 prepared for Hall effect measurement.

The holder is then placed under a magnetic field. As discussed in section 3.2.2 and 3.2.3, the current is applied to one pair, and the developed voltage across the other pair is measured. Then the resistivity, mobility and carrier concentration can be calculated from Eqs. 3.11, 3.19, and 3.8, respectively.

4.3.6 The atomic force microscopy

Surface morphology of the film could be made to be a picture by the atomic force microscope (AFM). An AFM consists of a cantilever with sharp tip or probe as shown in Fig. 4.17. The end of its tip is used to scan the surface. The force between the sample and the surface leads to a defection of the cantilever according to Hook's law. There are many kinds of force used for AFM such as mechanical force, van de Waal force, electrostatic force, and etc. Then, the deflection of cantilever was measured by using a laser spot reflected from the top surface of the cantilever into an array of photodiodes. Finally, the picture of surface morphology was created.

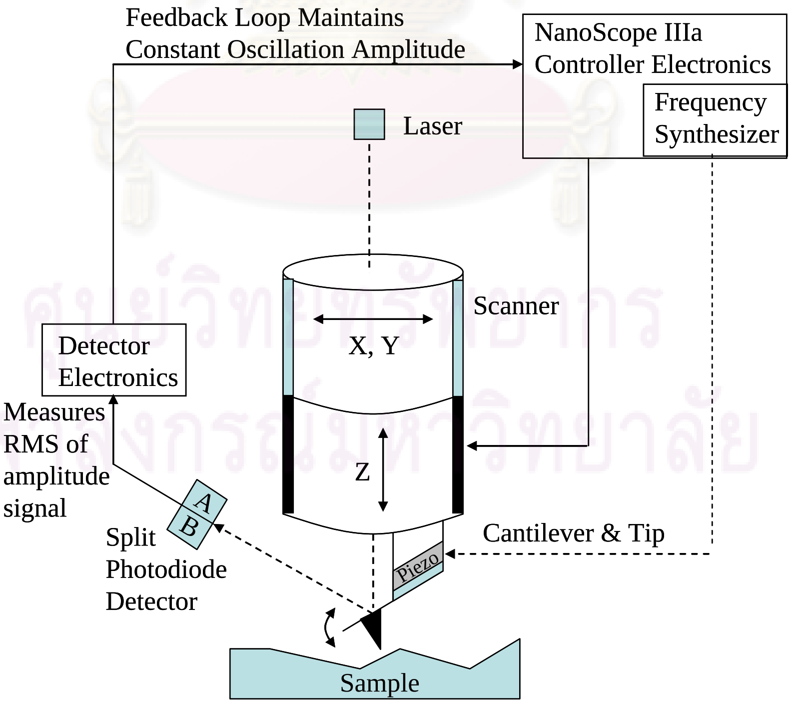

Figure 4.17: Diagram of scanning probe microscope.

4.3.7 Raman spectroscopy

From section 3.5, Raman spectroscopy is a spectroscopic technique used to study vibration modes in a system. It relies on an inelastic scattering of monochromatic light (such as laser) which interacts with phonons or other excitations in the system. As a result, the scattering light will exhibit lower or higher frequency. Finally, it is collected with a lens and sent through a monochromator and a detector. The Raman spectroscopy can be configured with excitation laser with different wavelength such as 514, 633, and 785 nm.

4.4 Research procedures

The research procedures of p-type ZnO were conducted using two kinds of starting materials: a fabrication from ZnO ceramic target, and a fabrication from Zn metallic target. The procedures are illustrated in a diagram shown in Fig. 4.18. In addition, the diagram of research strategy is depicted in Fig 4.19.

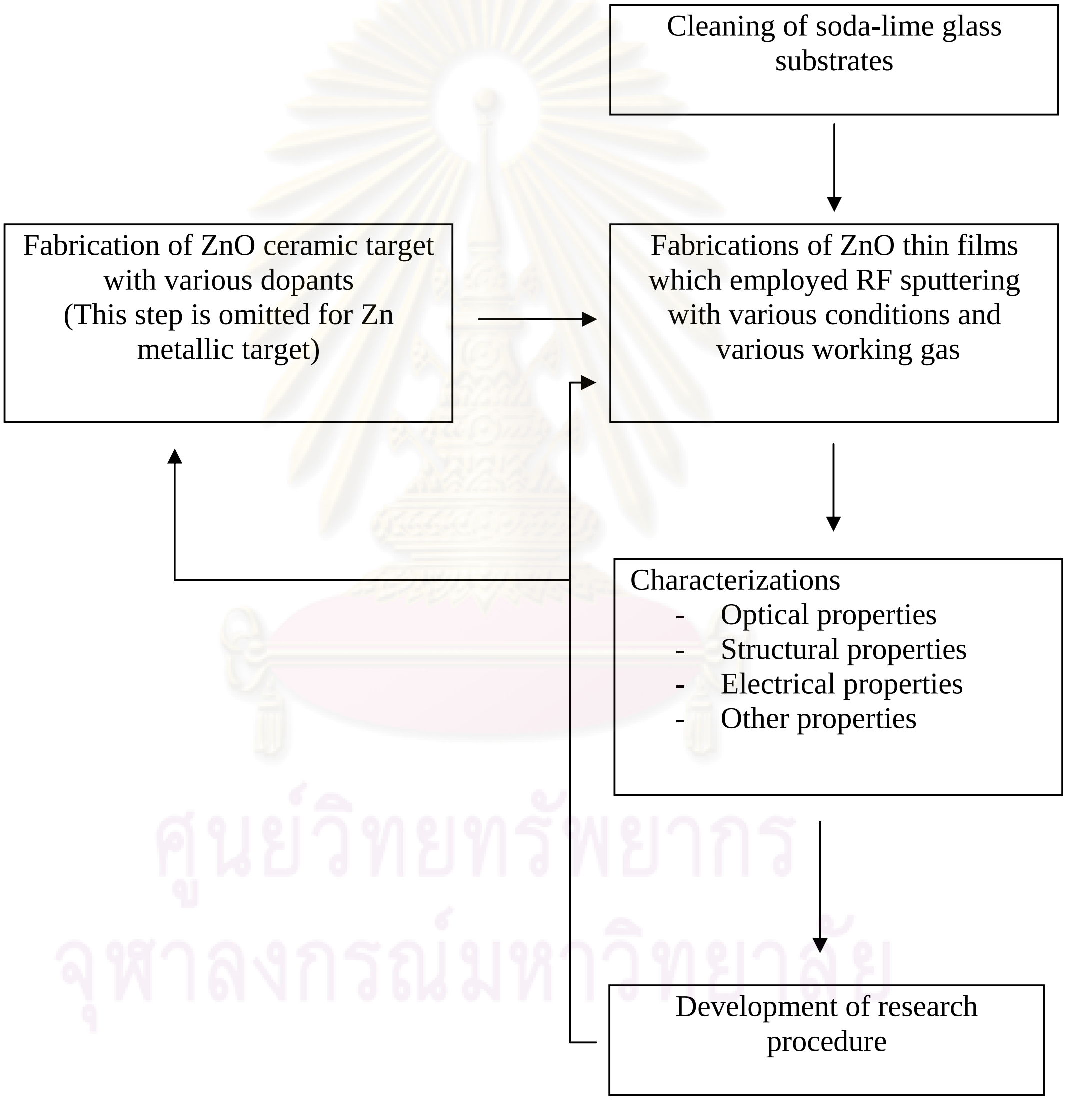

Figure 4.18: A diagram of research procedure.

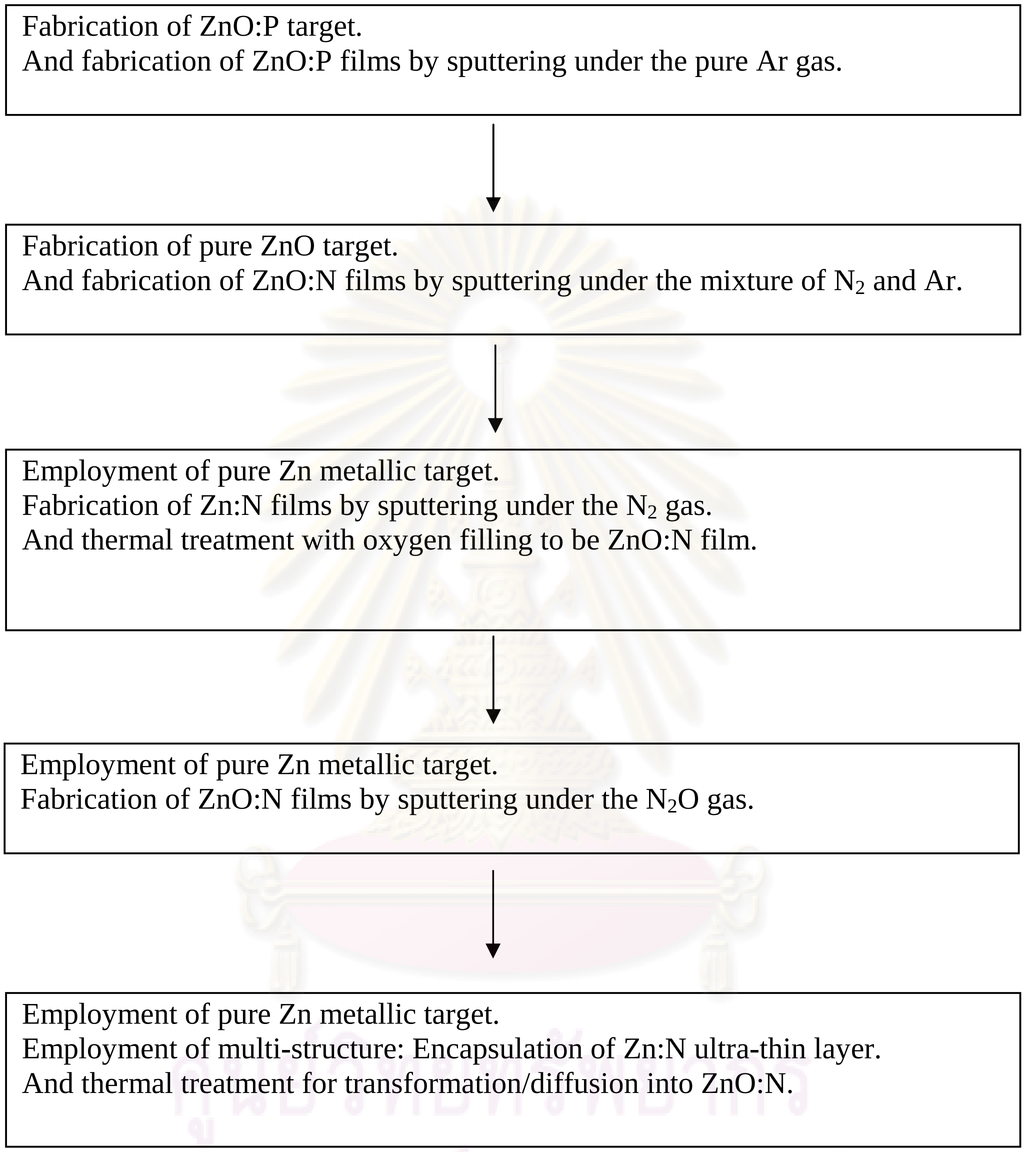

Fabrication of ZnO:P target.
And fabrication of ZnO:P films by sputtering under the pure Ar gas.

Fabrication of pure ZnO target.
And fabrication of ZnO:N films by sputtering under the mixture of N_2 and Ar.

Employment of pure Zn metallic target.
Fabrication of Zn:N films by sputtering under the N_2 gas.
And thermal treatment with oxygen filling to be ZnO:N film.

Employment of pure Zn metallic target.
Fabrication of ZnO:N films by sputtering under the N_2O gas.

Employment of pure Zn metallic target.
Employment of multi-structure: Encapsulation of Zn:N ultra-thin layer.
And thermal treatment for transformation/diffusion into ZnO:N.

Figure 4.19: A diagram of research strategy.

CHAPTER V

RESULTS AND DISCUSSIONS

This chapter begins with a reference n-type ZnO thin film. Then, a phosphorus doped ZnO thin fim is discussed. Finally, nitrogen doped ZnO thin films, our main themes, are discussed.

5.1 Aluminum-doped ZnO films: a reference of n-type ZnO

Aluminum doped ZnO (ZnO:Al) thin film, a kind of transparent conducting oxide (TCO) thin film, is used as window layer of thin film solar cells. If the target fabrication procedure discussed in section 4.1 is applicable, the high quality ZnO:Al thin film (good transmission, structure and electrical properties) can be obtained. The common conditions used for fabrication of ZnO:Al are summarized in Table 5.1. After fabrication, the as-grown films were characterized for their optical, structural, and electrical properties and summarized in Table 5.2. From Fig. 5.1, the high quality optical transmittance is about 90% at the wavelength of 450 - 800 nm (close to visible region of 400 - 700 nm). The lower transmittance at the wavelength greater than 800 nm corresponds to free carrier absorption. From Table 5.2, the optical gap is 3.54 eV, greater than that of 3.3 eV of the intrinsic ZnO, corresponding to the heavily doped mechanism of ZnO:Al that lower conducting states are filled up by conducting electrons and another electron will fill up the higher and higher states.

Table 5.1: Common conditions for fabrication of ZnO:Al films.

Target	ZnO (2.5wt% Al_2O_3)
Substrate	5×6 cm^2, soda-lime glass
Orientation of Substrate	60^o relative to target surface
Distance of substrate to target	6.5 cm (center to center)
Substrate temperature	Ambient temperature
Base pressure	$< 6.0 \times 10^{-6}$ mbar
Sputtering pressure	6.0×10^{-3} mbar
Sputtering gas	99.999% Ar
Sputtering power	RF 80 Watt
Sputtering time	75 minutes

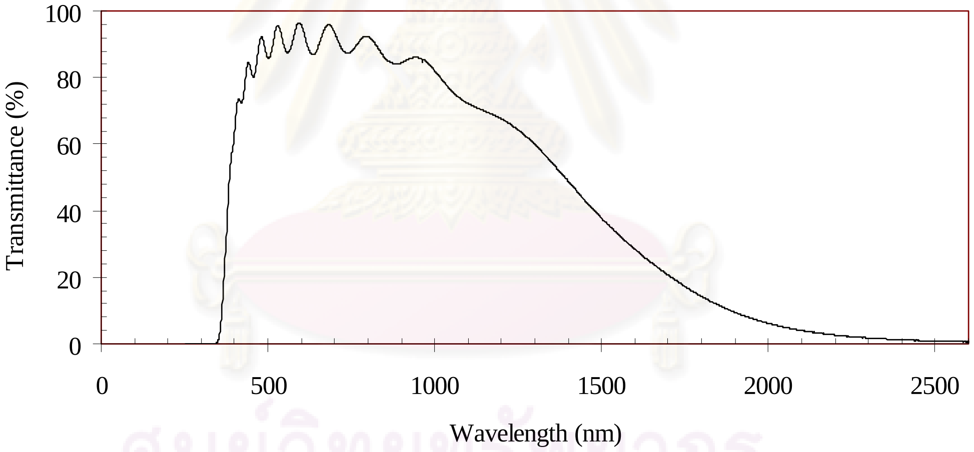

Figure 5.1: Optical transmittance of the as-grown ZnO:Al film.

From Fig. 5.2, the XRD spectrum can be identified for the (100), (002), and (004) planes. After fitting the preferred orientation peak (002), the c parameter as shown in Table 5.2 is 5.2072 Å, 0.01% (low tensile strain) greater than that of the standard ZnO [24]. Due to the narrow width of peak (002), the average grain size is 52 nm. Low tensile strain and large grain size refers to high structural quality.

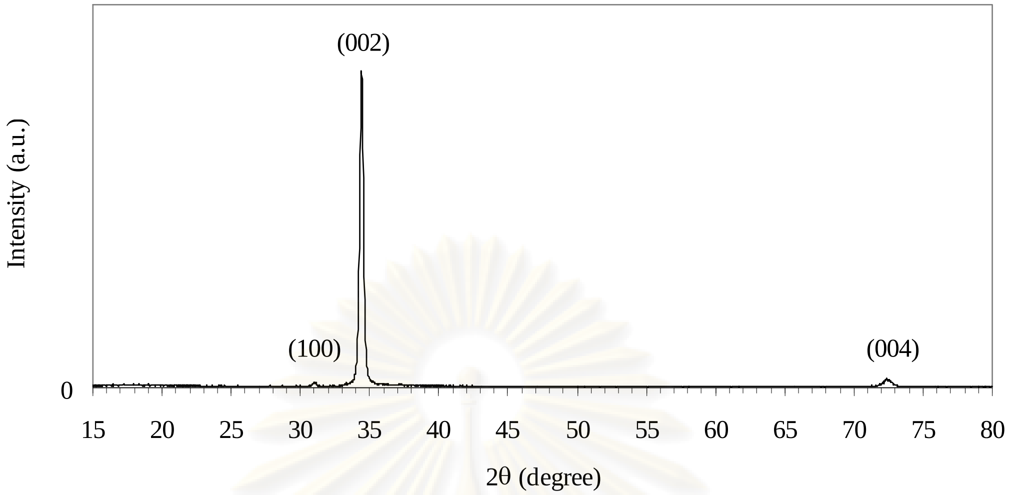

Figure 5.2: X-ray diffraction pattern of the as-grown ZnO:Al film.

Table 5.2: Physical properties of the as-grown ZnO:Al film.

Film thickness	1.40 μm (at center)
Deposition rate	18.7 nm/minute
Optical gap	3.54 eV
Lattice parameter: *c*	5.2072 Å , 0.01% larger than normal [24]
Average grain size	52 nm
Resistivity	2.42×10^{-3} Ω·cm
Mobility	7.31 $cm^2/V \cdot s$
Type of carrier	n-type
Carrier concentration	3.55×10^{20} cm^{-3}

The films exhibit low resistivity, high mobility, and high carrier concentration of 2.42 $\times 10^{-3}$ Ω·cm, 7.31 $cm^2/V \cdot s$, and 3.55×10^{20} cm^{-3}, respectively. These are the good electrical properties for application. It can be concluded that ZnO target fabrication procedure is applicable.

5.2 Phosphorus-doped ZnO films

Theoretical prediction was that p-type ZnO can be obtained by occupying of group-V elements into the oxygen site in ZnO crystal structure. Phosphorus, one of group-V element, can be easily used in a form of phosphorus oxide (P_2O_5) as a dopant in target fabrication process. Then, a P-doped ZnO (ZnO:P) thin film was obtained by rf sputtering. The common conditions used for fabrication ZnO:P film are summarized in Table 5.3. In order to enhance its optical, structural and electrical properties, the film was annealed at 200°C in vacuum for 50 minutes.

Table 5.3: Common conditions for fabrication of ZnO:P films.

Target	ZnO (2.5wt% P_2O_5)
Substrate	5×6 cm^2, soda-lime glass
Orientation of Substrate	60° relative to target surface
Distant of substrate to target	6.5 cm (center to center)
Substrate temperature	Room temperature
Base pressure	$< 6.0 \times 10^{-6}$ mbar
Sputtering pressure	6.0×10^{-3} mbar
Sputtering gas	99.999% Ar
Sputtering power	RF 80 Watt
Sputtering time	75 minutes

Consider Figure 5.3, the optical transmittance of the as-grown film is about 90% in the wavelengths between 450 – 1,000 nm and decreasing toward about 40% at 2,600 nm. Annealing process in vacuum leads to slightly increasing of transmittance near the band edge. The strong decreasing of transmittance in the long wavelength regions is typically due to the increasing of free carrier absorption. One can also see the shift of the cut-off wavelength which corresponds to the increase of optical gap as the physical properties of the ZnO:P are summarized in Table 5.3.

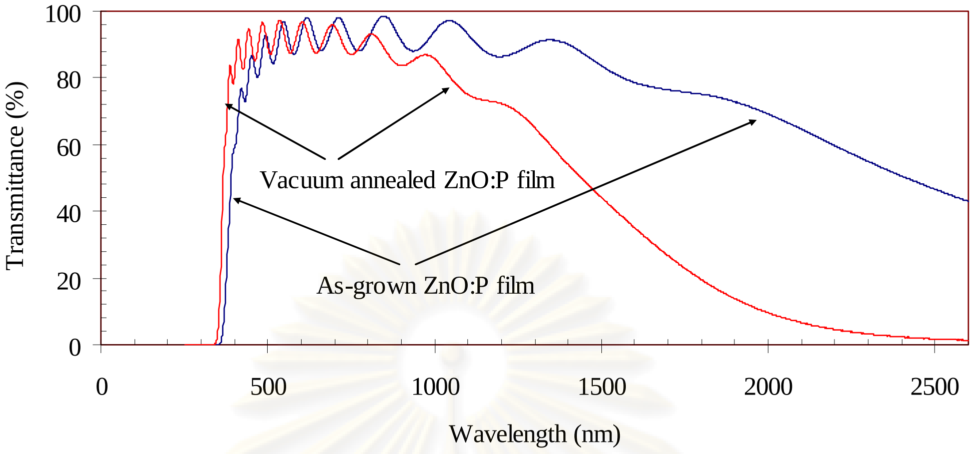

Figure 5.3: Optical transmittance of the ZnO:P films.

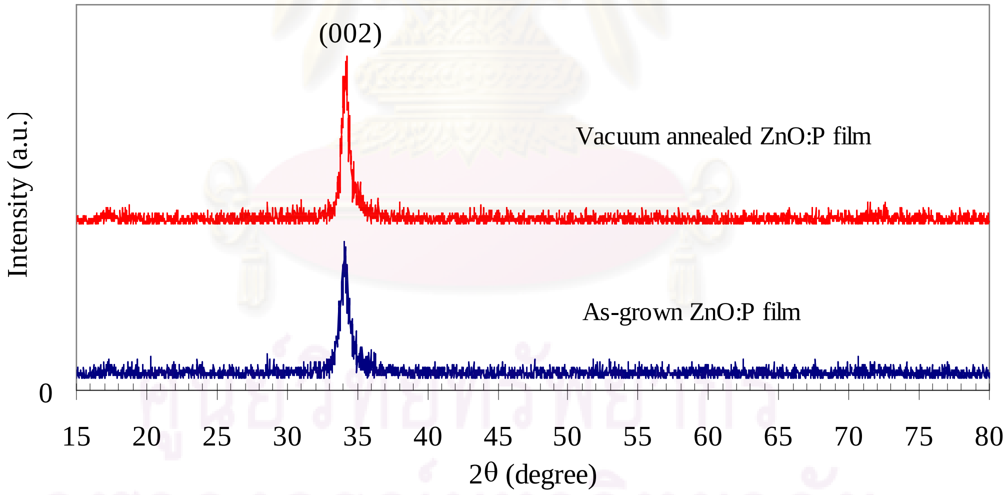

Figure 5.4: X-ray diffraction patterns of the ZnO:P films.

Consider Figure 5.4, the XRD patterns of the as-grown and vacuum annealed ZnO:P films exhibit low crystalline quality. Only preferred orientation (002) peaks are observed with low intensities.

Table 5.4: Physical properties of the ZnO:P films.

Film thickness	1.34 μm
Deposition rate	17.8 nm/minutes
Optical gap	3.44 eV (as-grown) 3.56 eV (vacuum annealed)
Lattice parameter: *c*	5.2528 Å (as-grown), 0.89% larger than normal [24] 5.2439 Å (vacuum annealed), 0.72% larger than normal [24]
Average grain size	18 nm (as-grown) 24 nm (vacuum annealed)
Resistivity	1.03×10^{-1} Ω·cm (as-grown) 6.22×10^{-3} Ω·cm (vacuum-annealed)
Mobility	4.21 cm^2/V·cm (as-grown) 6.59 cm^2/V·cm (vacuum-annealed)
Type of carrier	n-type
Carrier concentration	3.17×10^{19} cm^{-3} (as-grown) 1.55×10^{20} cm^{-3} (vacuum-annealed)

From Table 5.4, the lattice parameter *c* obtained from the XRD measurement of the as-grown and vacuum annealed ZnO:P film are 5.2528 Å (0.89% larger than normal at 5.2066 Å) and 5.2439 Å (0.72% larger than normal), respectively, which are caused by the tensile stain. The average grain size was 18 nm and 24 nm, respectively. The result suggests that the large atomic size of phosphorus leads to the low crystalline quality of the sputtered ZnO:P films. Thus, other group V elements with larger atomic size than that of phosphorus also lead to worst results due to higher tensile strain. The electrical properties obtained from the Hall effect measurement based on the van der Pauw configuration are shown in Table 5.4. We find the all the ZnO:P film exhibited n-type carrier. This suggests that the randomly incoming phosphorus atoms in the sputtering process do not occupy oxygen sites, but rather the zinc sites with more stability. As a result, accepter states from P cannot be obtained. Moreover, thermal energy from annealing process leads to the distribution of more donor states or more n-type carriers.

5.3 Nitrogen-doped ZnO films using ZnO target

With the ZnO:P obtained as strong n-type carriers as discussed in section 5.2, another choice of group-V element whose atomic size is smaller than phosphorus is nitrogen (N). The target for used in the sputtering process is a pure ZnO target (99.99% purity). The nitrogen dopants with unknown content are expected from the mixture of nitrogen (N_2) and argon (Ar) gases used during the sputtering. The ratios of the mixture are varied. The sputtering conditions used for fabrication nitrogen-doped ZnO are summarized in Table 5.5. Intrinsic ZnO (i-ZnO) films are fabricated under pure Ar or under the mixture of O_2 and Ar gases for a reference. The films are annealed at 500 ^oC in vacuum for 20 minutes for comparison. The thickness of the samples are about 400 - 500 nm.

Table 5.5: Common conditions for fabrication of ZnO:N films.

Target	ZnO (99.99%)
Substrate	5 × 6 cm^2, soda-lime glass
Orientation of Substrate	Planar
Distant of substrate to target	4.5 cm (center to center)
Substrate temperature	Room temperature
Base pressure	< 6.0×10^{-6} mbar
Sputtering pressure	6.0×10^{-3} mbar
Sputtering gas	N_2 and Ar with the ratios of 10:90, 25:75, 50:50, 100:0, and 0:100 for intrinsic ZnO (i-ZnO) (Including 2%O_2 + 98%Ar)
Sputtering power	RF 100 Watt
Sputtering time	10 minutes

The average optical transmission spectra of all the ZnO films are about of 90% with high transmission in the infrared region, as shown in Fig. 5.5, due to extremely low free charge carrier and thus resulting in high sheet resistance. In the narrower wavelength regions between 350 – 500 nm, the optical transmission spectra are different depending on the content of nitrogen gas during the sputtering, i.e. the transmittance spectra decrease with the increase of nitrogen partial pressure. Due to the decrease of the optical transmission spectra in the UV, violet, blue, and green regions (370 – 500 nm), only yellow, orange, red, and NIR waves can transmit through the films, thus most films show yellow shading. Consider Figure 4.6, when the films are annealed in vacuum at 500^{o}C for 20 minutes, all the optical transmission spectra in the region of 350 – 500 nm increased a little resulting in slightly yellow shading. We note that the optical transmission spectra of the intrinsic ZnO films before and after annealing remain the same. This suggests that nitrogen gas during sputtering is added to the films and contributes to defects in the ZnO films and it can be removed or redistributed during vacuum annealing. The optical gaps of the as-grown ZnO:N films increase from 3.25 eV to 3.28 eV with the increasing of N_2 partial pressure from 0% to 100% as shown in Fig. 5.7, while the optical gaps of annealed ZnO:N films are mostly constant at 3.26 eV except at 100% N_2 partial pressure, the optical gap decreases to 3.22 eV. These suggest that the vacuum annealed ZnO films are more stable, except the ZnO:N film with 100% N_2 film which perhaps contains excess amount of N_2. The stability of the crystal structure of the ZnO:N films are verified by the XRD spectra of all the as-grown and vacuum annealed ZnO:N as shown in Fig. 5.8.

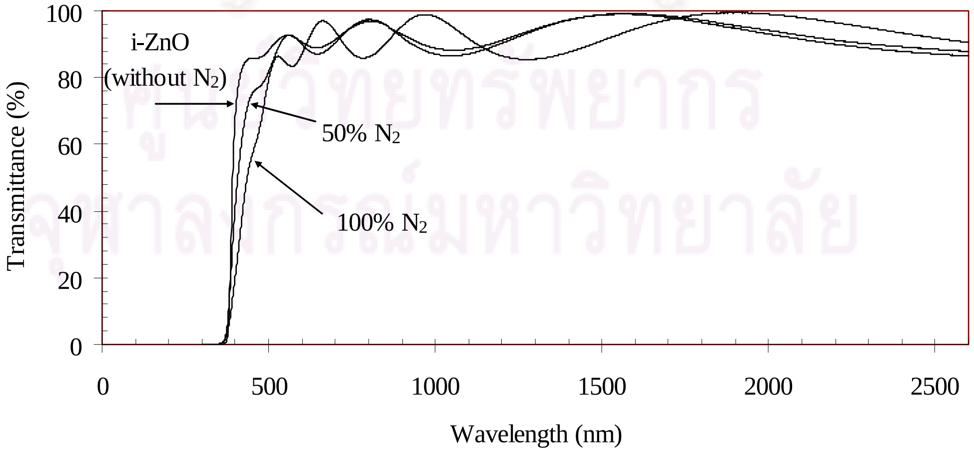

Figure 5.5: Optical transmittances of the as-grown ZnO:N films.

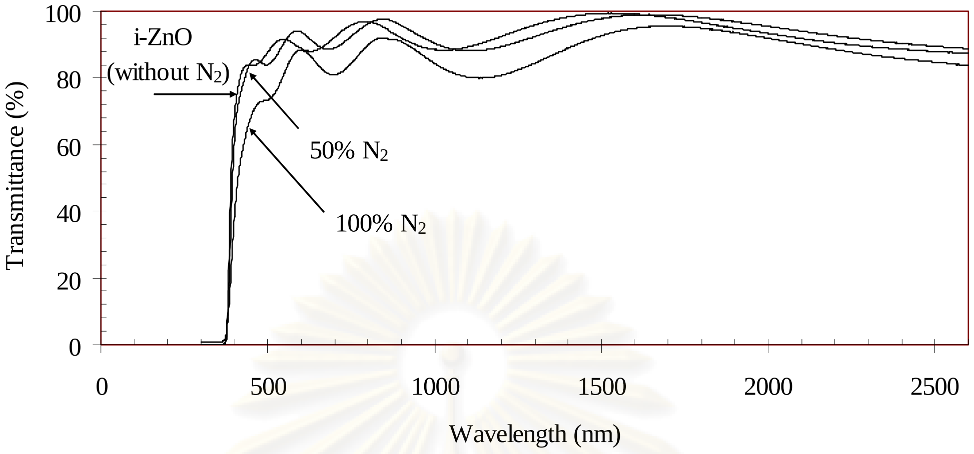

Figure 5.6: Optical transmittances of the vacuum annealed ZnO:N films.

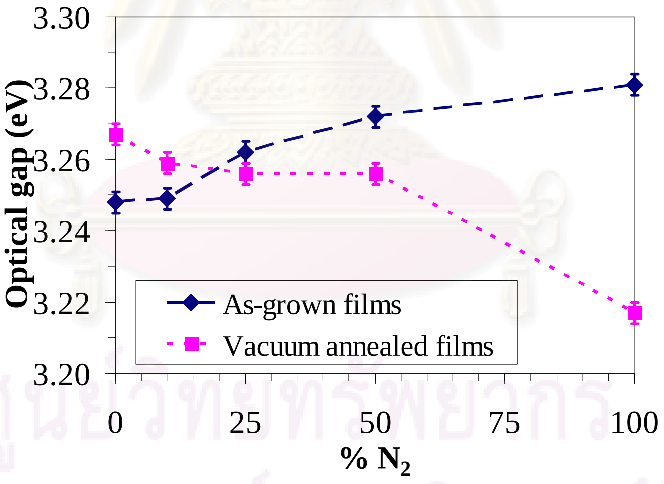

Figure 5.7: Comparison of calculated optical gaps of the as-grown ZnO films and vacuum annealed films with increasing nitrogen pressure from 0% to 100%.

It can be noticed that the only peak of (002) plane of the annealed films shift toward larger values of 2θ corresponding to smaller lattice spacing *c* as shown in Table 5.6.

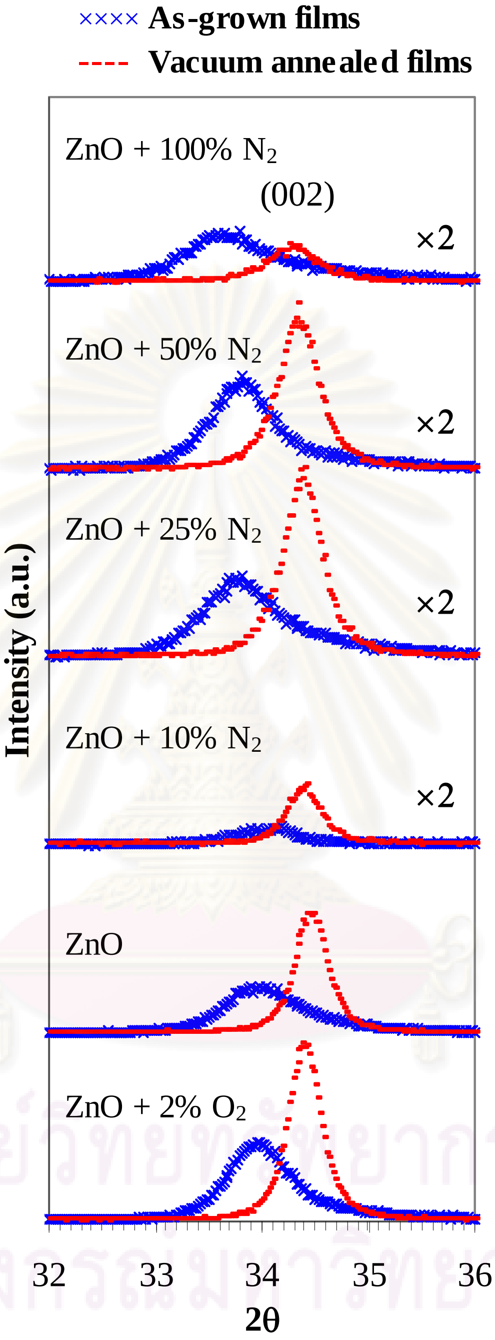

Figure 5.8: X-ray diffraction patterns of the vacuum annealed ZnO:N films comparing to intrinsic ZnO films.

The peak positions of vacuum annealed ZnO:N films are stable at about 34.42^o which is the plane (002) of ZnO. The lattice parameter *c* of the as-grown ZnO:N films are larger than that of vacuum annealed ZnO:N films which is the result of tensile strain along *c*-axis. In addition, the grain sizes become larger after annealing. This indicates that the crystalline of as-grown ZnO films are naturally disorder and contain many defects leading to larger lattice size than normal and small grain size, but it can be improved under vacuum annealing. Thermal energy stabilizes the crystal structure and minimizes defects leading to normal lattice size and larger grain size. We note that the ZnO film fabricated with 2% O_2 partial pressure has highest crystalline quality than the others. The lattice parameter *c* increases and the average grain size decreases with the increment of nitrogen partial pressure corresponding to the incorporation of nitrogen into the ZnO films.

The resistivity of the as-grown and vacuum annealed ZnO:N films are all high in the order of 10^5 Ω·cm as summarized in Table 5.7, thus, cannot be characterized for type and concentration of carriers by the existing Hall effect measurement set up. We not that the ZnO film grown with 100% Ar has its resistivity decreased dramatically when annealed in vacuum because the oxygen atoms could be driven out to create oxygen vacancies contributed to the increase of n-type carriers.

The surfaces morphologies over the area of 5 × 5 μm^2 of all the as-grown and vacuum annealed ZnO and ZnO:N films obtained from AFM are shown in Fig. 5.9 and the graph of roughness versus nitrogen partial pressure are shown in Fig. 5.10. The surfaces of both the as-grown and vacuum annealed ZnO films showing protrusions remain the same, Figs. 5.9 (a) – (d). It can be notice that the surfaces of the as-grown and vacuum annealed ZnO:N film with 10% N_2 partial pressure dramatically change showing a sponge-like surface shown in Figs. 5.9 (e) and (f) consistent with lower crystalline quality. The surfaces with rounded shape of the as-grown and vacuum annealed ZnO:N are observed with 25% - 50% N_2 partial pressure as illustrated in Figs. 5.9 (e) – (j). However, the surface morphology of the as-grown film fabricated with 100% N_2 partial pressure significantly change after annealing in vacuum, as can be seen in Figs. 5.9 (k) and (l).

Table 5.6: Lattice parameter c and average grain size of the as-grown and vacuum anneal ZnO:N films including i-ZnO films.

Sample	Lattice parameter (*c*) (Å)	% difference from normal (5.2066 Å) [24]	Average grain size (nm)
2% O_2 as-grown	5.2738	+ 1.29	25
2% O_2 vacuum annealed	5.2121	+ 0.10	47
100%Ar as-grown	5.2701	+ 1.22	20
100% Ar vacuum annealed	5.2040	- 0.05	44
10% N_2 as-grown	5.2633	+ 1.09	22
10% N_2 vacuum annealed	5.2135	+ 0.13	44
25% N_2 as-grown	5.3026	+ 1.84	21
25% N_2 vacuum annealed	5.2150	+ 0.16	40
50% N_2 as-grown	5.2973	+ 1.74	24
50% N_2 vacuum annealed	5.2209	+ 0.27	37
100% N_2 as-grown	5.3195	+ 2.17	17
100% N_2 vacuum annealed	5.2290	+ 0.43	29

Table 5.7: Thickness and resistivity of the ZnO:N films.

Sample	Calculated thickness of the as-grown film (nm)	Resistivity of the as-grown film (Ω·cm)	Resistivity of the vacuum annealed film (Ω·cm)
2% O_2	494	1.14×10^5	1.89×10^5
100%Ar	419	3.25×10^5	81.7
10% N_2	567	6.18×10^5	5.20×10^5
25% N_2	394	4.05×10^5	3.40×10^5
50% N_2	418	5.67×10^5	5.54×10^5
100% N_2	490	8.06×10^5	3.76×10^5

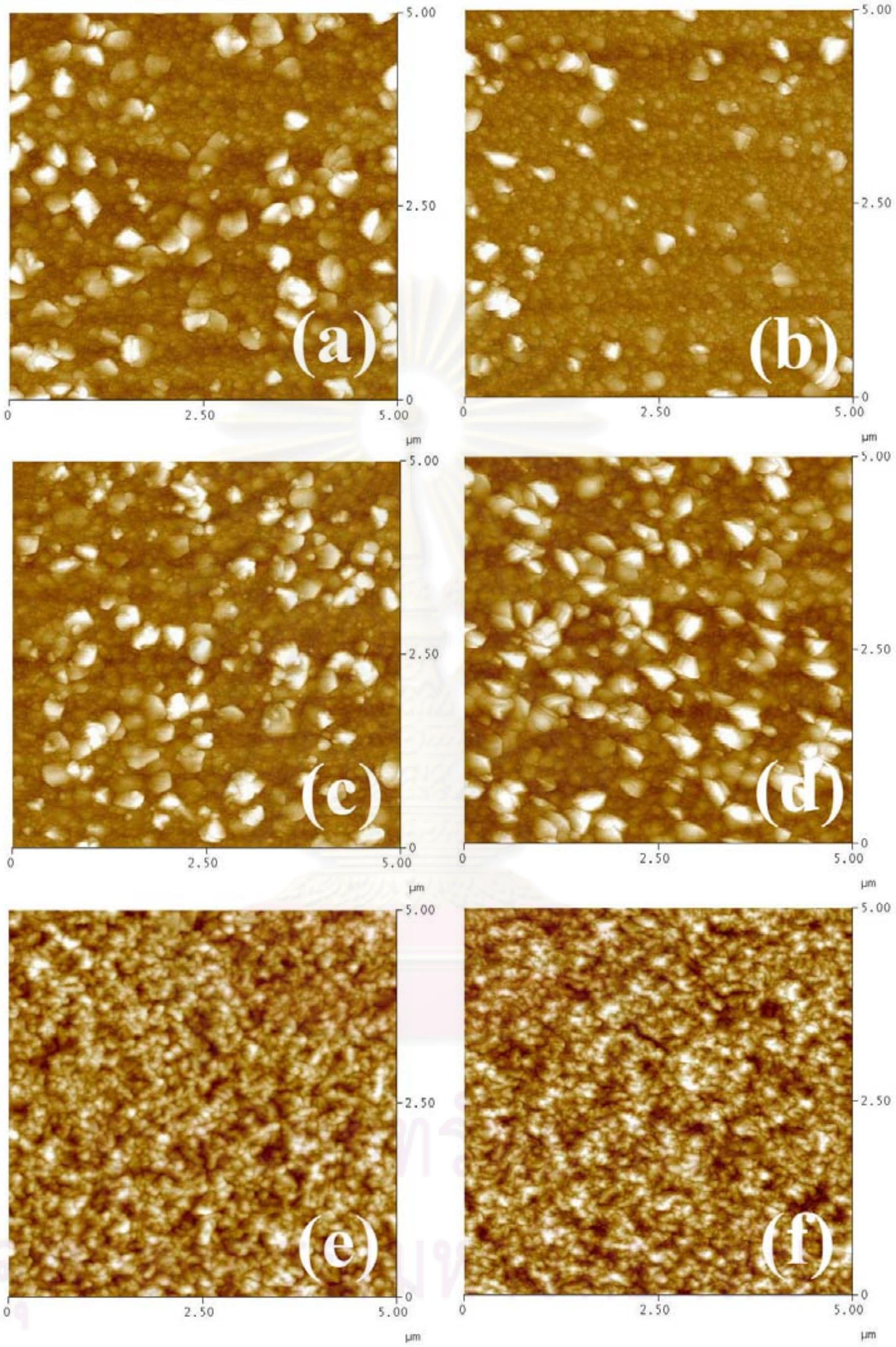

Figure 5.9: Comparison of 5 × 5 μm^2 *images from AFM of the as-grown ZnO films and vacuum annealed films with various partial pressure of reactive gas: (a), (b) 2%* O_2*; (c), (d) Pure Ar; and (e), (f) 10%* N_2*.*

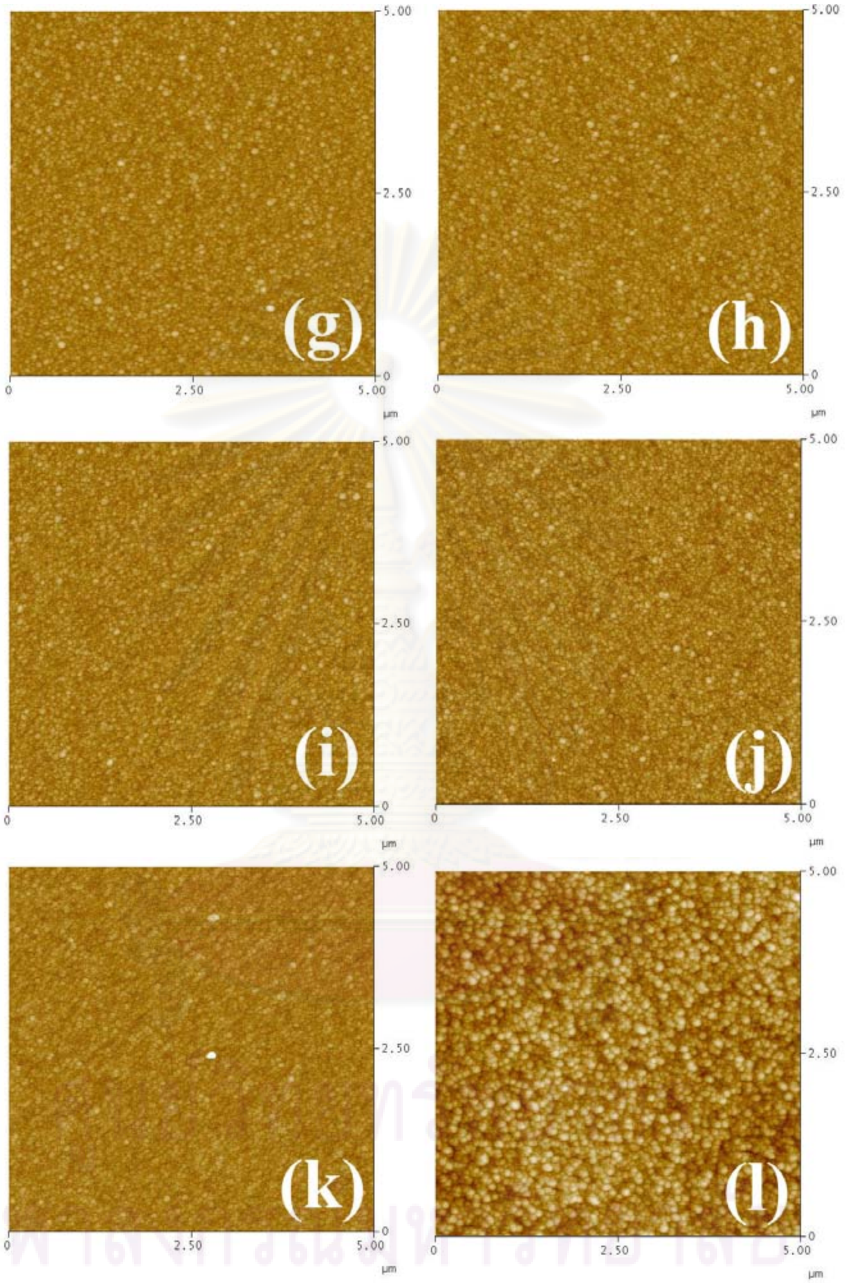

Figure 5.9 (continued): Comparison of $5 \times 5\ \mu m^2$ *images from AFM of the as-grown ZnO films and vacuum annealed films with various partial pressure of reactive gas: (g), (h) 25%* N_2*; (i), (j) 50%* N_2*; and (k), (l) 100%* N_2*.*

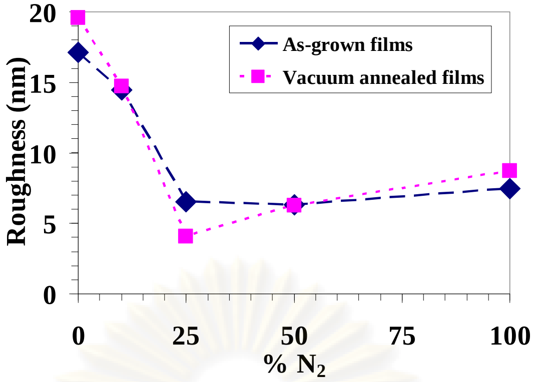

Figure 5.10: Comparison of calculated roughnesses of the as-grown ZnO films and vacuum annealed films with increasing nitrogen pressure from 0% to 100%.

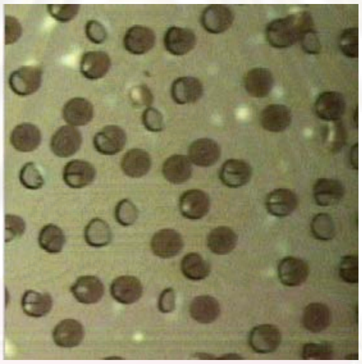

Figure 5.11: Microscope picture over the area of $150 \times 150\ \mu m^2$ *of exploded surface of vacuum annealed ZnO with 100%* N_2 *film.*

In addition, when observed the vacuum annealed film 100% N_2 partial pressure using optical microscope over the area of 150 × 150 μm^2 (Fig. 5.11), the bursting of the film including bubbles created inside the film is observed with the average diameter and density of about 10 μm and 3,200 mm^{-2}, respectively.

It can be inferred from the experimental results that nitrogen can be incorporated into the ZnO film in the form of diatomic molecules (as N_2) and merely substitute Zn or O sites resulting in high resistivity which will be further discussed. In other words, N_2 molecules mixed with Ar gas barely break up in the sputtering process in order to give N as dopants, neither n-type nor p-type. The exact locations of N_2 molecules cannot be verified with existing apparatus. The results lead us to believe that the excess N_2 molecules are trapped in the gaseous form in the ZnO since it can be driven out of the the film when given the thermal energy during vacuum annealing causing the bursting of the ZnO film. Note that the bursting is only observed in vacuum annealing films.

5.4 Nitrogen-doped ZnO using pure Zn metallic target

5.4.1 N_2 sputtering gas with O_2 filling in post-annealing process

With the difficulty of nitrogen atoms in occupying oxygen sites in ZnO structure as discussed in section 5.3, another idea to help N to compete with O in forming ZnO:N is using a pure Zn metallic target. Firstly, the Zn:N compound is forming as thin film when sputter Zn metallic target using nitrogen as sputtering gas. The oxygen atoms are later introduced into the crystal structure by post-annealing under the mixture of O_2 and Ar gases. The growth conditions used in the fabrication Zn:N films are summarized in Table 5.8, and the post annealing conditions and their electrical resistivities are summarized in table 5.9.

Table 5.8: Common conditions for fabrication of Zn:N films.

Target	Zn (99.99%)
Substrate	5 × 6 cm^2, soda-lime glass
Orientation of Substrate	Planar
Distant of substrate to target	4.5 cm (center to center)
Substrate temperature	Ambient temperature
Base pressure	$< 6.0 \times 10^{-6}$ mbar
Sputtering pressure	6.0×10^{-3} mbar
Sputtering gas	99.999% N_2
Sputtering power	RF 100 Watt
Sputtering time	10 minutes

Table 5.9: Post-annealing conditions and resistivities of the Zn:N films.

Annealing conditions	Resistivity (Ω·cm)
As-grown (468 nm)	6.52×10^3
Vacuum annealing at 500°C for 20 min.	3.62×10^5
10% O_2 + 90% Ar (6.0×10^{-3} mbar) at 500° for 20 min.	1.08×10^6
2-stage annealing:	
(a) Vacuum annealing, 500°C for 20 minutes and then	3.62×10^3
(b) 10% O_2 + 90% Ar (6.0×10^{-3} mbar), 500°C for 20 minutes	

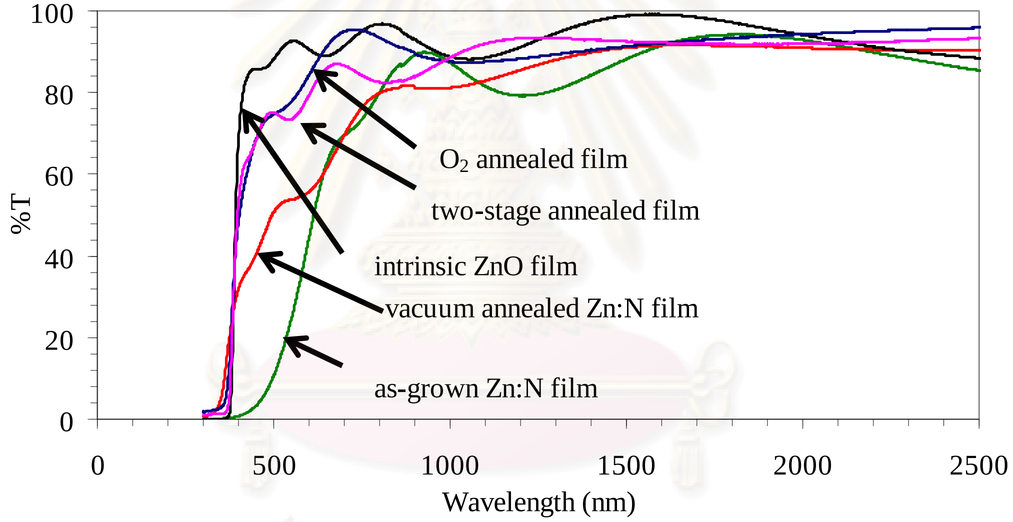

Figure 5.12: Optical transmittances of the Zn:N films.

The as-grown Zn:N compound thin films have brown shading and changed to lighter brown shading after annealing under various procedure as can be seen from the change in optical transmission spectra in Fig. 5.12. All the spectra show the average optical transmittance of about 90% above the cut-off. The high transmission spectra in the near infrared region (>700 nm) corresponds to the nature of extremely low free charge carrier resulting in high resistivities as summarized in Table 5.9. The films exhibit brown shading because of the low optical transmittances in the visible (VIS) region of 400 to 700 nm as shown in Fig. 5.12. With the various annealing conditions described in Table 5.9, the optical transmission spectra in the VIS region of the oxygen annealed film (OA film) and two-stage annealed film (2SA film) increased to be about 70 to 90%. The optical transmittance of vacuum annealed films (VA film) increases about 40 to 70%. Both optical spectra of OA film and 2SA film look like qualitatively similar to that of intrinsic ZnO thin film which was obtained by sputtering pure ZnO target under pure Ar gas, discussed previously. This suggests that annealing process can redistribute and/or reduce defect states in the Zn:N compound thin films, and leads to the formation of ZnO.

XRD spectra of the as-grown film (AG film) and various annealed films are shown in Fig 5.13(a) – (c) showing peaks Zn, Zn_3N_2, and ZnO based on the JCPDS files, summarized in Table 5.12. The XRD spectrum of the AG film exhibits the low intensity of (102) peak due to the amorphous like and low crystallinity of the Zn film with excess N_2. The XRD pattern of the VA film reveals both Zn peaks and Zn_3N_2 peaks. This result suggests that the crystalline Zn_3N_2 can be improved by the thermal energy in annealing process in vacuum where the excess N_2 is repelled out of the VA film. The peaks corresponding to Zn, Zn_3N_2, and ZnO in the OA film are obsverved, while only the sharp peaks of ZnO are observed in the 2SA film. These indicate that the thermal energy can activate oxygen to replace the nitrogen in the compound and then covert to ZnO. However, the residual Zn and Zn_3N_2 are observed in the OA film. The OA process is not effective to form ZnO because the remained unstable nitrogen atoms of which ionic size of 1.46 Å in the AG films will hinder the incoming oxygen atoms of which ionic size of 1.38 Å. In contrast, two-stage annealing has two mechanisms: (1) removing of unstable nitrogen defects off the film in first stage and (2) filling oxygen to the films in the second stage. The calculated grain sizes via Scherrer' formula are ~ 4 nm for OA film and ~10 nm for 2SA film. The XRD result indicates that the VA film is likely to be Zn_3N_2 of which energy gap is indirect [29]. Then we used the relation of indirect band-gap from the Eq. 3.28. Then we plotted $(\alpha h\nu)^{1/2}$ versus photon energy ($h\nu$) as shown in Fig. 5.14 and yielded the energy gap of 1.74 eV.

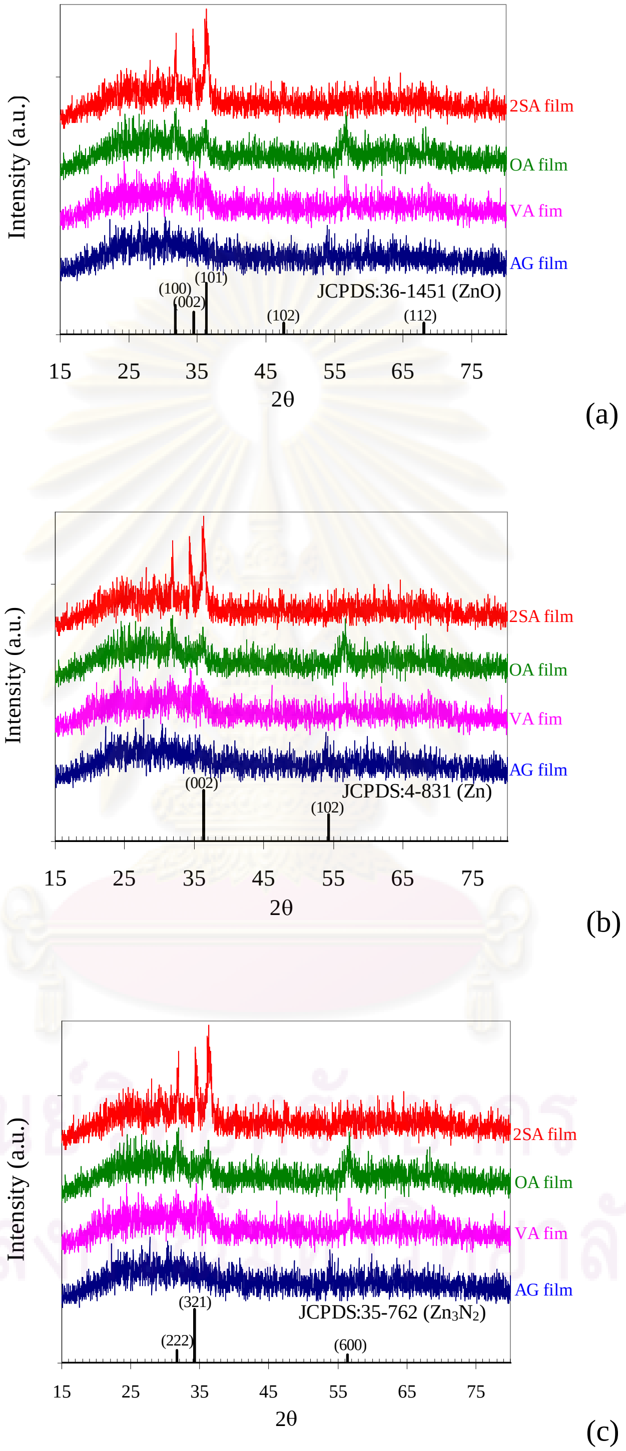

Figure 5.13: Identification of phase in the as-grown and annealed Zn:N films by comparing the XRD spectra to the standard ZnO, Zn, and Zn_3N_2 from JCPDS files.

Table 5.10: Observed peaks of Zn:N films under various annealed conditions (comparing to JCPDS files).

$Zn:N_2$ Sample	Observed peaks		
	Zn (JCPDS: 4-831)	Zn_3N_2 (JCPDS: 35-762)	ZnO (JCPDS: 36-1451)
(As-grown) AG film	(102)	-	-
(Vacuum annealed) VA film	(002) (102)	(222) (321) (600)	-
(Oxygen annealed) OA film	(002)	(222) (600)	(100) (101) (112)
(Two-step annealed) 2SA film	-	-	(100), (002) (101), (102) (112)

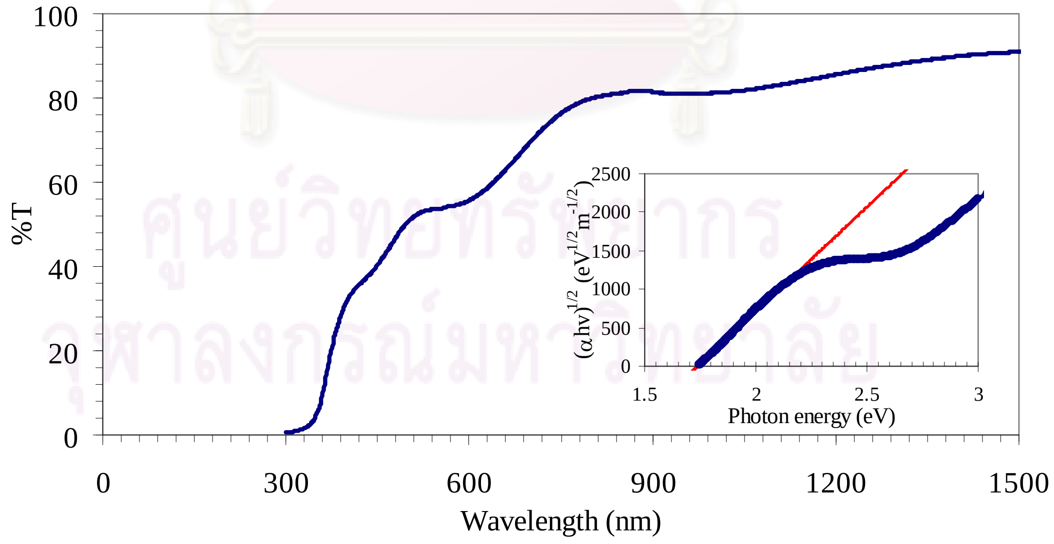

Figure 5.14: Optical transmittance of the vacuum anneal Zn:N film and determination of the optical gap as indirect gap of Zn_3N_2.

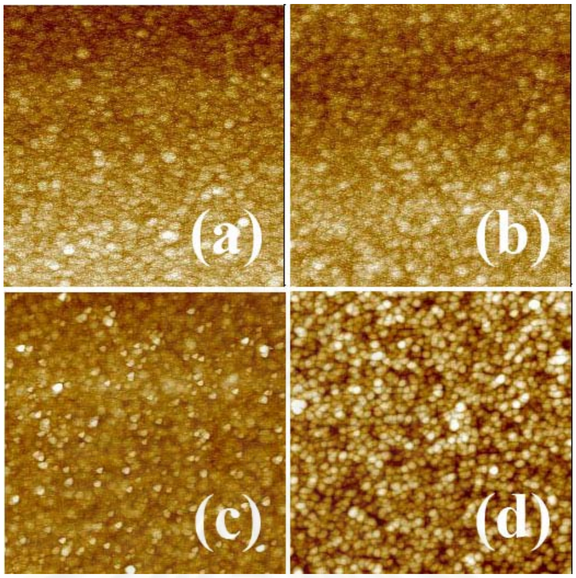

Figure 5.15: Comparison surface images from AFM in the area of 2.5×2.5 μm^2 of (a) AG film, (b) VA film, (c) OA film, and (d) 2SA film.

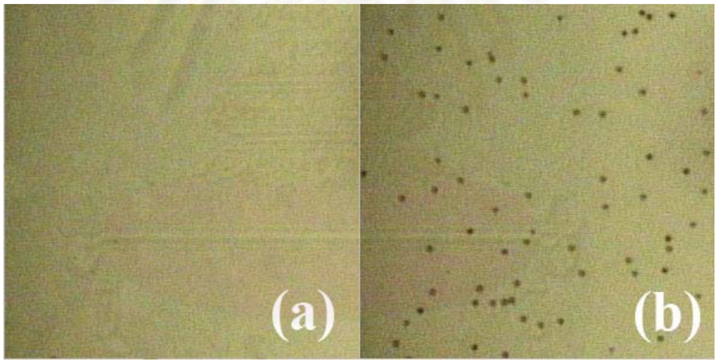

Figure 5.16: Microscope pictures in the area of 100×100 μm^2 of (a) AG film and (b) exploded surface of VA film.

The AFM image over the 2.5 × 2.5 μm^2 of all the Zn:N compound thin films are shown in Fig. 5.15. The surfaces AG and VA films in Fig. 5.15(a) and (b) are somewhat similar with the average roughness of about 5.5 nm. The surface of the OA, Fig. 5.15(c) film looks more dense with about the same roughness. Oxygen atoms during annealing may likely to form ZnO from the outside while the inside of the film contains the remained unstable nitrogen atoms. Figure 5.15 (d) show the surface of 2SA film with the average roughness of about 6 nm. This is the result of the reaction between oxygen atoms and zinc atoms forming ZnO throughout the film of which the unstable nitrogen atoms were already removed. In addition to what previously described in section 5.3, the bursting of the films is also observed in vacuum annealing, oxygen annealing, and two-stage annealing with approximately the same density about about 500 mm^{-2}. This indicates that annealing removes unstable nitrogen and slightly changes the microscopic surfaces of annealed films and dramatically changes the macroscopic surfaces.

From the obtained results, in order to obtain ZnO films, annealing under oxygen is inadequate because it will give residual Zn and Zn_3N_2. We suggest that to obtain pure crystalline ZnO film, the films should be annealed under vacuum to firstly remove unstable nitrogen and then they should be annealed under oxygen pressure. Due to the low intensity of XRD spectra with high resistivity in the order of 10^3 - 10^5 Ω·cm, the procedure described here could not provide high crystalline ZnO:N films with p-type conductivity. It suggests that an extremely small fraction of single N atoms can be obtained from dissociation collision process of N_2 molecule that will be described in the next section.

5.4.2 N_2O sputtering gas with Zn_3N_2 phase in the films

It is expected that the chemical bond of N_2O molecule can be broken easier in the dissociation collision of the sputtering process than that of N_2 molecule. That will help N atom to occupy the O sites of ZnO easier giving rise to the p-type carriers. In this part of the work, pure Zn target was used as the sputtering target and the N_2O : Ar ratios of are varied in order to obtain p-type ZnO. The sputtering parameters are summarized in Table 5.11. The substrates are pre-heated to 100^{o}C before sputtering in order to improve the crystalline quality of the films. The samples are fabricated using dc sputtering on the Zn metallic target, and the working pressure decrease to 4×10^{-3} mbar in order to obtain high energy electrons. All films are annealed at 500^{o}C for 20 minutes in vacuum. Due to the yellow shading of the as-grown ZnO:N films and the superposition peak in the XRD results as Fig. 5.20, it can make an assumption that the films contain Zn_3N_2 phase and ZnO phase.

Table 5.11: Common conditions for fabrication of ZnO:N film.

Target	Zn (99.99%)
Substrate	5 × 6 cm^2, soda-lime glass
Orientation of Substrate	Planar
Distance of substrate to target	4.5 cm (center to center)
Substrate temperature	100^oC
Base pressure	$< 6.0 \times 10^{-6}$ mbar
Sputtering pressure	4.0×10^{-3} mbar
Sputtering gas	N_2O and Ar with the ratio of 15:85, 20:80, 25:75, and 30:70
Sputtering power	DC 50 Watt
Sputtering time	15 minutes

The spectra can be identified as the superposition of two different peaks consisting of ZnO (002) peak and Zn_3N_2 (321) peak on the lower angle. Due to the defect of the crystalline leading to the large tensile strains, their inter-planar spacings are greater than normal, leading to the left shift of the peak positions (2θ for standard ZnO (002) at 34.422^o [24] and 2θ standard for Zn_3N_2 (321) at 34.280^o [27]). The fitted spectra are also shown in Fig 5.20. It indicates that Zn_3N_2 has low formation energy at quasi-stable phase in Zn-O-N system, after annealing Zn_3N_2 transform to be the more stable ZnO phase. So, zinc nitride (321) peak decreases for the vacuum annealed films and disappear for the annealed ZnO:N films that prepared under 20% N_2O partial pressure or more.

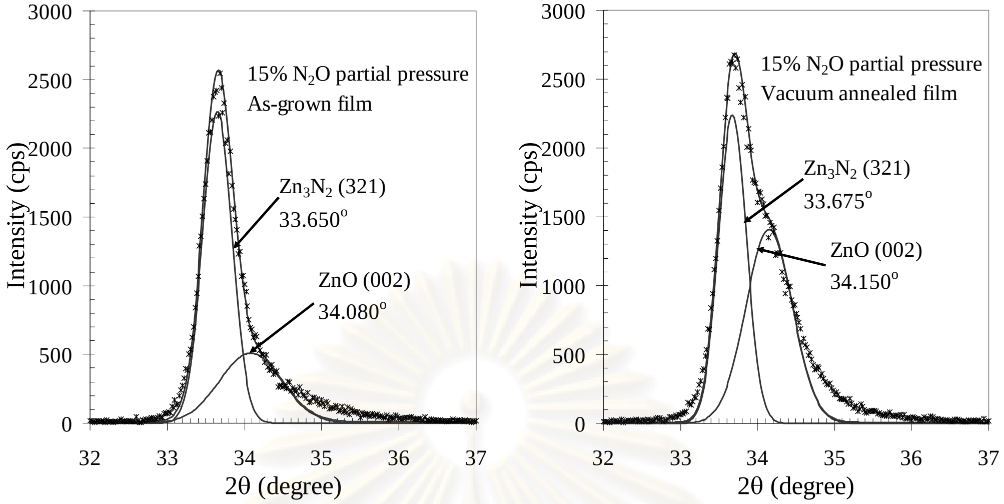

Figure 5.17: Fitting of the as-grown and vacuum annealed films of 15% N_2O partial pressure.

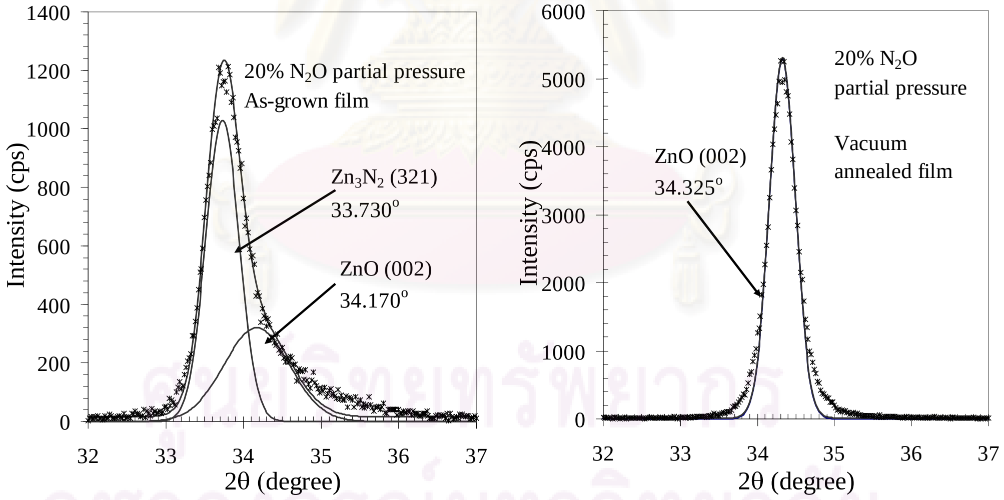

Figure 5.18: Fitting of the as-grown and vacuum annealed films of 20% N_2O partial pressure.

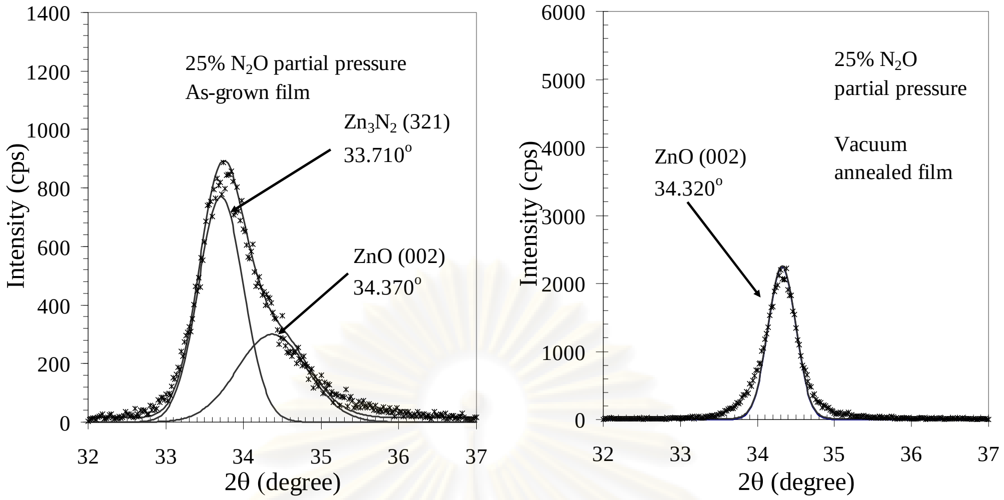

Figure 5.19: Fitting of the as-grown and vacuum annealed films of 25% N_2O partial pressure.

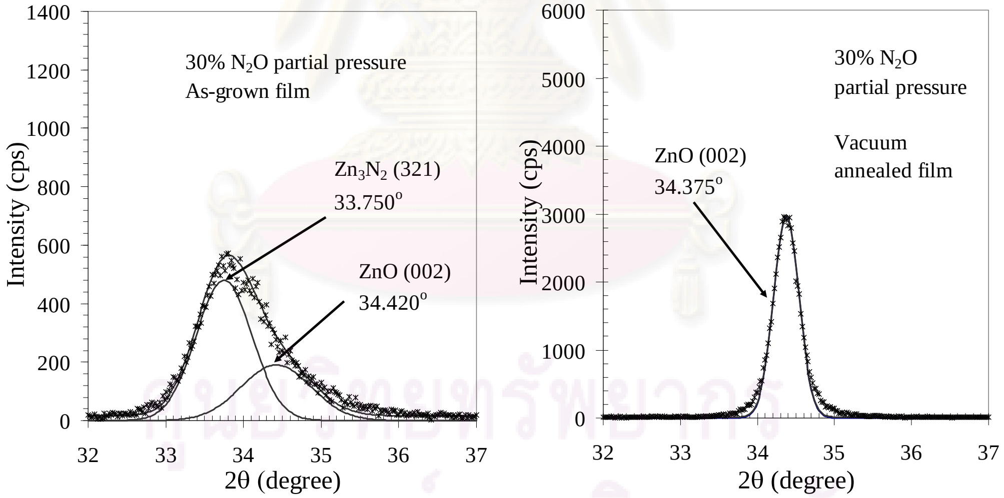

Figure 5.20: Fitting of the as-grown and vacuum annealed films of 30% N_2O partial pressure.

Table 5.12: Fitted peak parameters of XRD spectra of the as-grown (AG) and vacuum annealed (VA) ZnO:N films. (Note that lattice parameter $c = 2\times d_{002}$*)*

Sample	Peak identification	Peak position (degree)	Inter-planar spacing d_{002} (Å)	Peak Area (%)	Average crystallize size (nm)
15% N_2O AG	Zn_3N_2 (321)	33.650	2.6611	68	38
	ZnO (002)	34.080	2.6285	32	18
15% N_2O VA	Zn_3N_2 (321)	33.675	2.6592	49	40
	ZnO (002)	34.150	2.6233	51	24
20% N_2O AG	Zn_3N_2 (321)	33.730	2.6550	62	33
	ZnO (002)	34.170	2.6218	38	17
20% N_2O VA	ZnO (002)	34.325	2.6103	100	42
25% N_2O AG	Zn_3N_2 (321)	33.710	2.6565	62	25
	ZnO (002)	34.370	2.6070	38	16
25% N_2O VA	ZnO (002)	34.320	2.6107	100	40
30% N_2O AG	Zn_3N_2 (321)	33.750	2.6534	67	20
	ZnO (002)	34.420	2.6033	33	16
30% N_2O VA	ZnO (002)	34.375	2.6066	100	44
Standard Zn_3N_2	Zn_3N_2 (321)	34.280	2.6136	-	-
Standard ZnO	ZnO (002)	34.422	2.6032	-	-

We summarize the peak parameters for various N_2O partial pressures in Table 5.12 with average crystallite size obtained by Scherrer's formula. From the fitted XRD result, Zn_3N_2 phase along with ZnO phase in the as-grown ZnO:N films preferred to form low temperature (100^{o}C). The ratios of peak area of Zn_3N_2 (321) to that of ZnO (002) are about the same value of 2 because the ratio of N to O obtaining from N_2O sputtering gas is fixed. Average crystallite sites of ZnO are about the same of lower 20 nm. This should be the temperature limit of the ZnO formation with larger crystallite site. In contrast, average crystallite site of Zn_3N_2 is reduced from 38 nm to 20 nm with the increase of N_2O partial pressure from 15% to 30%. This should be the effect of oxygen to Zn_3N_2 crystalline. After annealing the as-grown ZnO:N films at 500^{o}C in vacuum, ZnO phase is more stable, so the quasi-stable zinc nitride phase decrease or re-crystallize to be more stable ZnO phase. The average crystallite sizes of ZnO phase of all vacuum annealed films increase to be about 40 nm which are larger than that of the as-grown films. This refers to the oxygen sufficiency which leads to the improvement of ZnO crystallinity by the thermal energy. Most of the films, except for 15% N_2O partial pressure or oxygen deficient case, show the absence of Zn_3N_2 phase after annealing. For the film grown at 15% N_2O partial pressure, the remainder of ZnO (321) peak of vacuum annealed film refers to the remainder of Zn_3N_2 phase after annealing. The Zn_3N_2 phase of this vacuum annealed film shows the average crystallite of 40 nm which is about the same value of its as-grown film referring to that the heat treatment does not increase Zn_3N_2 crystalline quality. Due to keeping the working pressure constant, the lower N_2O partial pressure corresponds to the higher Ar quantity leading to higher Zn sputtered atoms. Because of low N_2O quantity, O is deficient to catch Zn to form whole ZnO, the reminder of Zn atoms catch N atom to form Zn_3N_2 with high crystallite size referring to high crystallinity which still remains after annealing. For higher N_2O partial pressure or lower Ar pressure, Zn sputtered atoms is lower leading to oxygen sufficient causing that the system prefers forming only ZnO after annealing instead of the mix of ZnO and Zn_3N_2. The Zn_3N_3 could be formed in the as-grown film, but it should be quasi-stable state that was destroyed by the thermal energy.

In addition, with increasing the N_2O partial pressure, this ZnO (002) peak shifts to the right hand side corresponding to the decrement of inter-planar spacing of plane ZnO (002) or d_{002}. Their inter-planar spacing decrease and close to 2.6032 Å of standard ZnO. Comparing to inter-planar spacing of JCPDS file, all the as-grown films exhibit tensile strains in *c*-axis for ZnO phase (hexagonal) and *a*-axis for Zn_3N_2 (cubic). These should be the result of defects in film crystalline. It suggests that the defects could be all possible atoms or molecules yielding from the decomposition of N_2O gas such as NO, N_2, N and O during sputtering process, and occupying in possible locations such as oxygen site and interstitial. The defects or possible nitrogen defects should be reduced by vacuum annealing corresponding to the decrement of tensile strains.

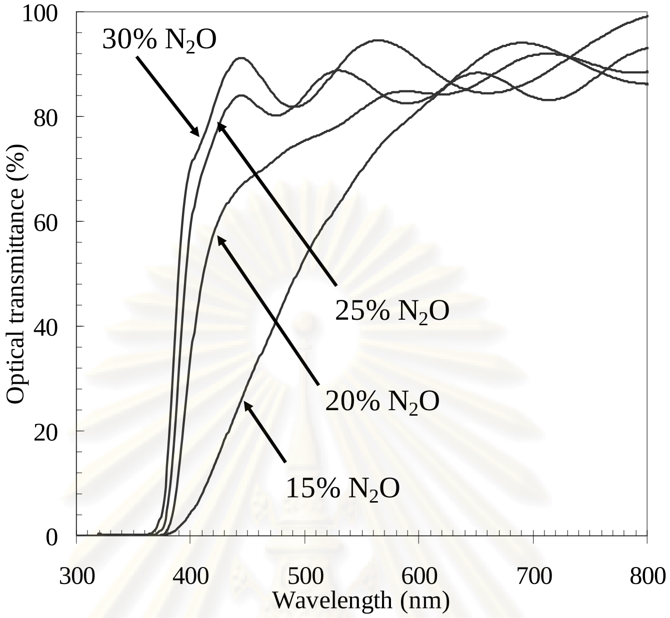

Figure 5.21: Optical transmittances of the as-grown ZnO:N films.

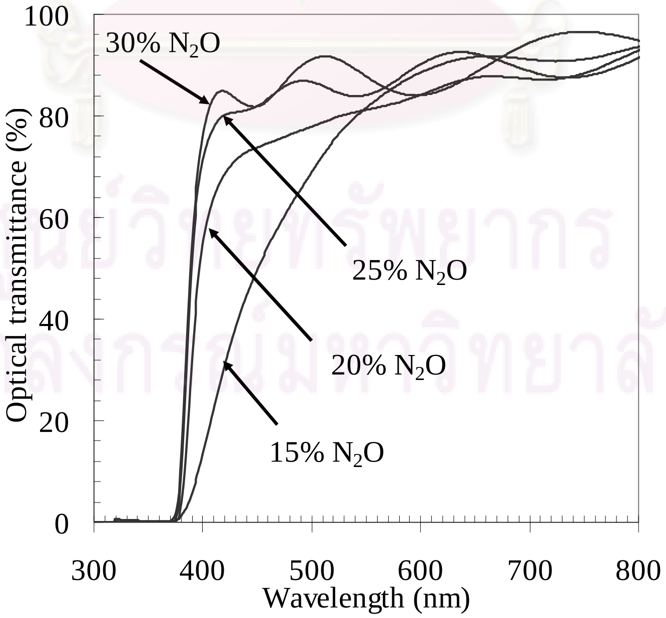

Figure 5.22: Optical transmittances of the vacuum annealed ZnO:N films.

Table 5.13: The Calculated thicknesses and the optical gaps of the as-grown (AG) films and vacuum annealed (VA) ZnO:N films.

Film	Thickness (nm)	Heat Treatment	Optical gap (eV)
15% N_2O	839	As-grown	3.18
		Vacuum annealed	3.23
20% N_2O	738	As-grown	3.25
		Vacuum annealed	3.27
25% N_2O	531	As-grown	3.26
		Vacuum annealed	3.27
30% N_2O	428	As-grown	3.27
		Vacuum annealed	3.27

*Table 5.14: Resistivity, Mobility and Carrier concentration for as-grown (AG) films and vacuum annealed (VA) ZnO:N films. (Note that * refers to slightly p-type by hot probe measurement and ** refers to ambiguous type.)*

Film	Heat Treatment	Resistivity ($\Omega\cdot$cm)	Mobility ($cm^2/V\cdot s$)	Type	Carrier concentration (cm^{-3})
15% N_2O	As-grown	1.3	5.9	n	1.4×10^{18}
	Vacuum annealed	4.9×10^{3}	1.3	n	1.6×10^{15}
20% N_2O	As-grown	1.2×10^{5}	-	*	-
	Vacuum annealed	1.6×10^{3}	0.67	n	9.6×10^{15}
25% N_2O	As-grown	3.3×10^{5}	-	**	-
	Vacuum annealed	2.7×10^{5}	-	**	-
30% N_2O	As-grown	2.6×10^{5}	-	**	-
	Vacuum annealed	2.0×10^{5}	-	**	-

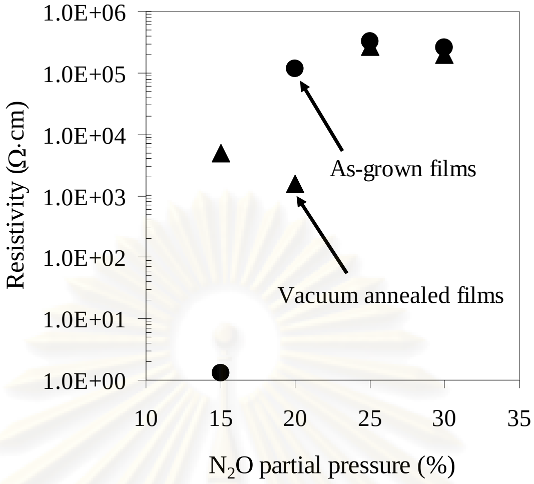

Figure 5.23: Resistivity versus N_2O partial pressure of the as-grown and vacuum annealed ZnO:N films.

The optical transmittance of the as-grown 15% N_2O partial pressure ZnO:N film exhibits lower transmittance in the region of 370 – 600 nm, corresponding to its yellow shading while all other films with 20% - 30% N_2O partial pressure have relatively higher transmission in the same region of wavelength corresponding to clearer color as the spectra are shown in Fig. 5.21. After annealing, the film with 15% N_2O partial pressure shows slightly increase of the optical transmittance as seen in Fig. 5.22. The as-grown ZnO:N films grown under low N_2O partial pressure generally exhibit yellow shading corresponding to the mixture of crystalline of Zn_3N_2 and ZnO. The increase of optical transmittance, when the N_2O partial pressure is increased corresponds to the decrement of the unstable Zn_3N_2 phase is driven out after obtaining addition thermal energy. The transmittances of 20% to 30% N_2O partial pressure films are close to the same cutoff wavelength. The calculated thicknesses and optical gaps are illustrated in Table 5.13. The optical gaps of the as-grown and vacuum annealed film for 15%N_2O exhibit lower value than the other. It suggests that the optical gap may be the mixed value of the optical gap of i-ZnO (3.27 eV) and that of Zn_3N_2 (2.12 eV [29]). That should be the result of the distribution of ZnO grain and Zn_3N_2 grain throughout the as-grown ZnO:N film surface. For 20% N_2O partial pressure or more, the calculated optical gaps of vacuum annealed ZnO:N films are close to the optical gap of i-ZnO or 3.27 eV. This result is significant difference from the work of Fusuhara *et al*. [39], sputtering ZnO target under the mixture of N_2 + Ar gases, leaded to the decrement of optical gap down to 2.30 eV [39] and cannot be observed the superposition peaks of their zinc oxynitride ($Zn_xO_yN_z$) films. It suggests that $Zn_xO_yN_z$ films should contain more unwanted nitrogen defects that should possibly be nitrogen interstitial $(N_2)_i$ than our ZnO:N films that contain Zn_3N_2 phase. In order to obtain nitrogen doped ZnO, sputtering Zn target under N_2O should reduce the unwanted nitrogen defects in ZnO:N film comparing to sputtering ZnO target under N_2, however, Zn_3N_2 phase in ZnO:N film is obtained. By using linear four-point-probe and Hall effect measurement, the some electrical properties e.g. resistivity, mobility, carrier concentration and type of carrier are obtained and summarized in Fig. 5.23 and Table 5.16.

The increase of N_2O partial pressure leads to the increase of resistivity of the as-grown films indicated as the circle up to 10^5 Ω·cm. For 25% and 30% N_2O, their resistivities exceed 10^5 Ω·cm. This indicates the compensation of p-type carrier to the native n-type carrier. Thus, their types of carrier cannot be exactly identified or slightly p-type detected by hot probe measurement. In addition, their resistivities of vacuum annealed ZnO:N films indicated as the triangle slightly decreases. After annealing, the resistivity of 15%N_2O increase to the order of 10^3 Ω·cm corresponding to the formation of ZnO phase. For the as-grown and vacuum annealed films for 25% or more N_2O ratio, their resistivities are too high to measure for correct carrier concentrations. It suggest that, for more amount of N_2O or enough oxygen quantity leads to a small amount of nitrogen occupying oxygen site (N_O) and thermal energy leads to the formation of unwanted stable defects that exhibit n-type conductivity. These could be substitutional diatomic molecules (SDM) such as $(N_2)_O$ [40, 41]. In addition, possible defects which provide p-type carriers among SDM's is $(NO)_O$, but it is unstable because of higher formation energy than $(N_2)_O$ [40]. As a result, annealing process leads to the decrease of p-type carrier. The thermal energy reduces the quasi-stable stage of acceptor in ZnO. From the results of high resisivities with no distinct p-type conductivity in the as-grown films and the ratios of peak area of ZnO phase to that of Zn_3N_2 were about 2:1 in the as-grown films, this is due to the higher chemical activity (electronegativity) of the oxygen than that of nitrogen leaving a very small fraction of nitrogen to occupy oxygen sites.

In order to increase p-type carrier, nitrogen or its compounds should be trapped in the i-ZnO films and then be chemically distributed by suitable thermal treatment which will discussed in the next section.

5.4.3 Encapsulation of ultra-thin Zn:N layer

In this part of the work a method to trap nitrogen in the structure ZnO is designed. A 3-layer encapsulation of ultra-thin Zn:N layer between the ZnO films is used to trap and redistribute nitrogen and filnally substitute oxygen in the films in order to obtain p-type conduction. The schematic diagram of encapsulation including thermal treatment used in the fabrication of ZnO:N are summarized in Table 5.15 and Table 5.16, respectively.

Table 5.15: Common conditions for fabrication of ZnO:N films.

Target	Zn (99.99%)
Substrate	5 × 6 cm^2, soda-lime glass
Orientation of Substrate	Planar
Distance of substrate to target	4.5 cm (center to center)
Substrate temperature	Room Temperature
Base pressure	$< 6.0 \times 10^{-6}$ mbar
Sputtering pressure	1.0×10^{-2} mbar
3-layer structure	Consider table 4.18
Sputtering power	RF 200 Watt

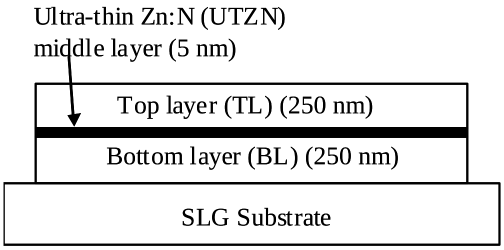

Figure 5.24: Schematic of the ZnO/Zn:N/ZnO film coated on SLG substrate.

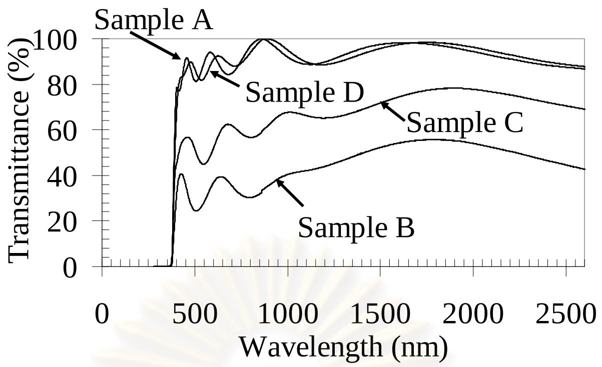

Fig. 5.25: Optical transmittances of the films.

Table 5.16: Samples and their growth conditions.

Sample	Sputtering condition	Treatment condition
A	85%Ar + 15%O_2, 4 min. (No middle layer or UTZN)	Up to 400^{o}C in 3 min. or short time vacuum (STV) annealing
B	BL: 85% Ar + 15% O_2, 2 min. UTZN: 50% Ar + 50% N_2, 2 sec. TL: 85% Ar + 15% O_2, 2 min.	As-grown
C	Same as B	STV
D	Same as B	Up to 500^{o}C in 20 min. and dwelling for 20 min. or long time vacuum (LTV) annealing

Table 5.17: Thicknesses, optical gaps, inter-planar spacings, and average grain sizes of the films.

Sample	Calculated thickness (nm)	Optical gap (eV)	Inter-planar spacing (Å)	Average grain size (nm)
A	505	3.27	2.6262	20
B	510	3.26	2.6458	15
C	487	3.27	2.6103	32
D	497	3.27	2.6011	48

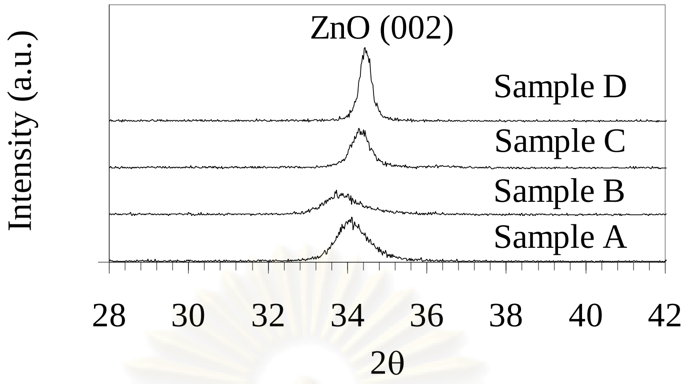

Fig. 5.26: XRD spectra of the films.

Table 5.18: Electrical properties of the films.

Sample	Resistivity ($\Omega\cdot$cm)	Type of carrier	Carrier concentration (cm^{-3})	Mobility ($V\cdot s/cm^2$)
A	3.6×10^5	Ambiguous	-	-
B	7.8×10^5	Ambiguous	-	-
C	2.3×10^{-2}	p	5.2×10^{19}	8.6
D	5.6×10^{-1}	n	3.1×10^{17}	57

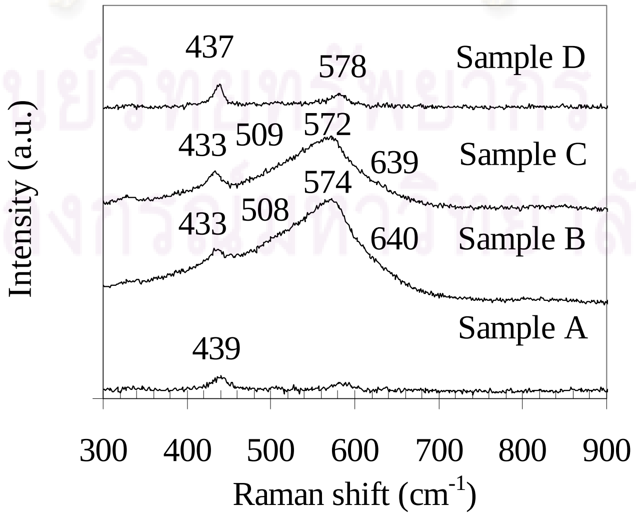

Fig. 5.27: Raman spectra of the films.

The optical transmission spectra of the samples summarized in Table 5.16 are illustrated in Fig 5.25. The optical transmittance of sample A is relatively high about 85% in the VIS region. Sample B exhibits very low transmittance with dark gray shading due to the property of the ultra-thin Zn:N compound (UTZN) layer. Sample C exhibits intermediate transmittance of about 60% in the VIS region with the appearance of gray shading, while sample D exhibits higher optical transmittance close to that of sample A. The results indicate that the thermal energy in both annealing processes increases the optical transmittance by the re-crystallization of the UTZN layer and the ZnO layers. The gray shading of sample C comes from the distribution of nitrogen related defect complex (NRDC) in the film. The calculated thicknesses from the interference patterns are about 500 nm and their optical gaps are about 3.27 eV closing to that of sample A or intrinsic ZnO. Due to the initial UTZN layer being considered as defects, the optical gap of the as-grown film (sample B, 3.26 eV) is slightly less than the others as summarized in Table 5.17.

The crystal structures of the films obtained from the XRD are shown in Fig. 5.26. Sample B exhibits lowest crystalline quality with wider peak of the (002) plane of ZnO. After the STV annealing, so called sample C, its crystalline quality was improved in terms of the decrement of inter-planar spacing and increment of grain size as summarized in Table 5.17. For the LTV annealing, namely sample D, the film exhibits the highest crystalline quality with average grain size of 48 nm. The stabilized inter-planar spacing of 2.6011 Å is close to that of 2.6032 Å [24] of standard ZnO powder. The shift of (002) peaks in both sample C and D (compared with sample B) corresponds to the decrease of inter-planar spacing by re-crystallization with the decrement of any interstitial atoms leading to the quasi-stable positions of N substituted in O sites (N_O) or stable positions of Zn and O.

The electrical properties of the sample A - D are summarized in Table 5.18. The results show that the ZnO:N film using UTZN middle layer followed by STV annealing, namely sample C, exhibits low resistivity in the order of 10^{-2} $\Omega\cdot$cm with the p-type carrier concentration in the order of 10^{19} cm^{-3}. However, this nitrogen-doped ZnO (ZnO:N) film should still contain Zn_3N_2 phase obtaining from UTZN layer with STV annealing. The annealing temperature up to 400°C should provide a chemical reaction of Zn and N_2 to be more stoichiometric Zn_3N_2 [20]. In other words,

Zn_3N_2 is the key substance to obtain ZnO:N with substitution of O into N site of Zn_3N_2 and the conversion of oxygen-doped Zn_3N_2 to be ZnO:N [21]. During the STV annealing, Zn_3N_2 phase forms simultaneously with the occupying of O into its N sites, and continuously with the formation of ZnO:N. As a result, there is no explicit Zn_3N_2 structure observed from XRD spectra. In contrast, the films without UTZN layer (sample A) and/or without any post annealing (sample B) exhibit extremely high resistivity in the order of 10^5 Ω·cm with ambiguous type of carrier. Due to the non-distribution of film crystalline structure, the top layer of sample B (with UTZN layer) still exhibits high resistivity. Furthermore, the LTV annealed film (sample D) leads to the n-type conductivity with carrier concentration of 10^{17} cm^{-3} and higher mobility. When the films are annealed at too high temperature as 500°C for a long time, the quasi-stable nitrogen defects such as N_O which provide p-type carrier should be redistributed by the excess thermal energy. In addition, substitutional diatomic molecules (SDM) [40, 41] which provide n-type carriers such as $(N_2)_O$ are expected to form with more stability and compensate the remained p-type carriers. Finally, the film exhibits n-type conductivity with higher mobility corresponding to the high crystalline quality in the XRD result.

The ZnO:N film using UTZN middle layer followed by STV annealing would have N or NRDC occupying in the O site. Then, NRDC would exist and could be detected by Raman spectroscopy as illustrated by Stoke Raman lines in Fig. 5.27. The positions of Raman shift are identified based on our best fitted peaks (not shown in the figure). Comparing to the works of L.L. Kerr *et al.* [23] and M.L. Tu *et al.* [14], their most dominant peaks in Raman shift of their p-type ZnO:N are of 570 and 581 cm^{-1}, respectively, which were interpreted as LO phonon mode [14]. The as-grown film with UTZN layer without annealing (sample B) exhibits the highest intensity at 574 cm^{-1}. It may be inferred as a result of NRDC containing in the film. With the STV annealing, sample C shows the main peak at 572 cm^{-1} corresponding to the existence of NRDC. In contrast, sample A (no UTZN) exhibits only small peak at 439 cm^{-1}. The Raman shifts at 433 - 439 cm^{-1} correspond to the intrinsic ZnO film [23]. Finally, sample D which contains UTZN layer with the LTV annealing exhibits similar Raman shift result similar to the intrinsic ZnO. It implied that excess thermal energy from the LTV annealing would cause the redistribution of NRDC in quasi-stable state to the more stable state leading to the compensation from the p-type carrier to the n-type carrier. The low intensity of Raman shift at 578 cm^{-1} of sample D reveals the small NRDC residue but not enough contribution to the p-type conductivity. Annealing in a high temperature and/or for a long time should remove unstable nitrogen related defect complexes and form more stable defects which exhibit n-type conductivity. Finally, post annealing is the mechanism to improve more optical transmittance and higher crystalline quality of the ZnO:N thin films but more thermal energy would destroy nitrogen related defect complexes leading to the n-type conductivity.

5.4.4 Evolution of crystal structure of Zn:N films in vacuum under high temperature

From section 5.4.3, in order to describe the mechanism of the middle layer, we demonstrate a systematic study of the temperature effect on the structural properties of the Zn:N thin film under vacuum that would transform to be Zn_3N_2 thin film. The sputtering conditions discussed in Table 5.15 were used, but this Zn:N film was fabricated for 4 minutes and the thickness of the as-grown films was about 0.5 μm. XRD measurement was used to examine and compare both lattice parameters and grain size of crystalline structure of pure Zn and Zn:N films. High temperature x-ray diffraction (HTXRD) measurement using Philips X’pert from ambient temperature (25^{o}C) to 554^{o}C, and scanning from 2θ of 30^{o} to 60^{o}, was used to examine the evolution of structural properties of the Zn:N film under vacuum. The Zn:N film was heated by platinum heater under vacuum of 10^{-5} mbar. The temperatures of platinum heater and Zn:N film were measured by an in-contact thermocouple (type-S) and non-contact pyrometer at 1.55 μm, respectively. The observed peaks in XRD patterns were fitted using Gaussian distribution for the calculation of structural parameters of the films.

The room temperature XRD spectra of the pure Zn and Zn:N films are shown in Fig. 5.28. The planes (002), (100), and (101) of Zn structure were similar observed similary in both spectra. Because the peak positions are close to Zn standard [42], the films are identified as zinc films. The larger peak width of Zn:N corresponds to the smaller average grain size calculated from Scherrer’s formula as shown in Table 5.19.

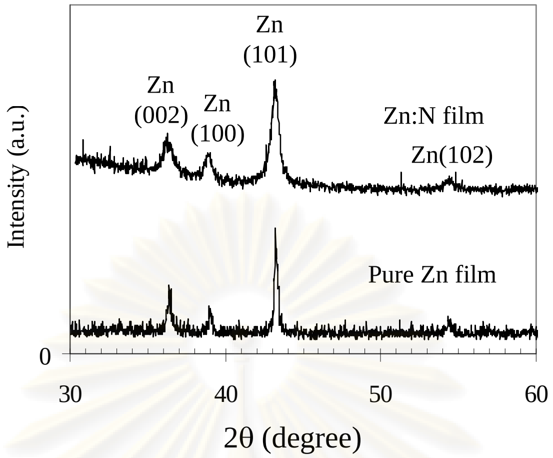

Figure 5.28: XRD spectra of pure Zn film and Zn:N film at ambient temperature.

Table 5.19: Lattice parameters (a & c of hexagonal structure) of pure Zn film and Zn:N film at ambient temperature, and average grain size.

Films	*a* (Å)	Difference from normal (2.6650 Å)	*c* (Å)	Difference from normal (4.9470 Å)	Average grain size (nm)
Pure Zn	2.6634	- 0.06%	4.9346	-0.25%	58
Zn:N	2.6686	+ 0.13%	4.9459	-0.02%	28

The lattice parameters *a* and *c* calculated from Zn peaks (100), (002) and (101) of Zn:N film also larger than those of pure Zn film. It suggests that nitrogen could incorporate into the Zn film in the form of defects without explicit Zn_3N_2 phase observed from the XRD spectrum. These defects could be in the forms of interstitials of nitrogen or Zn-N related compounds. The XRD patterns of the Zn:N film under vacuum at various temperatures are illustrate in Fig. 5.29. The lattice parameters of hexagonal structure of Zn from various XRD patterns or different temperatures were fitted, where the calculated lattice parameters *a* and *c* base on the least square fitting were depicted as Fig. 5.30(a) and (b), respectively. Average grain sizes of the Zn:N film from the transformation of Zn phase to Zn_3N_2 phase were also shown as Fig.

5.31. At the higher temperature from 124°C to 269°C, the left shifts corresponding to the increment of lattice constants of Zn were observed. The lattice parameter *a* from all temperatures is about 0.15% – 0.25% greater than 2.6650 Å of standard Zn [42]. In addition, at 269°C, the lattice parameter *c* increases rapidly to 0.7% greater than 4.9470 Å of standard Zn [42]. This corresponds to the large increase of tensile strain along *c*-axis of the Zn structure of the Zn:N thin film with the increase of temperature. The average grain size of the Zn phase is approximately 29 nm from ambient temperature to 203°C, then increase to about 33 nm from 269°C to 320°C followed by the change from Zn to Zn_3N_2 phase with the average grain size about 15 nm as shown in Fig 5.31. At temperature of 320°C, the decrement in amplitude of Zn (002), (100), and (101) peaks also was observed. In contrast, small peaks, e.g. (222) and (321) of Zn_3N_2 were also observed. This should be typical phase of Zn_3N_2 or Zn_xN_y created by the chemical reaction between Zn and N at high temperature under vacuum.

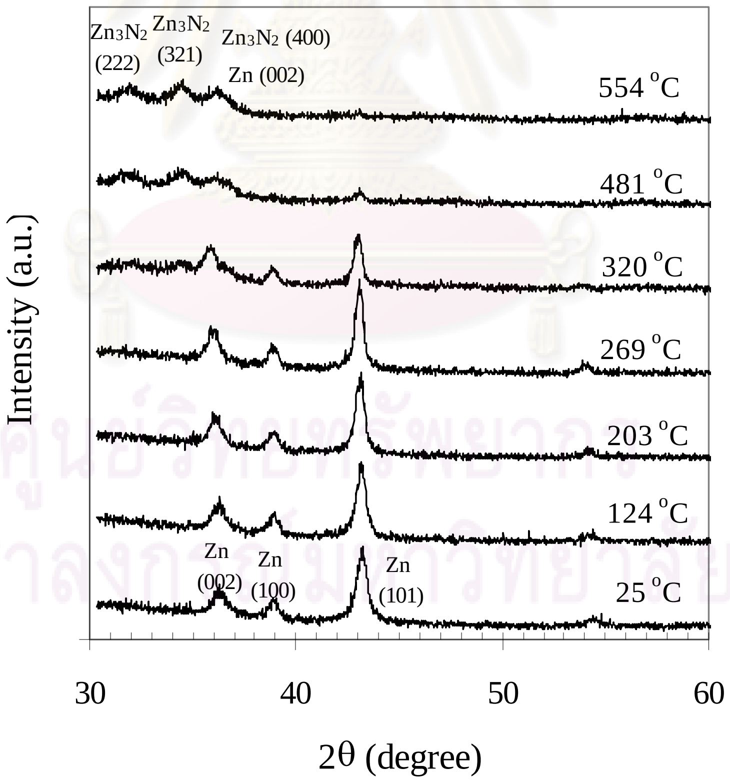

Figure 5.29: XRD spectra of the Zn:N film under various temperatures.

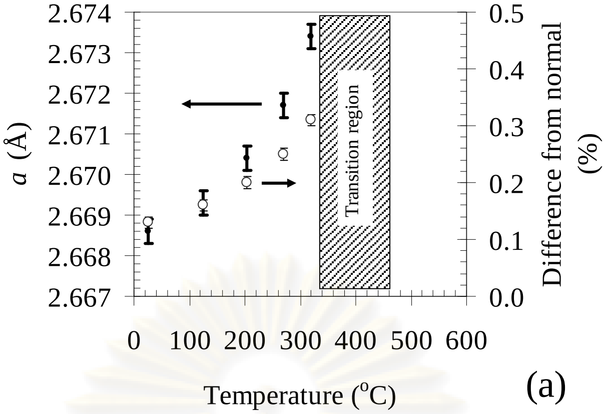

(a)

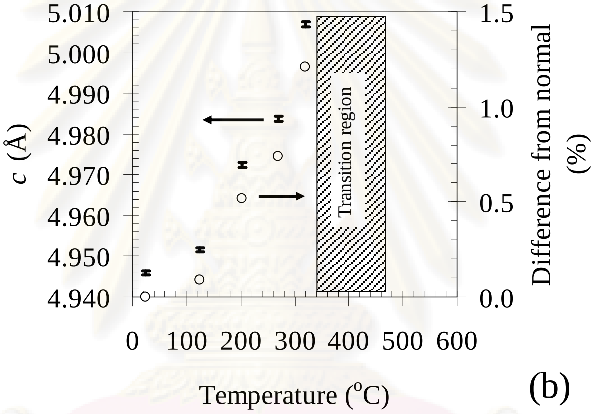

(b)

Figure 5.30: Lattice parameters (a) a and (b) c of the Zn:N film (Zn phase) under various temperatures.

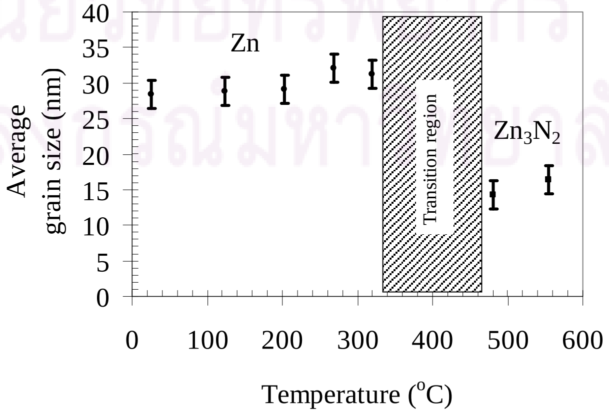

Figure 5.31: Average grain sizes of the Zn:N film under various temperatures.

Table 5.20: Lattice parameter a of Zn_3N_2 phase and average grain size of the Zn:N film at 481°C and 554°C.

Temperature (°C)	a (Å)	Difference from normal (9.7769 Å)	Average grain size (nm)
481	9.7503	-0.27%	14
554	9.7532	-0.24%	16

At temperature of 481°C and 554°C, the planes (222), (321), and (400) (overlaps with the peak (002) of Zn) of Zn_3N_2 structure were observed with the decrement of Zn peaks. This can be identified as the formation of Zn_3N_2 phase leading to incomplete phase transition from Zn:N to Zn_3N_2.

The calculated lattice parameter *a* of a cubic structure of Zn_3N_2 phase and its average grain size is summarized in Table 5.20. The lattice parameter *a* is less than standard Zn_3N_2 [27] by approximately 0.3%. The residual Zn phase is due to the nitrogen deficient of the Zn_3N_2 film at high temperature. The result revealed that some of nitrogen could be removed under vacuum by thermal energy during the formation of Zn_3N_2 phase. Thus, the phase transition from Zn:N to Zn_3N_2 is not a completely chemical reaction.

From the results, from ambient temperature to approximately of 270°C, the Zn:N film exhibits Zn phase in hexagonal structure. The lattice parameters *a* and *c* of in Zn:N film are greater than those of of pure Zn film due to the nitrogen distribution. At higher temperature than 320°C, the film should rather be in the Zn_3N_2 or Zn_xN_y phases because of the large increment of lattice parameters *a* and *c* of Zn phase and the observation of the (222), (321), and (400) planes of Zn_3N_2 phases. The result suggests that the Zn:N film exhibits the phase transition from Zn:N to Zn_3N_2 at temperature higher than 320°C. At temperature above 500°C, the film exhibits Zn_3N_2 phase with the residual phase of Zn due to the nitrogen deficiency in the system.

CHAPTER VI

CONCLUSIONS

In order to obtain p-type ZnO, it requires the effort to dope group-V element into the O sites in ZnO structure. Due to large atomic size of P, the as-grown ZnO:P film exhibits low crystalline quality with tensile strain which cannot be improved by post-annealing. With the random incoming atoms in sputtering process, the incoming P atoms prefer to occupy Zn sites with more stability instead of the expected O sites. Thermal annealing should drive additional P into its stable sites, thus the n-type carriers increase. The n-type carrier concentrations of the as-grown and vacuum annealed ZnO:P films are of 3.17×10^{19} and 1.55×10^{20} cm^{-3}, respectively.

Nitrogen which has atomic site smaller than that of P is suitable in occupying the Zn site. Starting from ZnO target with N_2 sputtering gas (mixed with Ar) leads to the N_2 interstitials in the film which can be removed by annealing in vacuum. The films also exhibit very high resistance corresponding to the low carrier concentration. The problem is that nitrogen cannot compete against oxygen in occupying oxygen sites. In order to help nitrogen, other material or Zn metallic target was selected. Fill N to the film firstly in the form of Zn:N film and then anneal under oxygen. Then, the ZnO:N films were obtained. The complete ZnO structure without Zn or Zn_3N_2 was obtained by two-step annealing; firstly with vacuum annealing and secondly with oxygen annealing. The problems are that the structural properties were low and their resistivities were high without p-type conductivity. The problem of this method is that the nitrogen bond cannot be broken. Other gas used instead of N_2 is N_2O. Sputtering Zn target under N_2O partial pressure exhibits interested results of XRD spectra. The XRD spectra exhibit a superposition of Zn_3N_2 (321) peak and ZnO (002) peak. The ratios of peak area are the same for various N_2O partial pressures. Some of the as-grown film exhibit very low p-type conductivity by hot probe measurement. Most of them including the vacuum annealing, exhibit very high resistivities in the order of 10^5 $\Omega\cdot$cm with ambiguous type of carrier. The problem is that oxygen is more active than nitrogen. Another idea is that mechanically trap N or its compound in i-ZnO and chemically distributes by suitable thermal annealing. Nitrogen doped zinc oxide (ZnO:N) could be obtained from the insertion of ultra-thin Zn:N (UTZN) middle layer with the thickness of 5 nm into the ZnO film with the short time vacuum (STV) annealing (up to 400°C in 3 minutes). The key process to enhance hole carriers in ZnO:N film is to distribute the crystalline structure into quasi-stable states acting as acceptors. The use of STV annealing, in the mean time, creates Zn_3N_2 from the UTZN layer, contributes O into N sites of Zn_3N_2, and creates ZnO:N with p-type conductivity. Resistivity, mobility, and carrier concentration of the STV annealed film are of 2.3×10^{-2} Ω·cm, 8.6 V·s/m^2, and 5.2×10^{19} cm^{-3}, respectively. Due to quasi-stable state of p-type conductivity, they can be redistributed by the long time vacuum (LTV) annealing (up to 500°C in 20 minutes and dwelling for 20 minutes) to stable states with n-type conductivity. It can be concluded that the key parameters to obtain p-type ZnO film are temperature and time of post-annealing.

The suggestion for further investigation of p-type ZnO thin film is to use different methods such as co-doping, group-I doping, and annealing at the satisfied pressure. Co-doping could be use to tune accepter and donor levels of ZnO. Group-I doping leads to the occupied group-I element at the Zn site. As a result, group-I doped p-type ZnO could be possibly obtained. Annealing pressure effects the formation of Zn:N to Zn_3N_2. So, the p-type ZnO:N films which employ Zn_3N_2 formation should be tuned by the optimizing of annealing pressure.

References

[1] Look, D. C. Recent advances in ZnO materials and devices. *Mater. Sci. Eng.* **B80** (2001): 383-387.

[2] Lee, J. C., Kang, K. H., Kim, S. K., Yoon, K. H., Park, I. J., Song, J. RF sputter deposition of the high-quality intrinsic and n-type ZnO window layers for Cu(In,Ga)Se_2-base solar cell applications. *Sol. Energ. Mat. Sol. C.* **64** (2000): 185-195.

[3] Chen, M., Pei, Z. L., Sun, C., Gong, J., Huang, R. F., Wen, L. S. ZAO: an attractive potential substitute for ITO in flat display panels. *Mater. Sci. Eng.* **B85** (2001): 212-217.

[4] Look, D. C., Reynolds, D. C., Sizelove, J. R., Jones, R. L., Litton, C. W., Cantwell, G., Harsch, W. C. Electrical properties of bulk ZnO. *Solid Stat Commun.* **105 (6)** (1998) 399-401.

[5] Igasaki, Y., Kanma, H. Ar gas pressure dependence of the properties of transparent conducting ZnO:Al films deposited on glass substrates. *Appl. Surf. Sci.* **169-170** (2001) 508-511.

[6] Li, X., Asher, S. E., Limpijumnong, S., Keyes, B. M., Perkins, C. L., Barnes, T. M., Moutinho, H. R., Luther, J. M., Zhang, S. B., Wei, S. H., Coutts, T. J. Impurity effects in ZnO and nitrogen-doped ZnO thin films fabricated by MOCVD. *J. Cryst. Growth* **287** (2006) 94-100.

[7] Xiu, F. X., Yang, Z., Mandalapu, L. J., Liu, J. L. P-type ZnO films with solid-source phosphorus doping by molecular-beam epitaxy. *Appl. Phys. Lett.* **88** (2006) 152106-1 – 152106-3.

[8] Xiu, F. X., Yang, Z., Mandalapu, L. J., Liu, J. L., Donor and acceptor competitions in phosphorus-doped ZnO. *Appl. Phys. Lett.* **88** (2006) 152116-1 – 152116-3.

[9] Heo, Y. W., Ip, K., Park, S. J., Pearton, S. J., Norton, D. P. Shallow donor formation in phosphorus-doped ZnO thin films. *Appl. Phys. A* **78** (2004) 53-57.

[10] Lim, S. H., Kim, J. W., Kang, H. S., Kim, G. H., Chang, H. W., Lee, S. Y. Characterization of phosphorus doped ZnO multi-layer thin films to control carrier concentration. *Superlattice Microst.* **38** (2005) 377-384.

[11] Dulere, J. R., Ohaire, R., Meaney, A., Johnton, K., Reid, I., Tobin, G., Mosnier, J. P., Viry, M. G., Mcglynn, E., Henry, M. O. Fabrication of p-type doped ZnO thin films using pulsed laser deposition. *J. Mater. Sci-Mater. El.* **16** (2005) 421-427.

[12] Ryu, Y. R., Zhu, S., Look, D. C., Wrobel, J. M., Jeoung, H. M., White, H. W. Synthesis of p-type ZnO films. *J. Cryst. Growth* **216** (2000) 330-334.

[13] Vlasenflin, T. H., Tanaka, M. P-type conduction in ZnO dual-acceptor-doped with nitrogen and phosphorus. *Solid State Commun.* **142** (2007) 292-294.

[14] Tu, M. L., Su, Y. K., Ma, C. Y. Nitrogen-doped p-type ZnO films prepared from nitrogen gas radio-frequency magnetron sputtering. *J. Appl. Phys.* **100** (2006) 053705-1 – 053705-4.

[15] Yao, B., Guan, L. X., Xing, G. Z., Zhang, Z. Z., Li, B. H., Wei, Z. P., Wang, X. H., Cong, C. X., Xie, Y. P., Lu, Y. M., Shen, D. Z. P-type conductivity and stability of nitrogen-doped zinc oxide prepared by magnetron sputtering. *J. Lumin.* **122-123** (2007) 191-194.

[16] Wang, J., Sallet, V., Jomard, F., do Rego, A. M. B., Elamurugu, E., Martins, R., Fortunato, E. Influence of the reactive N_2 flow on the properties of rf-sputtered ZnO thin films. *Thin Solid Films* **515** (2007) 8780-8784.

[17] Wang, H., Gao, X., Duan, Q, Lu, J. Variation of surface properties of ZnO films by the implantation of N^+ ions. *Thin Solid Films* **492** (2005) 236-239.

[18] Wang, P., Chen, N., Yin, Z., Yang, F., Peng, C. Fabrication and properties of Sb-doped ZnO thin films grown by radio frequency (RF) magnetron sputtering. *J. Cryst. Growth* **290** (2006) 56-60.

[19] Zhong, F., Ma, H., Du, W., Ma, J., Zhang, X., Xiao, H., Ji, F., Xue, C. Optical band gap of zinc nitride films prepared on quartz substrates from a zinc nitride target by reactive rf magnetron sputtering. *Appl. Surf. Sci.* **252** (2006) 7983-7986.

[20] Kambilafka, V., Voulgaropulou, P., Dounis, S., Iliopoulos, E., Androulidaki, M., Tsagaraki, K., Šály, V., Ružinský, M., Prokein, P., Aperathitis, E. The effect

of nitrogen on the properties of zinc nitride thin films and their conversion into p-ZnO:N films. *Thin Solid Films* **515** (2007) 8573-8576.

[21] Wang, C., Ji, Z., Liu, K., Xiang, Y., Ye, Z. P-type ZnO thin films prepared by oxidation of Zn_3N_2 thin films deposited by DC magnetron sputtering. *J. Cryst. Growth* **259** (2003) 279-281.

[22] Sun, J. C., Liang, H. W., Zhao, J. Z., Bian, J. M., Feng, Q. J., Hu, L. Z., Zhang, H. Q., Liang, X. P., Luo, Y. M., Du, G. T. Ultraviolet electroluminescence from n-ZnO:Ga/p-ZnO:N homojunction device on sapphire substrate with p-type ZnO:N layer formed by annealing in N_2O plasma ambient. *Chem. Phys. Lett.* **460** (2008) 548-551.

[23] Kerr, L. L, Li, X., Canepa, M., Sommer, A. J. Raman analysis of nitrogen doped ZnO. *Thin Solid Films* **515** (2007) 5282-5286.

[24] *Powder Diffraction File, Joint Committee on Powder Diffraction Standards.* Card no. 36-1451.

[25] http://www.tcd.ie/Physics/People/Charles.Patterson/research_projects/zinc_cobolt_oxide.php

[26] Bass, M., DeCusatis, C., Enoch, J., Lakshminarayanan, V., Li, G., MacDonald, C., Mahajan, V., and Stryland, E. V. Handbook of Optics, Vol. 2, 2nd edition. McGraw-Hill, New York, 1994.

[27] *Powder Diffraction File, Joint Committee on Powder Diffraction Standards.* Card no. 35-762.

[28] Kuriyama, K., Takahashi, Y., and Sunohara, F. Optical band gap of Zn_3N_2 films. *Physical Review B.* **48(4)** (1993) 2781-2782.

[29] Du, W., Zong, F., Ma, H., Ma, J., Zhang, M., Feng, X., Li, H., Zhang, Z., and Zhao, P. Optical band gap of zinc nitride films prepared by reactive rf magnetron sputtering. *Cryst. Res. Technol.* **41(9)** (2006) 889-892.

[30] Vegas, A., Matin., R. L., and Bevan, D. J. M. Compounds with a ‘stuffed’ anti-bixbyite-type structure, analyzed in terms of the Zintl-Klemm and coordination-defect concepts. *Acta Crys.* **B65** (2009) 11-21.

[31] Li, B. S., Liu, Y. C., Zhi, Z. Z., Shen, D. Z., Lu, Y. M., Zhang, J. Y., Fan, X. W., Mu, R. X., and Henderson, D. O. Optical properties and electrical

characterization of p-type ZnO thin films prepared by thermally oxiding Zn_3N_2 thin films. *J. Mater. Res.* **18(1)** (2003) 8-13.

[32] Xiao, H. *Introduction to Semiconductor Manufacturing Technology*. New Jersey: Prentic-Hall, 2001.

[33] Ranyan, W. R. *Semiconductor Measurement and Instrumentation.* Tokyo: McGraw-Hill Kogakusha, 1975.

[34] Yu, P. Y., and Cardona, M. *Fundamentals of semiconductors: Physics and material properties.* Berlin: Spinger, 1996.

[35] Toress, J., Cisneros, J. I., Gordillo, G., and Alvarez, F. *A simple method to determine the optical constants and thicknesses of $Zn_xCd_{1-x}S$ thin films.* Thin Solid Films **289** (1996) 238-241.

[36] Pankove, J. I. *Optical process in semiconductors.* New York: Dover, 1971.

[37] Azaroff, L. V., *Elements of X-ray Crystallography.* New York: McGraw-Hill, 1968.

[38] Kittel, *C. Introduction to Solid State Physics 7th edition.* New York: John Wiley & Sons, 1996.

[39] Futsuhara, M., Yoshioka, K., and Takai, O. *Optical properties of zinc oxynitride thin films.* Thin Solid Films **317** (1998) 322-325.

[40] Limpijumnong, S., Li, X., Wei, S. H., and Zhang, S. B. *Substitional diatomic molecules NO, NC, CO, N_2 and O_2: Their vibrational frequenies effects on p doping ZnO.* Appl. Phys. Lett. **86** (2005) 211910-1 – 211910-3.

[41] Limpijumnong, S., Li, X., Wei, S. H., and Zhang, S. B. *Probing deactivations in nitrogen doped ZnO by vibration signatures:* A First principles study. Physica B **376 – 377** (2006) 686 – 689.

[42] *Powder Diffraction File, Joint Committee on Powder Diffraction Standards.* Card no. 4-831.

APPENDICES

APPENDIX A

LIST OF ABBREVIATIONS

2SA	Two-stage anneal
AG	As-grown
AFM	Atomic force microscopy
DC	Direct current
FWHM	Full width at half maximum
i-ZnO	Intrinsic ZnO
JCPDS	Joint Committee on Powder Diffraction Standards
LTV	Long time vacuum
MBE	Molecular beam epitaxy
MFP	Mean free path
MOCVD	Metal-organic chemical vapor deposition
NIR	Near infrared
N_O	Nitrogen which occupies oxygen site
$(N_2)_O$	Nitrogen molecule which occupies oxygen site
NRDC	Nitrogen related defect complex
OA	Oxygen anneal
PLD	Pulse laser deposition
RF	Radio frequency
SCCM	Cubic centimeter per minute at STP
STV	Short time vacuum
TCO	Transparent conductive oxide
UTZN	Ultra-thin Zn:N
UV	Ultraviolet
VA	Vacuum anneal
VIS	Visible
V_O	Oxygen vacancy
XRD	X-ray diffraction
Zn_i	Zinc interstitial

APPENDIX B
LIST OF CONFERENCES

1. Wantong, K., Chatraphorn, S., Yoodee, K., and Chityuttakarn, C. "Preparation of high quality aluminum-doped zinc oxide (AZO) target using warmly pressed technique" *The 32nd Congress on Science and Technology Thailand (STT32)*, Bangkok, Thailand, 10-12 October 2006.
2. Wantong, K., Chityuttakarn, C., Chatraphorn, S., and Yoodee, K. "Fabrication of phosphorus-doped ZnO thin films under partial pressure of nitrogen gas" *Siam Physics Congress 2007 (SPC 2007)*, Nakorn Pathom, Thailand, 22-24 March 2007.
3. Wantong, K., Chatraphorn, S., Yoodee, K., and Chityuttakarn, C. "Comparison of rf magnetron sputtering ZnO thin films using nitrogen sputtering gas" *Siam Physics Congress 2008 (SPC 2008)*, Nakorn Ratchasima, Thailand, 20-22 March 2008.
4. Wantong, K., Chatraphorn, S., and Chityuttakarn, C. "Effect of annealing Zn:N_2 films grown by rf magnetron sputtering technique" *5th Thailand Materials Science and Technology Conference (MSAT5)*, Bangkok, Thailand, 16-19 September 2008.
5. Wantong, K., Chatraphorn, S., and Chityuttakarn, C. "Incorporation of nitrogen into zinc oxide thin films using N_2O sputtering technique" *The 34th Congress on Science and Technology Thailand (STT34)*, Bangkok, Thailand, 31 October – 2 November 2008.
6. Chityuttakarn, C., Chatraphorn, S., and Wantong, K. "Zinc oxide thin films grown by sputtering technique under the N_2O partial pressure" *4th Mathematics and Physical Sciences Graduate Congress 2008 (MPSGC 08)*, National University of Singapore, Singapore, 17-19 December, 2008.
7. Wantong, K., Chatraphorn, S., Yoodee, K., and Chityuttakarn, C. "Evolution of ZnO thin film prepared by reactive dc sputtering technique using the mixed gas of N_2O and N_2, *Siam Physics Congress 2009 (SPC 2009)*, Petchburi, Thailand, 20-22 March 2009.

CURRICULUM VITAE

Kriangkrai Wantong was born on 13th September 1975 in Samut Prakan, Thailand. He has been a student in the special program called Development and Promotion for Science and Technology Talent Project (DPST). He received his Bachelor degree of Science (First Class Honors) in Physics from Chulalongkorn University in 1998, and received his Master degree of Science in Physics from Chulalongkorn University in 2002. During 2002 – 2005, he had been worked as a precious metal assayer at the Gem and Jewelry Institute of Thailand. He continued his Ph.D. degree in 2005.